NAVAL POSTGRADUATE SCHOOL

MONTEREY, CALIFORNIA

THESIS

AN EXPLORATION OF THE MARSUPIAL PARADIGM IN DEVELOPING AFRICAN EASTERLY WAVES FROM 2020: JOSEPHINE, ISAIAS, AND LAURA

by

Scott C. Britton

June 2021

Thesis Advisor: Michael T. Montgomery
Second Reader: Scott Powell

THIS PAGE INTENTIONALLY LEFT BLANK

REPORT DOCUMENTATION PAGE			*Form Approved OMB No. 0704-0188*

1. AGENCY USE ONLY *(Leave blank)*	**2. REPORT DATE** June 2021	**3. REPORT TYPE AND DATES COVERED** Master's thesis

4. TITLE AND SUBTITLE
AN EXPLORATION OF THE MARSUPIAL PARADIGM IN DEVELOPING AFRICAN EASTERLY WAVES FROM 2020: JOSEPHINE, ISAIAS, AND LAURA

5. FUNDING NUMBERS

6. AUTHOR(S) Scott C. Britton

7. PERFORMING ORGANIZATION NAME(S) AND ADDRESS(ES)
Naval Postgraduate School
Monterey, CA 93943-5000

8. PERFORMING ORGANIZATION REPORT NUMBER

9. SPONSORING / MONITORING AGENCY NAME(S) AND ADDRESS(ES)
N/A

10. SPONSORING / MONITORING AGENCY REPORT NUMBER

11. SUPPLEMENTARY NOTES The views expressed in this thesis are those of the author and do not reflect the official policy or position of the Department of Defense or the U.S. Government.

12a. DISTRIBUTION / AVAILABILITY STATEMENT
Approved for public release. Distribution is unlimited.

12b. DISTRIBUTION CODE
A

13. ABSTRACT (maximum 200 words)

This thesis applies the marsupial paradigm (MP) conceptual model of tropical cyclone (TC) formation previously used to describe the transition from a tropical disturbance to a tropical depression. A case study of three storms that formed from African easterly waves in the North Atlantic during the 2020 hurricane season, Isaias, Josephine, and Laura, provides insight into the pre-formation structures called wave-pouches. The analysis evaluates several variables including the Okubo-Weiss (OW) parameter, relative vorticity, relative humidity, and vertical shear in a comoving (quasi-Lagrangian) framework. Additionally, GOES-16 Channel 13 infrared imagery emphasizing cloud presence was coupled in sequence with the analyses to reveal connections between wave-pouch structure and observed developing convection. Furthermore, this work addresses pouch interactions with shear and other pouches or vortices. The study concludes with recommendations to forecasters on how to incorporate the MP into pre-TC analysis alongside the global numerical weather model outputs.

14. SUBJECT TERMS hurricane, Lagrangian, marsupial paradigm, MP, Okubo-Weiss, OW, pouch, prediction, tropical cyclone, TC	**15. NUMBER OF PAGES** 107
	16. PRICE CODE

17. SECURITY CLASSIFICATION OF REPORT	**18. SECURITY CLASSIFICATION OF THIS PAGE**	**19. SECURITY CLASSIFICATION OF ABSTRACT**	**20. LIMITATION OF ABSTRACT**
Unclassified	Unclassified	Unclassified	UU

NSN 7540-01-280-5500

Standard Form 298 (Rev. 2-89)
Prescribed by ANSI Std. 239-18

THIS PAGE INTENTIONALLY LEFT BLANK

Approved for public release. Distribution is unlimited.

AN EXPLORATION OF THE MARSUPIAL PARADIGM IN DEVELOPING AFRICAN EASTERLY WAVES FROM 2020: JOSEPHINE, ISAIAS, AND LAURA

Scott C. Britton
Lieutenant Commander, United States Navy
BA, College of Wooster, 2006

Submitted in partial fulfillment of the
requirements for the degree of

MASTER OF SCIENCE IN METEOROLOGY AND PHYSICAL OCEANOGRAPHY

from the

NAVAL POSTGRADUATE SCHOOL
June 2021

Approved by: Michael T. Montgomery
Advisor

Scott Powell
Second Reader

Wendell A. Nuss
Chair, Department of Meteorology

THIS PAGE INTENTIONALLY LEFT BLANK

ABSTRACT

This thesis applies the marsupial paradigm (MP) conceptual model of tropical cyclone (TC) formation previously used to describe the transition from a tropical disturbance to a tropical depression. A case study of three storms that formed from African easterly waves in the North Atlantic during the 2020 hurricane season, Isaias, Josephine, and Laura, provides insight into the pre-formation structures called wave-pouches. The analysis evaluates several variables including the Okubo-Weiss (OW) parameter, relative vorticity, relative humidity, and vertical shear in a comoving (quasi-Lagrangian) framework. Additionally, GOES-16 Channel 13 infrared imagery emphasizing cloud presence was coupled in sequence with the analyses to reveal connections between wave-pouch structure and observed developing convection. Furthermore, this work addresses pouch interactions with shear and other pouches or vortices. The study concludes with recommendations to forecasters on how to incorporate the MP into pre-TC analysis alongside the global numerical weather model outputs.

THIS PAGE INTENTIONALLY LEFT BLANK

TABLE OF CONTENTS

THIS PAGE INTENTIONALLY LEFT BLANK

LIST OF FIGURES

THIS PAGE INTENTIONALLY LEFT BLANK

LIST OF ACRONYMS AND ABBREVIATIONS

AEJ	African Easterly Jet
AEW	African Easterly Wave
CIMSS	Cooperative Institute for Meteorological Satellite Studies (Univ. of Wisconsin)
GDAL	Geospatial Data Abstraction Library
GFS	Global Forecast System
GIS	Geographic Information System
GOES	Geostationary Operational Environmental Satellite
IBTrACS	International Best Track Archive for Climate Stewardship (NOAA)
IR	Infrared
ITCZ	Intertropical Convergence Zone
LCL	Lifted Condensation Level
MP	Marsupial Paradigm
NHC	National Hurricane Center
NOAA	National Oceanic and Atmospheric Administration
OGR	Open Source Geospatial Foundation
OW	Okubo-Weiss parameter
PTC	Potential Tropical Cyclone
RH	Relative Humidity
SAL	Saharan Air Layer
SST	Sea Surface Temperature
TC	Tropical Cyclone
TD	Tropical Depression
TS	Tropical Storm
WGS84	World Geodetic System from 1984

THIS PAGE INTENTIONALLY LEFT BLANK

ACKNOWLEDGMENTS

Thank you, Dr. Michael T. Montgomery, for the guidance and support through this process. A special thanks to Mr. Mark Boothe for his technical expertise, sharp eye, and guidance within the wide world of Amazon Web Services.

A special shout out goes to Mr. Michael Guy on the AWS Navy team for helping me get my remote workstation set up during this COVID-19 pandemic.

Thank you to my wife, Emily, for the sustained support through these unprecedented times. Also, thank you to the ever-productive and curious boys, Cedar and Alder, for popping into my cave and saving me from the perils of a virtual world.

THIS PAGE INTENTIONALLY LEFT BLANK

I. INTRODUCTION

A. SYNOPSIS

Intrigue and destruction, symmetrical beauty and self-sustaining force, hard-to-predict transformation and reliable indicators: Tropical cyclones (TCs) continue to mystify and transfix those inside the Meteorological community as well as outside. The necessary conditions outlined by Gray (1975) of ocean heat content to 60 meters in depth (or high sea surface temperature (SST)), high relative humidity (RH) in the middle troposphere, cyclonic vorticity-inducing perturbations at low levels, weak vertical wind shear, moist instability from the surface to 500 hPa, and the effect of the Coriolis force away from the equator are necessary to the formation of TCs; yet alone, they are insufficient. Identified by organized deep convection with closed surface wind streamlines circulating around a well-defined center, TCs transfer energy from the ocean to the upper troposphere in a self-sustaining process (NHC). From a climatological perspective, the North Atlantic hurricane season from June to November marks a period of high TC activity. There are periods of quiet during the peak of the Atlantic TC season as well as anomalous cyclones that form outside the season. In the western North Pacific, typhoon season never ceases.

To better understand TC formation, the work of Dunkerton, Montgomery, Wang, Rutherford, and Boothe, among others, developed a conceptual model known as the marsupial paradigm (MP). Simply stated, translating from an Earth-relative to a Lagrangian or comoving reference frame provides a visual structure of TC formation that often precedes the development of a TC in the Earth-relative framework. This edge, the extra time and relative precision of detection within the comoving framework is desirable to gain additional insight into developing cyclones and can be useful for enhancing naval operations or saving lives and protecting infrastructure.

Foundational to the MP, Dunkerton et al. (2009) described and tested three hypotheses that evaluate and contribute to the characterization of the associated wave-relative flow structure called a “cat’s eye”.

> (H1) Proto-vortex cyclonic eddies instrumental in TC formation are intimately associated with the parent wave's critical latitude in the *lower troposphere*. The critical layer and Kelvin cat's eye within, formed as a result of the wave's finite-amplitude interaction with its own critical latitude, contain a region of cyclonic rotation and weak straining/shearing deformation in which synoptic waves and mesoscale vorticity anomalies, moving westward together, amplify and aggregate on a nearly zero relative mean flow. This multi-scale interaction provides a dynamical pathway to 'bottom-up' development of the proto-vortex from below. (p. 5594)

This first hypothesis advocates a bottom-up development for TC genesis referencing the critical latitude in the lower troposphere. Critical latitude is defined as the latitude or level where mean flow and wave phase speed are equal in the wave propagation direction (Dunkerton et al. 2009). A purely zonally oriented wave at the critical latitude would have a speed (c) equal to the zonal component of the mean wind vector (u): c=u. Important to the discussion is the trough axis that corresponds to an elongated area of low air pressure. The intersection of the trough axis and critical latitude constitutes the "sweet spot."

Another important feature is the Okubo-Weiss (OW) parameter, which distinguishes cyclonic rotation from strain and shear deformation. As a result, OW aids in identifying the proto-vortex cyclonic eddies that form within the parent wave. As a useful identifier of cyclonic rotation that exceeds strain or shear deformation, OW is defined mathematically as

$$OW = \zeta^2 - S_1^2 - S_2^2 = \left(V_x - U_y\right)^2 - \left(U_x - V_y\right)^2 - \left(V_x + U_y\right)^2. \quad (1)$$

In Equation (1), ζ represents the relative vertical vorticity, or the rotational flow or spin, S_1 represents horizontal strain deformation, and S_2 represents horizontal shear deformation. Squaring each value amplifies the magnitude of signal to aid in analysis and produces typical values in candidate disturbances of the order $10^{-9}s^{-2}$. Positive values of OW indicate rotationally dominant flow. Negative values of OW indicate strain or shear dominant flow (Montgomery et al. 2012). Generated images pertaining to this thesis focus on positive OW, which indicates areas of cyclonic rotational flow and, ultimately, areas

with potential for cyclogenesis. OW alone does not illustrate the entire structure, nor is it a sufficient singular diagnostic.

> (H2) The critical-layer cat's eye of the parent wave provides a set of quasi-closed material contours inside of which air is repeatedly moistened by convection, protected to some degree from lateral intrusion of dry air and impinging vertical shear, and (thanks to its location near the critical latitude) able to keep pace with the parent wave until the proto-vortex has strengthened into a self-maintaining entity. (p. 5594)

This second hypothesis focuses on the protective nature of nearly closed, wave-relative, flow streamlines, a flow structure broadly defining the so-called "pouch" analogous with a marsupial's pouch. Inside the nearly closed cyclonic streamlines, convective activity can concentrate vorticity under favorable conditions and remain protected from inhibitive effects of environmental dry air outside the pouch. Convective activity inside the pouch extracts moisture from lower levels and moistens the vertical column through the evaporation of previous clouds. The convection eventually concentrates around the intersection of the trough axis and critical latitude, which is most clearly characterized by high OW values. On the small scale of the proto-vortex and protective pouches, convection acts to moisten the column in contrast with the dehumidifying effect convection has on larger scales within the tropics (Dunkerton et al. 2009).

> (H3) The parent wave is maintained and possibly enhanced by diabatically amplified eddies within the wave (proto-vortices on the mesoscale), a process favored in regions of small intrinsic phase speed. (p. 5597)

The third hypothesis from Dunkerton el al. (2009) links the wave with the eddies contained therein. The eddies help maintain the wave as eddies build and sustain themselves in conditions conducive to cyclogenesis. From the positive correlation between the convective heating rate and the temperature anomaly within the pouch, the wave will be reinforced and the wave amplitude will increase. However, as genesis approaches, the wave loses amplitude as the proto-vortex within the pouch transforms into a tropical depression or cyclone and, under the influence of the beta effect, breaks off with increased poleward trajectory (Chan and Williams 1987; Smith 1991; Sutyrin and Flierl 1994). This process ultimately leaves the emergent vortex and the wave as separate flow structures: the

westward propagating wave greatly weakened in amplitude and the poleward moving vortex often tracking into unfavorable conditions. The term “parent wave” aptly describes the gestation and transition of a recirculating eddy structure within the cyclonic cat’s eye region of the wave-pouch into an independent tropical depression vortex.

To test these hypotheses, Dunkerton et al. (2009) evaluated 55 named wave/genesis events during August and September from 1998 to 2001. The results suggested that convective precipitation occurred within the comoving, nearly closed, streamline and that TC development occurred in close proximity to the intersection of the trough axis and the critical latitude. Embedded in their discussion was the wave-pouch relationship to moisture. Horizontal moisture advection was common when the wave-pouch structure was less well-defined, allowing for entrainment of moisture. However, once a well-defined or nearly closed streamline structure emerged, parcels became isolated within the pouch center. The closed streamline, creating a protective sheath around the center fosters column moistening within the pouch center while deflecting surrounding environmental dry air. While not conclusive, the source of moisture, in some cases, may fall exclusively within the comoving closed streamlines reinforcing the isolated pouch concept.

The first large-scale field test of the MP conceptual model capitalized on targeted areas for TC development during the Pre-Depression Investigation of Cloud-Systems in the Tropics (PREDICT) experiment (Montgomery et al. 2012). PREDICT provided a trove of in-situ measurements from areas of concern based on analysis of parameters like nearly closed streamlines, OW, relative vorticity, and vertical wind shear, all of which are key ingredients to the MP conceptual model. Not only were researchers able to direct timing and location of aircraft observation efforts, but the data collected during the experiment provided insight into a spectrum of phenomena, including waves that failed to develop, a previous TC with potential to redevelop that failed to do so, and finally, waves that became TCs. Coupling the in-situ measurements with model parameters and forecasts provided a foundational analysis for advancing the understanding of tropical cyclogenesis.

Specific PREDICT-related research examined, among other things, the non-redevelopment case of Ex-Gaston (Freismuth et al. 2016). The determination of pouch structure based on plots of Lagrangian manifolds overlaid on equivalent potential

temperature as a proxy for tropospheric moisture and temperature at a given pressure level coincident with vertical wind shear revealed potential dry air intrusion to the pouch. Ex-Gaston, despite indications of a closed pouch at lower levels, experienced dry air intrusion at mid- to upper levels throughout successive dropsonde events with corresponding analyses that suggested the pouch was open and susceptible to dry air intrusion at both the 500 hPa and 700 hPa levels. The results indicated that mid- to upper- level dry air intrusion weakened the convective activity in ex-Gaston on 2 September 2010. Analysis of the in-situ, dropsonde data supported the interpretations derived from model analyses. Together, this work provided an unprecedented illustration of the underlying dynamics and thermodynamics of a non-developing case at multiple vertical levels within the comoving reference frame.

Continued development of the MP conceptual model led to a more automated approach to characterizing pouches outlined by Rutherford et al. (2018). Much of the discussion in this study revolved around thresholds best used to identify tropical depressions (TDs), tropical storms (TSs), and hurricanes in an automated sense regarding the Lagrangian variables OW and relative vorticity. A significant finding was that developing TCs possessed strong Lagrangian rotation surrounded by a band of high lateral shear, known as a protective shear sheath. Additionally, horizontal strain (S_2) modulated the relationship between curvature vorticity and shear vorticity, both components of the strain tensor. Acknowledging the importance of thermodynamic characteristics for TC development, the authors stated that thermodynamic characteristics were present for a growing TC, but were statistically negligible when characterizing the pouch structure. Furthermore, the measure of strain-free rotation was sufficient to determine the position and intensity of a cyclone.

While the MP provides a conceptual framework for identifying and tracking pouches, research by Prieto et al. (2003), following Dritschell and Waugh (1992), evaluated interactions of cyclonic vortices. Five categories characterized by separation distance, radius ratio, and vorticity ratio outlined typical interactions of two vortices: elastic interaction, partial strain, complete strain, partial merger, and complete merger. Two distant vortices with similar vorticity intensities and sizes experience elastic interaction.

As the two vortices move closer together, they experience partial merger and then complete merger. Partial strain of a vortex occurs when one radius is larger than the other in relatively close proximity; complete strain occurs when the two vortices are nearby and one vortex has a radius much larger and more intense than the other (Prieto et al. 2003; Leweke et al. 2016).

Evaluating OW, relative vorticity, and potential temperature within the MP framework, Wang and Hankes (2013) examined 164 TS formation cases, specifically from AEWs during the months of July through October from 1989 to 2010. They found nearly 80% of wave-pouches east of 60W initially formed at 700 hPa, whereas about 68% of wave-pouches west of 60W developed at 850 hPa or 925 hPa first. Figure 1, from that study, provides a climatological context for the AEW axis and propagation, along with TC genesis locations in the low to mid-level troposphere. The image illustrates an idealized notion of the typical formation path and indicates the level at which TCs form. A compelling statistical finding revealed that 97% of named storms possessed a wave-pouch at 700 hPa twelve hours prior to genesis. Comparatively, this lessened to 90% at 850-hPa, 82% at 925 hPa, and 79% for all three levels just twelve hours prior to genesis. Additionally, relative vorticity and OW analyses indicated that circulations intensified quicker at 925 hPa (low-level) compared to 600 hPa (mid-level), supporting the view of a bottom-up approach for TC genesis. The magnitude and scale of the Wang and Hankes (2013) data set provided useful insight into TC formation patterns without diving into the dynamics of specific storms.

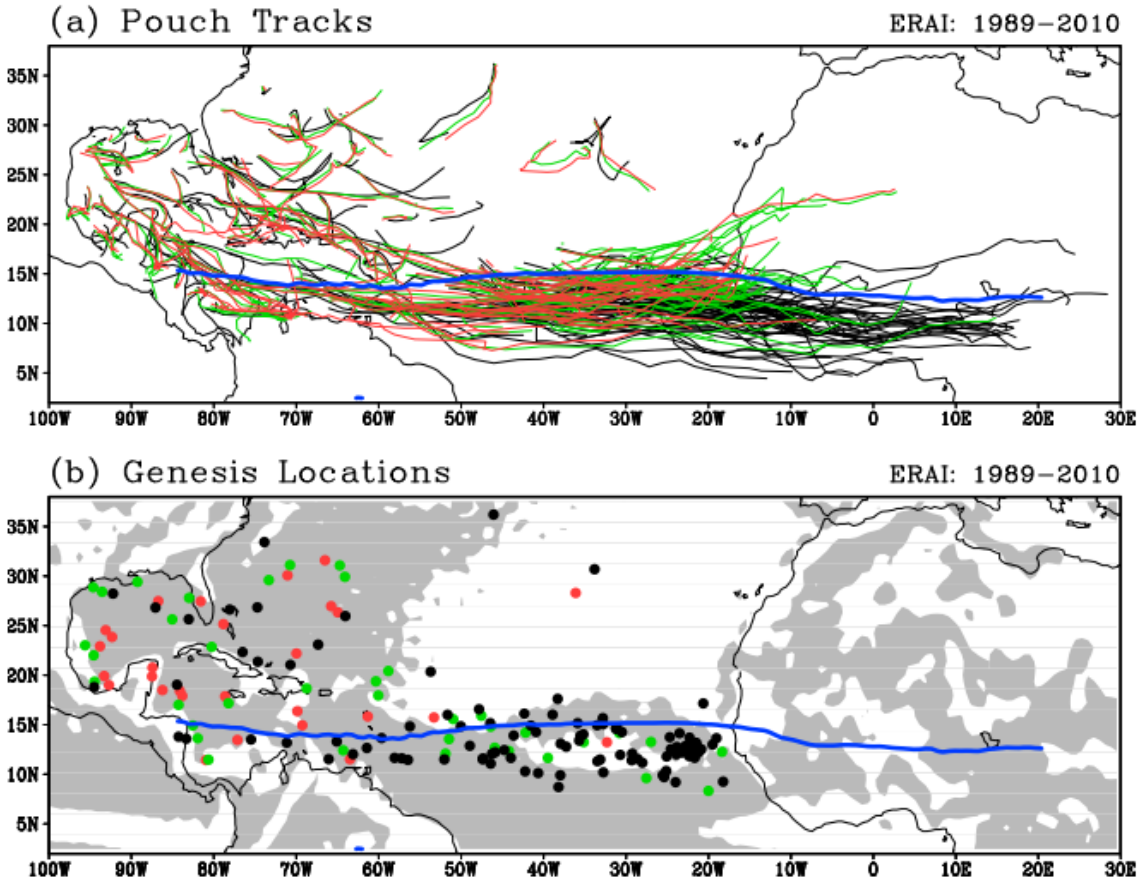

Wang and Hankes (2013) identified (a) wave-pouch tracks at a given level and (b) TC genesis locations during July to October from 1989 to 2010. Colors indicate the level of analysis: 700 hPa (black), 850 hPa (green), and 925 hPa (red). The blue solid curve is the long-term mean of the 700-hPa easterly jet throughout the analysis period (July to October 1989 to 2010). The grey shading (b) represents areas of mean convergence at 850 hPa from the long-term mean of the same time frame.

Figure 1. Pouch tracks (top) and TC genesis locations (bottom).
Source: Wang and Hankes (2013).

B. MOTIVATION

Aside from the mystery that lingers, TCs have an operational impact to the seas and coasts, including the property of the Department of Defense and the United States Navy. A critical ambition to develop and operationalize the MP underscores the potential to predict the occurrence of TCs with greater range and precision. Developing a familiarity within the comoving reference frame grants operational forecasters an additional tool and insight into TC formation, almost like lifting a veil obscuring an image.

Granting operational forecasters additional tools to increase TC forecasting range and precision provides decision-makers more time and context to determine evacuations, sorties, and base closures. Baked into a commander's decision is a risk analysis on how disruptive and costly an evacuation might be against the alternative. To consider the impact to operations, how does the conceptual model assist the operational forecaster? Is the conceptual model purely diagnostic, or can it contribute to improving forecast quality? The effort in this thesis is to use the MP to extract operationally relevant observations and insight into TC formation dynamics, beyond broad statistical generalizations. Herein lies the exploration of the conceptual model and its predictive potential during the formation of three TCs that originated as AEWs during the 2020 Atlantic hurricane season.

In summary, the MP presents a clean conceptual model from which to observe and analyze the atmospheric conditions and the TC formation process throughout the troposphere. While the MP is clean in concept, generating the images for analysis is more difficult, and finding ways to neatly automate and package the products for forecasters is still a challenging task. Currently, the analyses and forecasts are derived from the NOAA Global Forecast System (GFS) model with a desire to expand to other models.

C. TROPICAL EVENTS EXAMINED

The upcoming discussion examines pre-storm formation of three named TCs through analysis and narrative relying on National Hurricane Center's (NHC) graphics, advisories, and discussions. While no two events are alike, the three cases shared similar geolocation and tracks as tropical disturbances, depressions, and, in one case as a "potential tropical cyclone" (defined p. 10). The following text broadly outlines the 2020 conditions in the Atlantic along with each storm: Isaias, Josephine, and Laura.

1. Conditions in the Atlantic Ocean 2020

The 2020 Atlantic Hurricane Season Outlook issued 21 May 2020 by the National Oceanic and Atmospheric Administration (NOAA) estimated a more active than normal hurricane season. After a record nine named storms by 30 July, NOAA updated the outlook to reflect an extremely active season by 3 August (Bell et al. 2020). In the outlooks'

consideration, a combination of above average SSTs, weaker vertical wind shear, and low mean sea level air pressure would enhance TC formation. The combination of the Atlantic Multi-Decadal Oscillation (AMO), increasing SSTs, a strong and moist West African Monsoon, and the impending transition to La Niña (usually characterized by weak vertical shear over the North Atlantic basin) suggested very favorable TC conditions. In hindsight, the transition to La Niña only strengthened throughout the season.

Along with increasingly favorable conditions for TC formation, the Saharan air layer (SAL) was at its peak between June and into August (Figure 2). The exceptionally dry and warm air coincident with strong winds tends to inhibit TC formation. Perturbations in the African easterly jet (AEJ) developing into African easterly waves (AEW) act to modulate the SAL to the north and the warm moist air to the south in the Atlantic. The AEJ appears be the line of demarcation between the SAL and the Intertropical Convergence Zone (ITCZ). North of this latitudinal stratification, TC formation is inhibited in the North Atlantic by vertical wind shear and dry air from the SAL, while, south of the AEJ, a moist lower troposphere sustains favorable conditions for TC formation associated with the ITCZ.

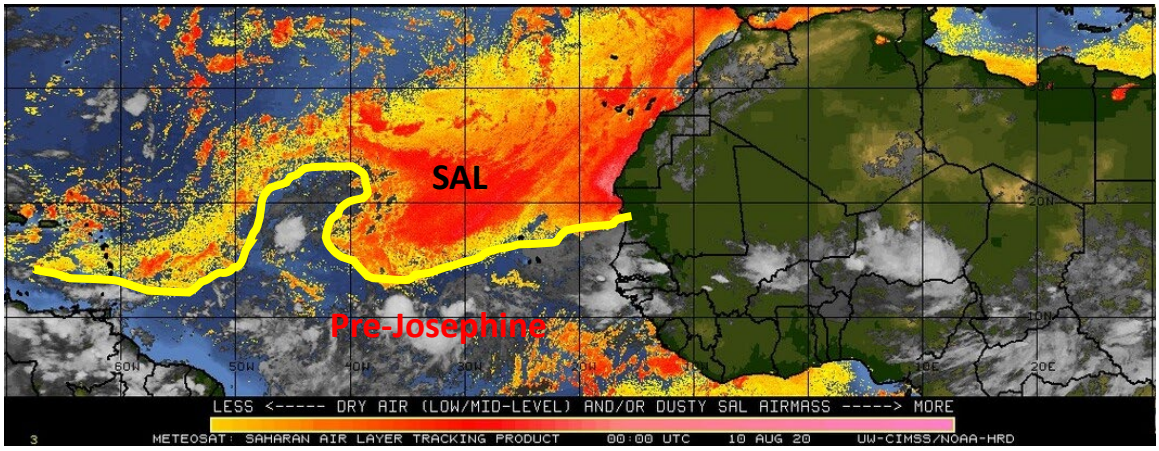

The SAL together with the expanse of dry air is the yellow to red shades. Pre-Josephine labeled below the yellow, which line highlights the boundary between drier air to the north and available moist air to the south in the North Atlantic. An unrelated disturbance is evident well northwest of the pre-Josephine disturbance.

Figure 2. Dry Air/Saharan Air Layer depicted at 00 UTC 10 August 2020.
Source: University of Wisconsin—CIMSS (2020).

The favorable conditions for TC formation and the interaction of a strong SAL provide context for the early hurricane season in the North Atlantic. Additional seasonal context includes the northward shift of the ITCZ bringing moisture and convective formations around 10°N-11°N. The westward propagating AEWs are thought of as the seeds of many TCs, and the existence of convection associated with an AEW, visible by satellite or model parameters, trigger operational forecasters to track the disturbance. Many AEWs are trackable starting in eastern Africa typically close to the 700-hPa level, which corresponds closely to the altitude of the AEJ that has its maximum easterly wind near the 600-hPa level. Both weak and strong waves have the potential to develop into TCs. Ultimately, the disturbance or pouch formation must extend to the lower troposphere, at 850 hPa and 925 hPa, to become a TD.

In all analyses of TC formation from AEWs, a prominent question is how does a 700-hPa AEW extend lower into the troposphere? There are three main pathways to establish the low-level cyclonic circulation. (1) Favorable TC conditions allow for the sustained propagation and deep convection over the ocean to extend a mid-level pouch to the lower levels. This is the standard or idealized process. (2) A lower-level disturbance aligns with a mid-level (700-hPa) AEW and promotes the low-level vertical alignment and vorticity advection within favorable conditions. (3) Low-level disturbances grow and develop vertically in favorable pouch-like conditions.

2. Parallels in TC Formation and Summary of NHC Forecasts

NHC first published a Tropical Weather Outlook (TWO), including a formation probability of <20% of pre-Isaias off the coast of Western Africa, at approximately 12°N on 23 July (NHC 2020b). The propagation remained predominantly westward during pre-genesis and formation prior to reaching the Leeward Islands. Operationally unique was the Potential Tropical Cyclone (PTC) status prior to becoming a named TS, skipping the designation as a TD, a result of sustained winds of TD or TS strength associated with the disorganized disturbance that lacked a well-defined center (Lattos et al. 2021; Brennan 2021). The wave-pouch contended with a strong SAL to the north, yet the adjacent SAL

did not prevent Isaias from forming. See the Appendix Section B for more operational forecast discussion from NHC.

Similarly, observations of pre-Josephine indicated a wave off Western Africa also at approximately 12°N on 8 August. The propagation remained predominantly westward during pre-genesis. The wave-pouch contended with a strong SAL to the north, yet the storm persisted and became a TS prior to dissipating on a northwestward track in the North Atlantic. See the Appendix Section A for more operational forecast discussion from NHC.

Akin to the others, the observations of pre-Laura indicated yet another wave off the coast of Western Africa on 16 August. The propagation remained predominantly westward during pre-genesis. The wave-pouch contended with the SAL, but arguably to a lesser degree than the two preceding storms. Storm formation occurred near the Leeward Islands and continued into the Caribbean and strengthening in the Gulf of Mexico. See Appendix Section C for more operational forecast discussion by NHC.

Although no storm is the same, identifying similarities in track and formation location assists in comparing pouch scale and mesoscale impacts to storm formation. The tracks in Figure 3, from International Best Track Archive for Climate Stewardship (IBTrACS) and NHC, provide insight into the variation among the three candidate storms in addition to variation between tracking methods. At first glance, the IBTrACS paths appear smoothed in comparison to the NHC-derived tracks. This smoothing in IBTrACS tracks reflects a more complete representation of a TC track based on all available data and information compiled following the conclusion of the storm or season. The NHC tracks are the working best track and represent the TC forecast or outlook as a snapshot for a given day and time. Both tracks are helpful in this work in developing the storm narrative. IBTrACS provides a strong consensus from multiple sources of data and information after the event that may not be immediately available to a forecaster issuing guidance in real time for a developing TC. The variability between the two track comparison images in Figure 3 highlights the distinction of post event consensus and real-time forecasting.

The area and time of interest highlighted by orange rectangles (Figure 3) comprises the critical timeline for the analysis of each storm. While these times arguably represent an

arbitrary decision point on selecting the three storms, the tracks cluster closely and significant development occurred in the area for each storm. With regard to this discussion, the operational forecast will contain much of the mesoscale and synoptic influences, as well as the pouch-scale observations. Characteristics of wave-pouches within the context of the MP help to identify precursors to formation of pouches with isolated areas of deep cumulus convection. The subsequent analysis then attempts to tease out critical elements that drive genesis, generally prior to TC formation for cases in which TC formation is inevitable.

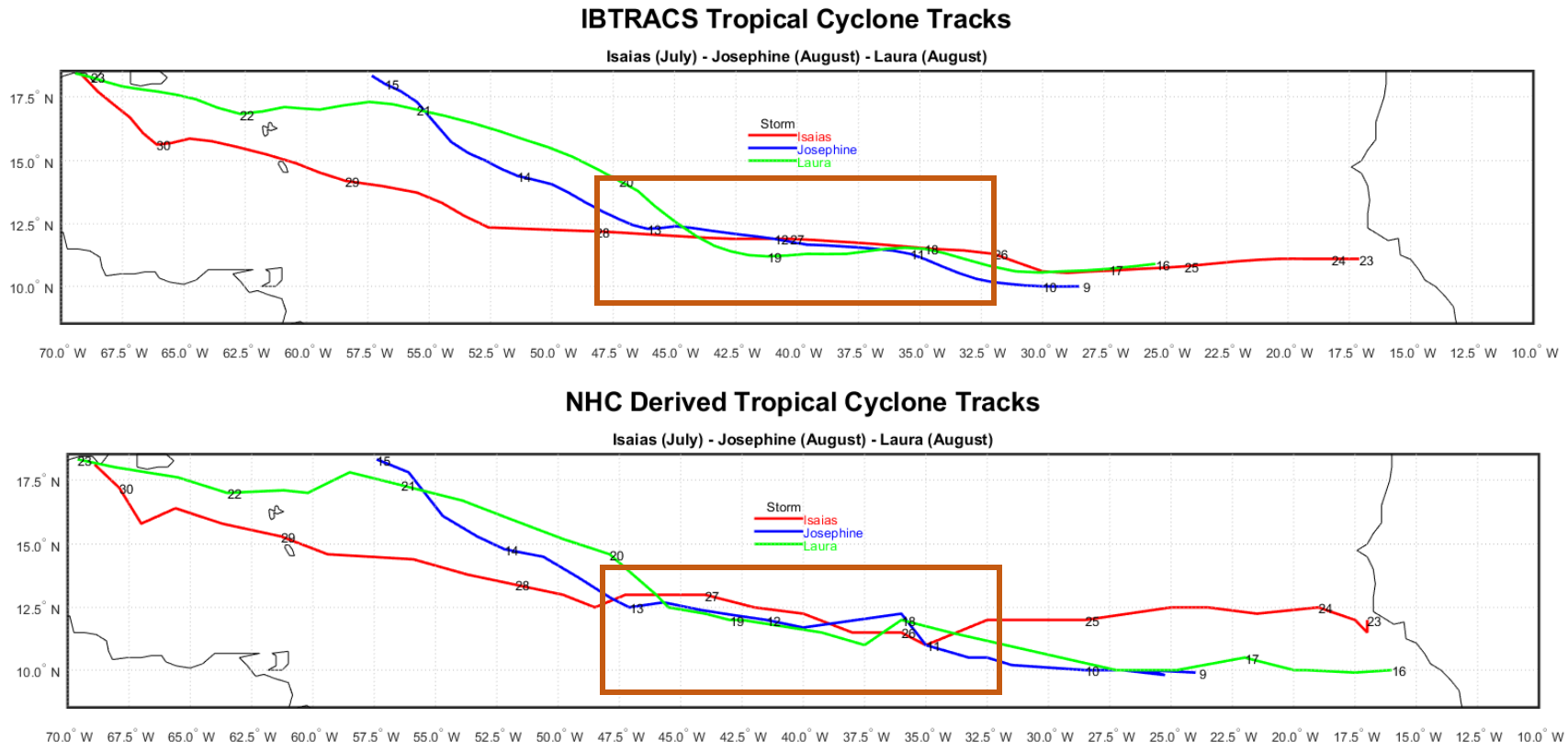

Figure 3. Tropical Cyclone tracks from IBTRACS (top) and NHC derived (bottom). Adapted from Knapp et al. (2018) (top) and NHC (2020b) (bottom).

THIS PAGE INTENTIONALLY LEFT BLANK

II. METHODOLOGY

A. APPLYING THE MARSUPIAL POUCH PARADIGM

The Montgomery Research Group at the Naval Postgraduate School produces several products, among them analysis and forecasting images in the comoving reference frame from Global Forecasting System (GFS) model outputs. The principal method assessed in this thesis generates images in the Earth-relative and comoving framework to detect the structural formation of the wave-pouch for three pre-depression storms. The pouch structure of three 2020 North Atlantic storms—Josephine, Isaias, and Laura—is examined using .25°-spatial resolution GFS analyses and every six hours.

The process begins with an initial point, notionally determined by the first estimated position of the developing storm mentioned in NHC's TWO bulletin. Additionally, NHC provides estimated system velocity (wave phase speed) supplying context to generate the comoving fields. Visual inspection of moisture and meridional wind in Hovmöller plots of 120-hour forecasts provides an additional estimate of the wave-pouch zonal phase speed. An estimate of zonal and meridional phase speed provides the adjustment to produce GFS analyses of comoving streamlines. The streamline plots overlaid with OW at 700 hPa or 850 hPa cue the user on the location of the pouch. This process repeats successively earlier in six-hour time increments (00, 06, 12, and 18 UTC) backward until the presence of nearly closed streamlines is not found at any level, cessation of the OW or relative vorticity disturbance, or the track and position of the disturbance appears unrealistic. Careful and repeated examination of these earlier analyses allows for the assignment of a unique, accurate zonal phase speed at each of these earlier analysis times. Meanwhile, estimated pouch positions often depict meridional motion in addition to zonal motion. The output produces several images each depicting a different variable: RH, OW, relative vorticity, potential vorticity, horizontal wind direction and speed, and vertical wind shear. Each variable is plotted at 925 hPa, 850 hPa, 700 hPa, and 500 hPa independently and stacked in one eight panel image to provide insight to the vertical structure.

The two-step visual determination of phase speed and pouch location lends itself to iteration: (1) refining the position and phase speed, and (2) working backward (or forward) in six-hour increments to produce the same catalogue of images for different analyses. Working this way, given the tools, provides a relatively accurate process to visualize pouch structures and development. This diagnostic process embraces the scientific method through rigorous evaluation of the images, but possesses artistic element also, involving perception and judgment.

The balance of science and art through iteration is clearest when preserving positional and phase speed continuity between analysis catalogues. Easily trackable are disturbances that propagate due west; however, as a disturbance shifts north or south, this introduces some difficulty in assessing the correct phase speed iteratively in six-hour increments. The first iterative step of refining position and phase speed become recursively iterative, where adjusting the phase speed might lead to an observable change in trough and critical latitude position. An adjustment in position then changes the phase speed. The art of the process is confirmatory when the recursive nature akin to that of Newton's Method, producing, through each iteration, a solution closer to the real position and phase speed. Considering positional and phase speed continuity validates the analyses between time steps, ensuring a latitudinal or longitudinal jump did not erroneously manifest between evaluations, along with ensuring speed and direction remain realistic with a change in position.

During the iterative process there are key structures that help identify a pouch (Figure 4, left). The intersection of the trough axis and critical latitude, considered the "sweet spot," is central to positioning the pouch (Dunkerton et al. 2009; Wang et al. 2010). Additionally, in the comoving plot, nearly closed and concentric streamlines should be evident at the tropospheric level evaluated (Figure 4, right). Within the nearly closed streamlines, the OW parameter should be high in value as a representation of parcel spin relative to the sweet spot, the location of which helps reinforce the structure at the evaluated level. In a well-developed pre-storm, the sweet spot (trough axis crossing the critical latitude), closed and concentric streamlines, and high OW value will coincide at multiple, if not all, levels. If the sweet spot, closed and concentric streamlines, and high OW do not

coincide, there is either a problem from user input or there is no discernable structure to track. In cases when pouches are difficult to identify, evaluating multiple levels at a given analysis, as well as examining additional analyses times may provide context for the prevailing atmospheric conditions resulting in no trackable pouch or a resumption of pouch tracking.

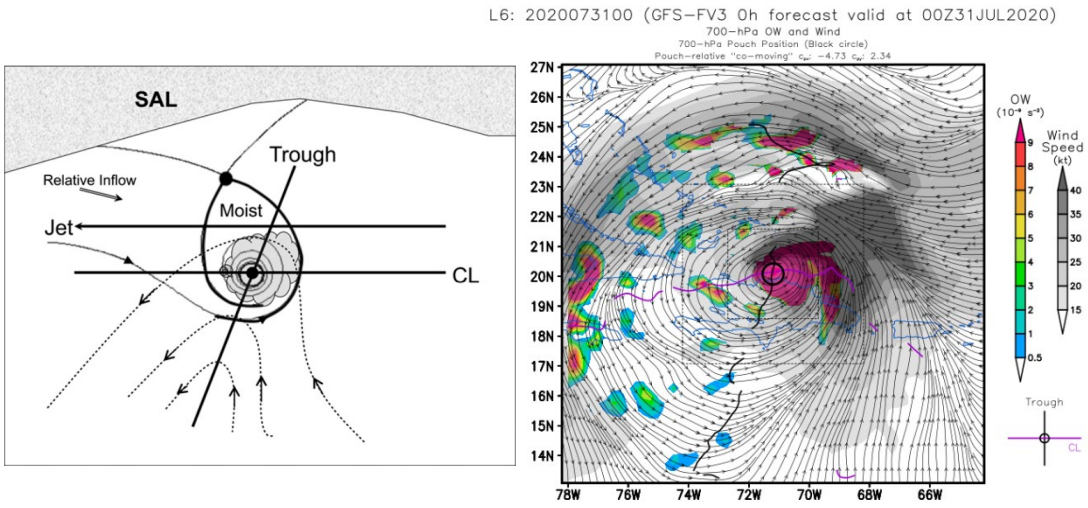

The left image characterizes the structure of a developing pouch from a wave-trough typically moving westward from the African coast in the North Atlantic. The right image depicts the GFS analysis of OW (color shading) and comoving streamlines and isotachs (grey shading) at 700 hPa for Tropical Storm Isaias at 00 UTC 31 July 2020. Notable characteristics include the intersection of the trough axis (black solid line) and the critical latitude (pink solid line) marking the "sweet spot." The concentric and nearly closed streamlines surrounding the intersection correspond to a concentrated area of high OW values.

Figure 4. Depiction of an idealized pouch at 700 hPa. Source: Wang et al. (2010) (left) and Rutherford (2020) (right).

The levels considered in the analysis include 200 hPa and 500 hPa. However, analysis levels for consideration were primarily at 700 hPa, 850 hPa, or 925 hPa levels. The geospatial context of land or sea along with RH, relative and potential vorticity, and vertical shear coincident with the pouch provide additional cues for pouch existence and robustness. Two forms of vertical wind shear help in the evaluation of a pouch: deep-layer vertical wind shear, the difference between wind velocity at 200 hPa and 850 hPa, and

pouch-layer vertical wind shear, the difference between wind velocity at 500 hPa and 850 hPa. In some cases, deep-layer shear obfuscates the encouraging pouch conditions at lower levels where the pouch shear can provide insight in comparison.

From the initial NHC assessment, working backward in six-hour increments, the goal is to track the pouch structure to a realistic place of origin. While post-analysis has the benefit of hindsight, working backwards in this method allows observation and analysis of what is useful to track and for how long. Keeping perspective and narrowing scope to determine pre-depression structures leading to TC formation limits the duration and geographic extent of the analysis.

B. VALIDATION AND UNCERTAINTY DISCUSSION

To validate, reinforce, and observe the connection between the MP and the real world, selected satellite images were ingested into a Geographic Information System (GIS) and then compared with MP figures in the results and discussion. The Cloud and Moisture Imagery from GOES-16 channel 13 clean longwave infrared (IR) provides distinct cloud detection and heights and provides insight to TS intensity (Schmit et al. 2017). The desired output was a World Geodetic System-1984 (WGS84) georeferenced translation of satellite imagery requested from NOAAs Comprehensive Large Array-Data Stewardship System (CLASS) using the Geospatial Data Abstraction Library (GDAL/OGR contributors 2021). Once in the WGS84 geotiff format, the series of images were overlaid in Quantum GIS with pouch determined and NHC identified positions. The focus herein consisted of increments every six hours in imagery and positions to corroborate locations and dynamics in the GFS pouch field plots with the clouds and convection in the satellite imagery.

As a preamble to this coarse analysis, trackable pouches were identified prior to the first NHC TWO for each storm, though with a high degree of uncertainty. The NHC position for pre-depression disturbances is marked by a colored "x," which provided for the approximate location of the disturbance and the color indicating probability of formation in the next 48 and 120 hours. The approximated positions were then transcribed for use in a GIS application incurring additional uncertainty. As an ideal wave-pouch structure propagates westward and develops, the amount of uncertainty diminishes as

closed streamlines become more apparent and reliable in the comoving reference frame. Comparably, the uncertainty for NHC positions reduces during this time as well. Closed streamlines appear in the Earth-relative reference frame, increasing fidelity for TC position. In this analysis, it is the examination of the pre-cyclone formation period between pouch or NHC identification of an area of concern to the clear formation of a TD or TS. Additionally, the use of model analysis fields assumes that those fields represent the real atmosphere, but they do not, which contributes to additional uncertainty or modeling artifacts when analyzing pouches and their positions across analyses. Similarly, uncertainty exists in the forecasts, advisories, and statements from the NHC often used as a base with which to compare results. Positional uncertainty exists when applying coordinates to a GIS, particularly when geo-referencing multiple sources that are inherently uncertain.

THIS PAGE INTENTIONALLY LEFT BLANK

III. DATA AND RESULTS

Invariably, analyses and forecasts of TCs generally focus on track and intensity. The flow of this discussion will start with the MP pouch-determined track plotted alongside the NHC operational "working best track" positions. The use of the "working best track" provides a direct comparison between methods and tools used for real-time operational forecasts. The discussion then transitions to specific times and days with corresponding satellite imagery and 700-hPa level tracked pouch eight-panel plots in comoving and Earth-relative coordinates as a way to examine the tropical disturbances on a pouch scale. Additional images and discussion contribute to the narrative revealed by the pouch analyses.

A. PRE-JOSEPHINE

Consider pre-Josephine as the control case. Pre-Josephine formation followed the expected or typified AEW to TC formation sequence described in Dunkerton et al. (2009), Montgomery et al. (2010b), and Wang and Hanks (2013). While NHC's TWO identified a disturbance on 9 August, post-storm MP analysis identified a 700-hPa pouch associated with an AEW near the coast of West Africa as early as 06 UTC 7 August (Figure 5).

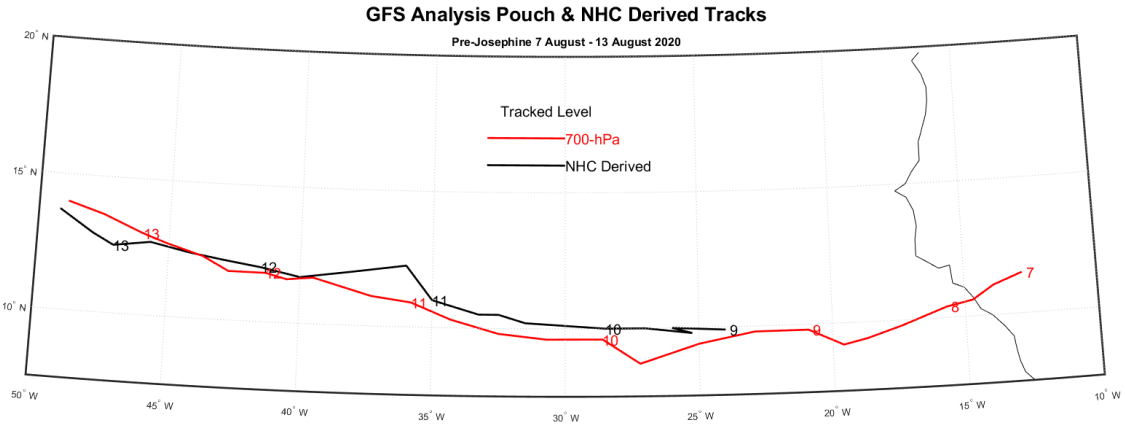

Days marked at 00 UTC analyses, except 06 UTC on 7 August.

Figure 5 GFS analysis pouch and NHC-derived tracks for pre-Josephine. Adapted from NHC (2020b).

The propagation path in Figure 5 shows westward propagation fluctuating in latitude from 12°N on an initial southwest path, then nearly westward at 10°N before taking a northwestward track toward 15°N. The MP track ends on 13 August, when NHC named TS Josephine. In this typified TC narrative, pre-Josephine battled vertical shear inimical to cyclogenesis and dry air coincident with the SAL north of the propagation path. Throughout the entire period in the discussion of pre-Josephine that follows, the 700-hPa level tracked pouch structure remained consistent in GFS analyses fields. The large basin scale depictions of relative vorticity and OW in Figure 6 (left and right, respectively) illustrate the synoptic scale subtropical ridges between 20°N and 30°N and easterly tropical wind flow between 10°N and 15°N. The streamlines are Earth-relative with the pouch marked by a grey circle in both panels. A tropical ridge centered near 9°N, 25°W appears to keep high relative vorticity bands northward and divide areas of high OW value areas (Figure 6, left and right, respectively).

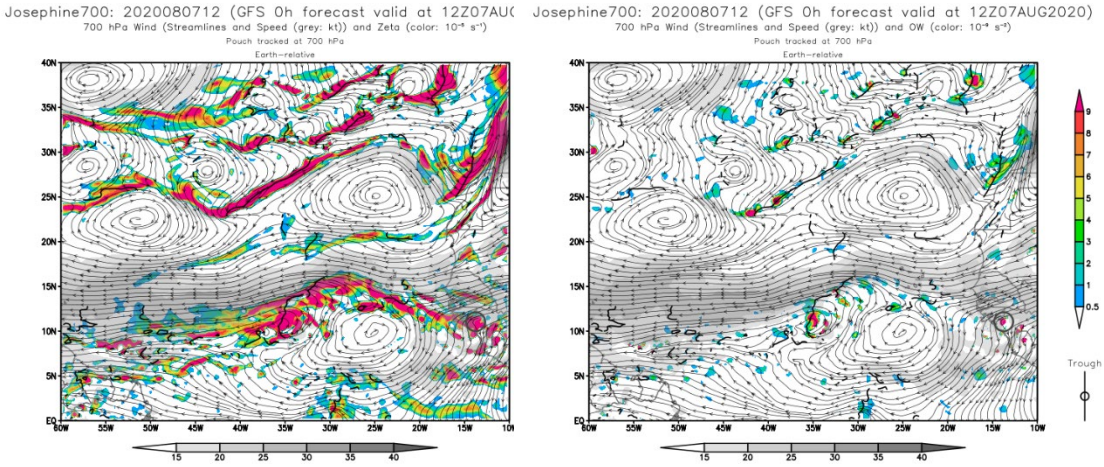

The grey circle indicates the 700-hPa level tracked pouch near the Africa coast in both images. The larger basin scale imagery depicts two prominent subtropical ridges and a tropical ridge that buoy wave-troughs in the westward flow between 10°N and 15°N in the North Atlantic. Additionally, comparing relative vorticity (left) to OW (right) helps identify groupings of high vortical centers.

Figure 6. GFS 700-hPa level analyses of relative vorticity (left) and OW (right) overlaid with Earth-relative streamlines at 12 UTC 7 August 2020.

On 7 August the detection of a pouch among a broad area of relative vorticity (Figure 7, left) was clearly indicated by the OW and "sweet spot" (Figure 7, right). The NHC and MP positions of pre-Josephine remained relatively close (within a quarter degree) and embedded in an area of disorganized convection as depicted by GOES-16 IR imagery at 12 UTC 9 August 2020 (Figure 8 top, left column). The GFS 700-hPa analysis shows high OW values within the closed streamlines in the comoving reference frame based on a phase speed of 8 m/s westward and 3 m/s southward (Figure 8 top, center column). The NHC and MP positions separated as convection waned by 18 UTC 9 August (Figure 8 bottom, left column). Areas of high OW values within closed streamlines appear larger in at 850 hPa and 925 hPa in the GFS analyses plot compared to six hours prior (Figure 8 bottom, center column).

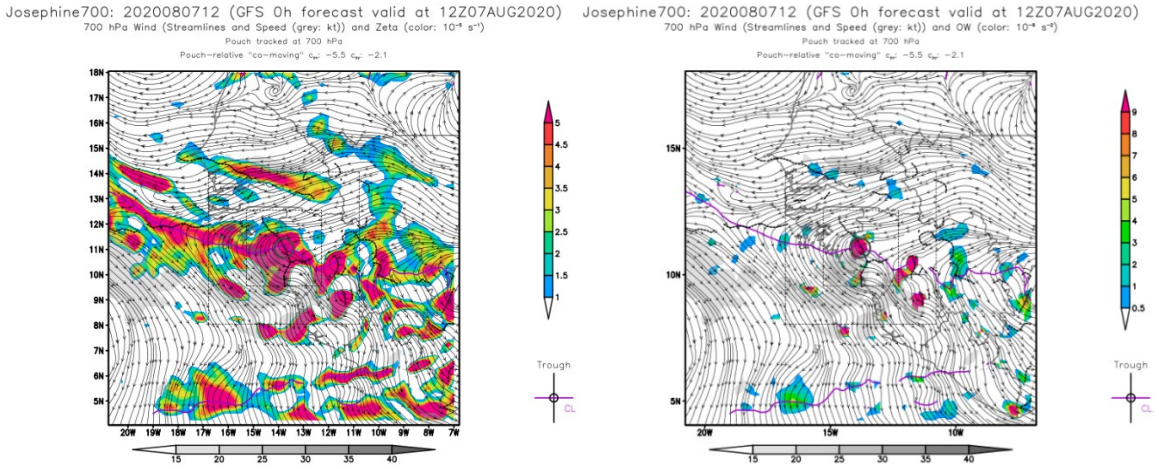

Comoving streamlines with a westward propagation velocity of 5.5m/s and southward propagation velocity of 2.1m/s overlaid on relative vorticity (left) and OW (right) at 12 UTC 7 August 2020. A grey circle highlights the 700-hPa trough-critical latitude intersection that coincides with high relative vorticity (left) and localized area of high OW (right).

Figure 7. GFS analyses of 700-hPa comoving streamlines with relative vorticity and OW, respectively.

A resurgence of localized convection appeared to the northwest of the NHC and pouch positions at 00 UTC 10 August 2020 (Figure 9 top, left column). The GFS OW and streamline analysis illustrated the same extent of closed streamlines with a vertically aligned pouch in the comoving reference frame at each level (Figure 9, center column) as

well as the Earth-relative reference frame in all but the 500-hPa level (Figure 9, right column). By 06 UTC 10 August, an outer band of convection stretching northeastward from the main convective element developed.

Similar to the latter half of 09 August, convection weakened later on 10 August (Figure 10 left column). Despite weakened convection, GFS comoving analyses show pre-Josephine as a well-defined, vertically aligned pouch throughout the 500 to 925hPa layer at 12 and 18 UTC 10 August (Figure 10 center column). Pre-Josephine appears with closed circulation in the Earth-relative reference frame at all levels except 500-hPa (Figure 10, right column).

Similar to the start of 10 August, convection returned at 00 UTC and increased at 06 UTC 11 August 2020 (Figure 11, left column). While two convective clusters were present at 06 UTC 10 August (Figure 9, left column), on 11 August the western cluster had dissipated while the eastern cluster remained and was close to the center of the pouch (Figure 11, left column). From the pouch plots, there is no pouch structure able to prevent environmental dry air from inhibiting convective activity in the area of convection west of pre-Josephine, around 40°W. However, the well-defined pouch now associated with the area of convection at 32°W persists.

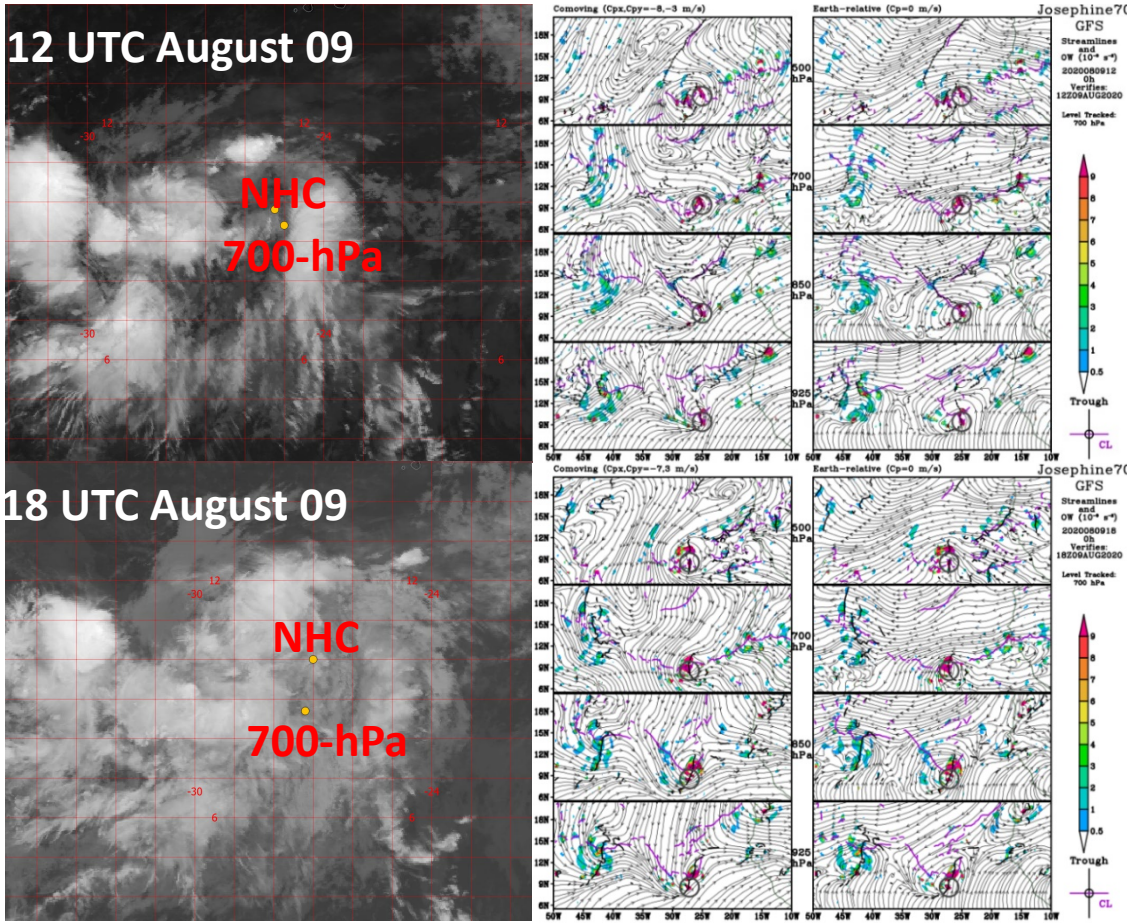

GOES-16 Channel 13 IR (left column) and GFS analyses of OW values with comoving (center column) and Earth-relative (right column) streamlines at four levels: 500 hPa (top), through 700 hPa, 850 hPa, and 925 hPa (bottom). Approximated NHC and MP-derived 700-hPa pouch locations denoted on GOES-16 imagery with yellow dots. Same 700-hPa pouch location denoted by a grey circle on all GFS plots, regardless of underlying level plotted.

Figure 8. Pre-Josephine IR imagery alongside comoving and Earth-relative streamline plots overlaid on OW at 12 and 18 UTC 09 August 2020.

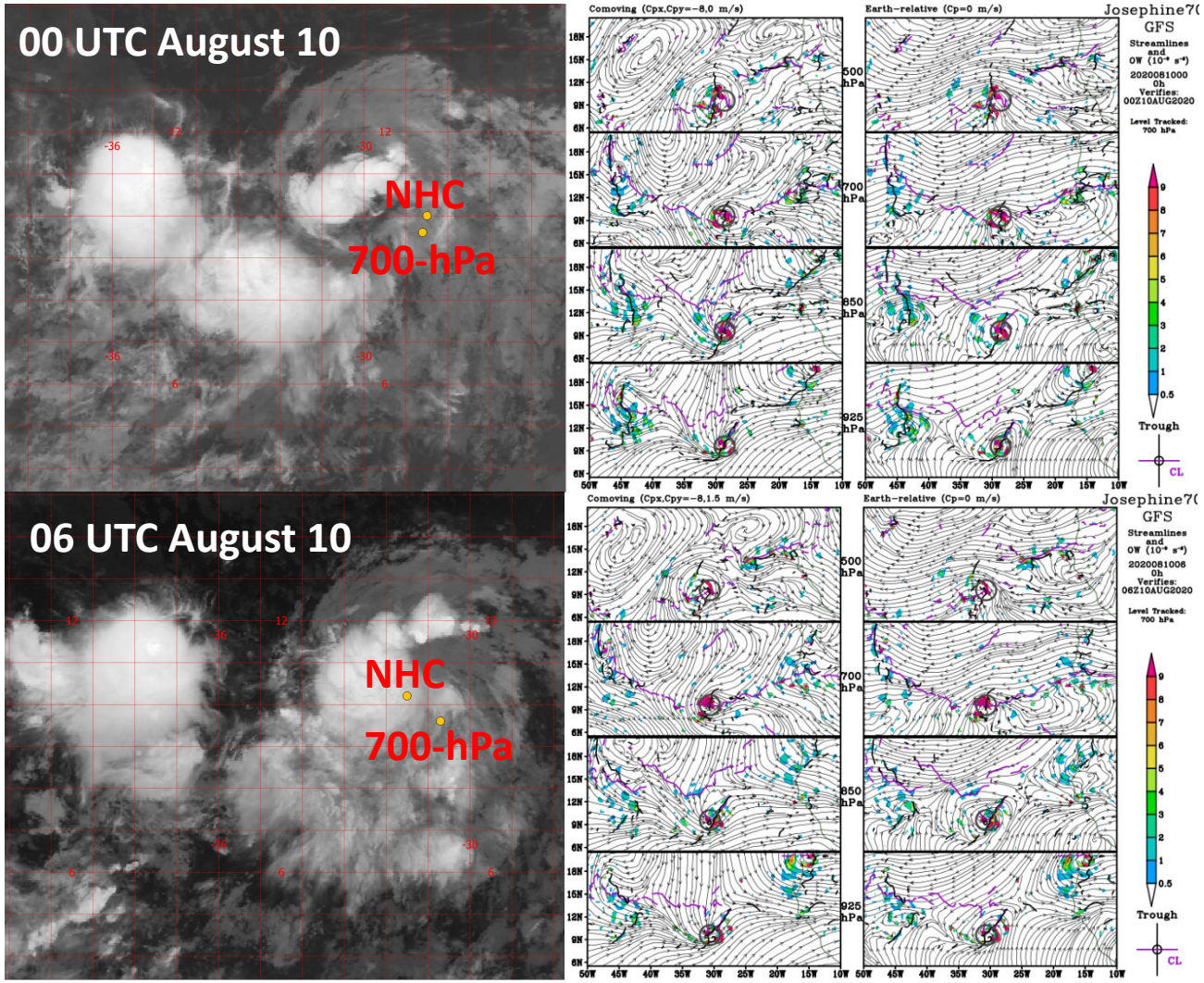

Figure 9. Same as Figure 8, except at 00 and 06 UTC 10 August 2020.

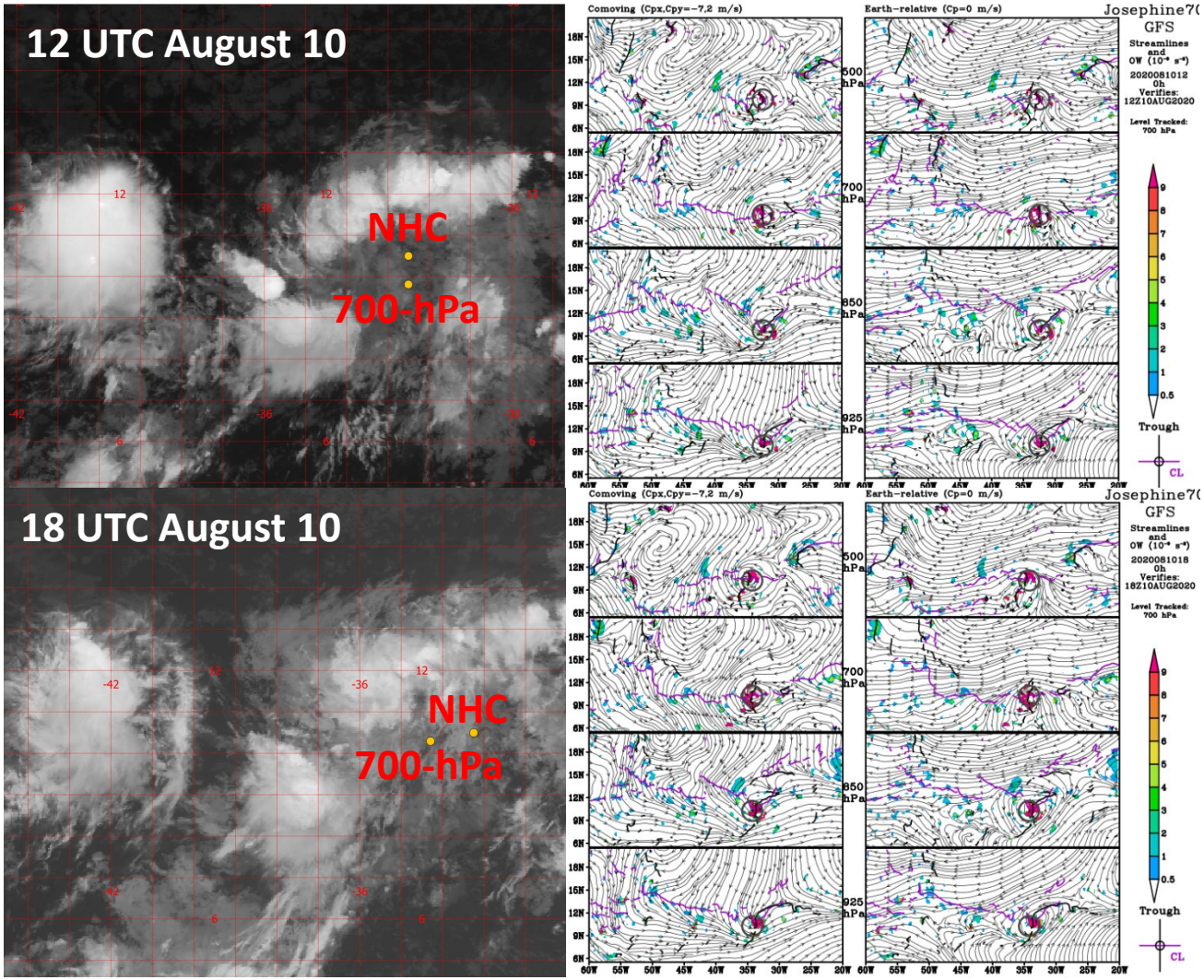

Figure 10. Same as Figure 8, except at 12 and 18 UTC 10 August 2020.

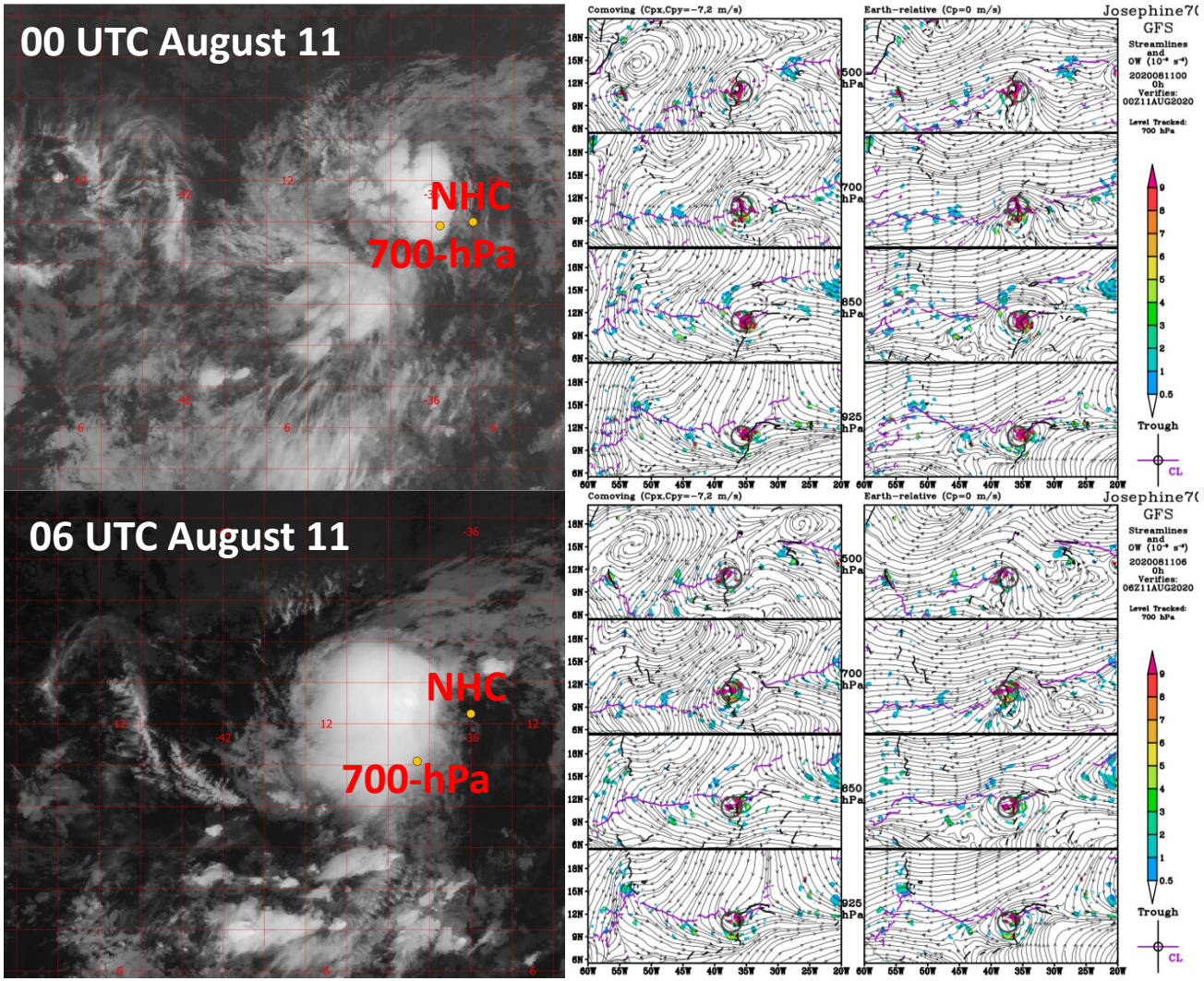

Figure 11. Same as Figure 8, except at 00 and 06 UTC 11 August 2020.

As an AEW originating trough, a pouch was present at 700 hPa for the duration of the formation process from 8 to 11 August. At 12 UTC 9 August the pouch extended down to 850 hPa and 925 hPa, and coincided with some areas of convection near the pouch center. Pouch-layer vertical shear (Figure 12) and coincident dry SAL air (Figure 2) temporarily inhibited development of pre-Josephine evidenced by weakening convection from 9–10 August (Figure 8 through Figure 10, left column) and reduced RH in GFS analyses (Figure 13 and Figure 14).

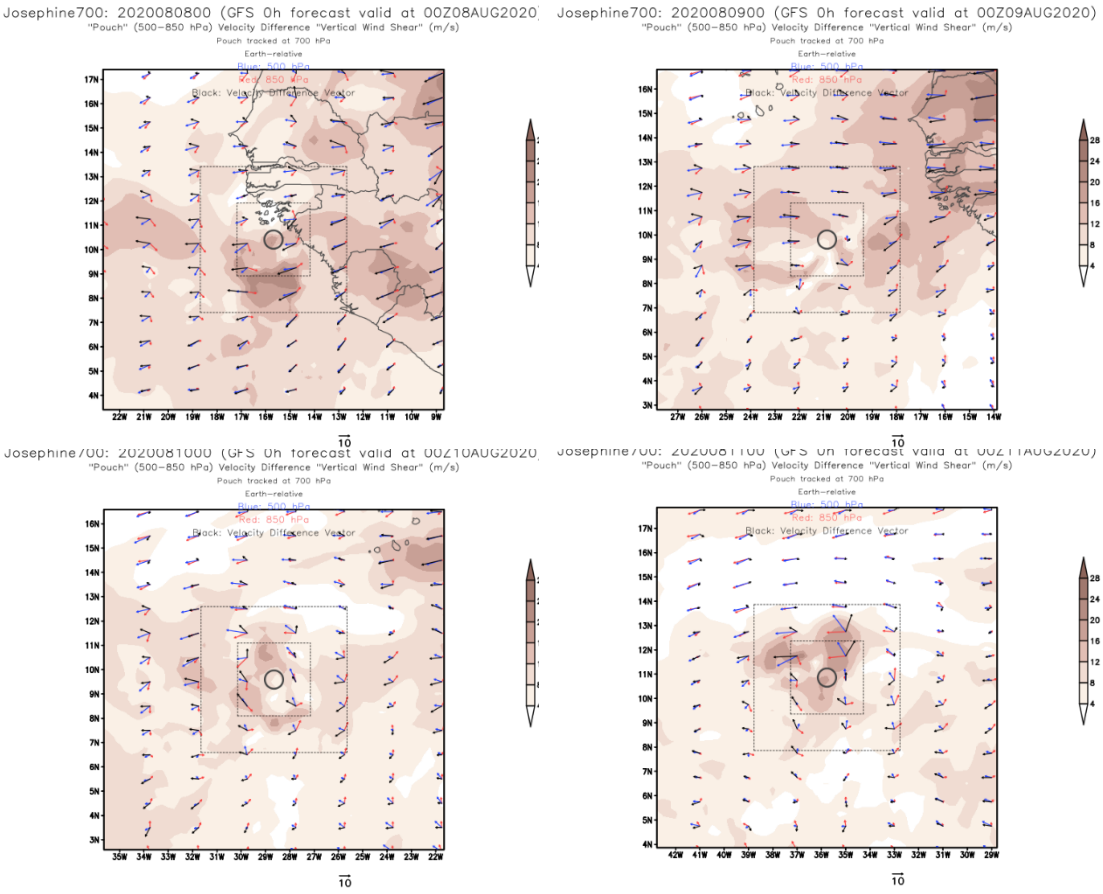

Pouch-layer shear (500-850 hPa) starting from left to right, top to bottom. The tropical wave propagates westward away from the coast of Africa. The blue arrow represents the wind vector at 500 hPa; the red arrow represents the wind vector at 850 hPa; and the black arrow is the vector difference between the 500 hPa and 850 hPa levels.

Figure 12. Pouch-layer vertical shear 00 UTC 8, 9, 10, and 11 August 2020.

The pouch-layer vertical wind shear and dry air reduced moisture availability to the north and east of the pouch and impinged the pouch at 700 hPa and 850 hPa throughout 10 August. By 00 UTC 11 August, moisture westward of the center remained, see Figure 13 and Figure 14. As pre-Josephine propagated westward the easterly pouch-level vertical shear decreased. By 00 UTC 11 August the pouch remained intact and RH throughout the column increased (Figure 15) providing an opportunity for another burst of convection associated with the pouch.

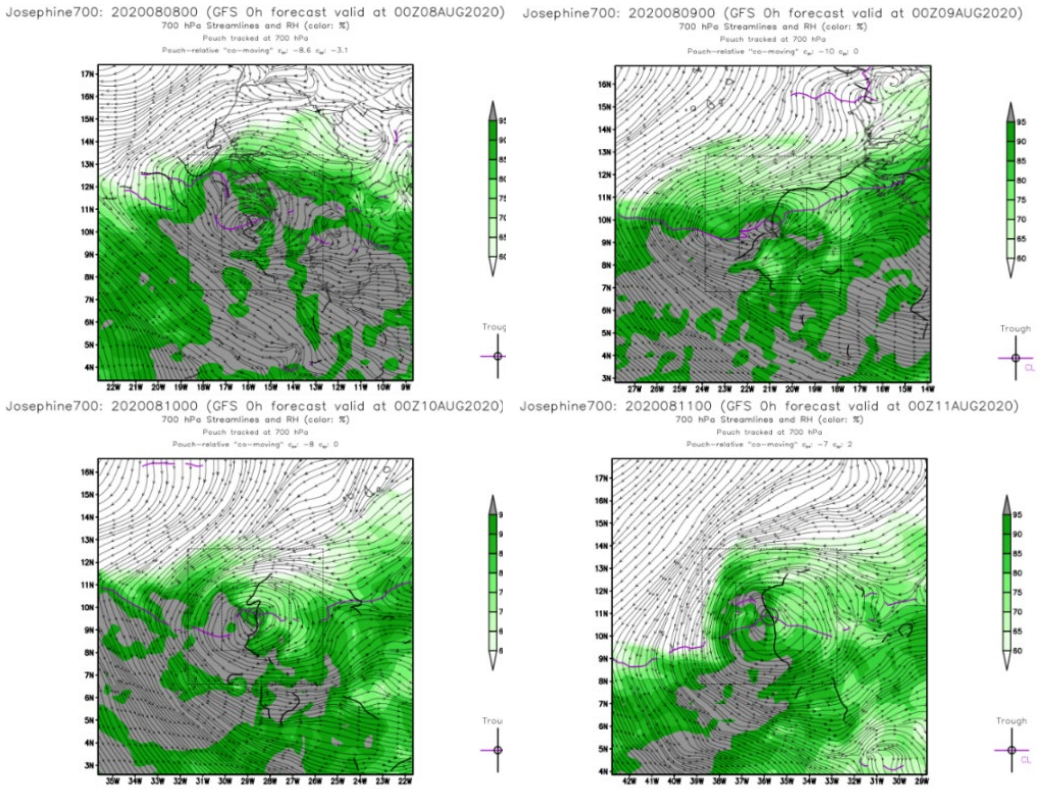

Figure 13. GFS analyses of RH at 700 hPa at 00 UTC 8, 9, 10, and 11 August with comoving streamlines.

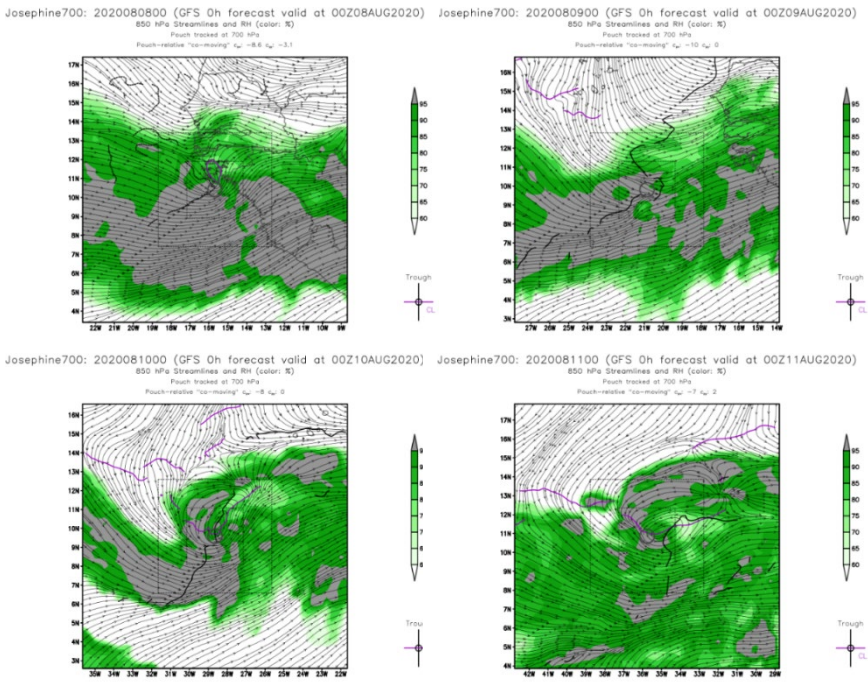

Figure 14. Same as Figure 13, except RH at 850 hPa.

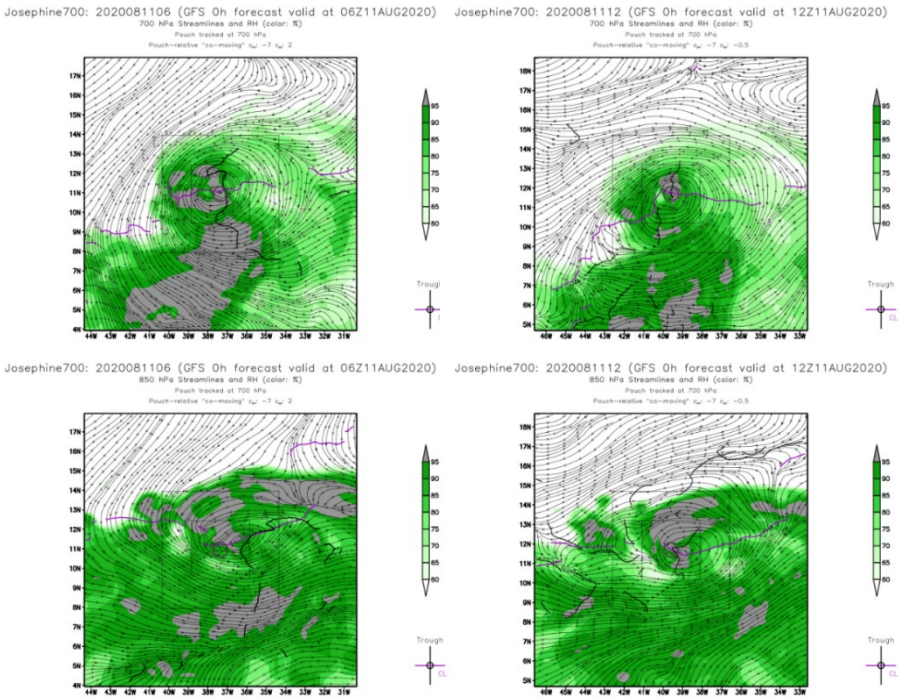

GFS analyses of RH overlaid on comoving streamlines at 750 hPa level (top row) and is 850 hPa level (bottom row).

Figure 15. GFS analyses of RH at 06 and 12 UTC 11 August 2020.

The development, pause, and redevelopment of Josephine from 9 through 11 August provides insight into how mesoscale vertical shear affects the pouch and formation similar to that of Typhoon Nuri (Montgomery et al. 2010a). While the closed streamline structure remained intact at the 700 and 850-hPa levels coincident with concentrated high OW values at each level, the available moisture and the convection from the IR imagery fluctuated (Figure 8 to Figure 11, left column). As the pouch-layer vertical shear weakened on 11 August, the already deep and vertically aligned pouch was able to remoisten the column and convection returned. Unsurprisingly, the effect of pouch-layer vertical shear is detrimental to the development of TCs; however, the formation of Josephine highlighted the modulating nature of moderate pouch-layer vertical shear on the sustained deep convection in a well-defined and deep pouch structure.

Dry air from the SAL coincident with the vertical shear may have limited early development of Josephine. However, the pre-Josphine pouch extended down to 850 hPa in a band of moisture and areas of convection by 18 UTC 9 August (Figure 8 bottom, left). Nearing the boundary between the ITCZ and SAL (Figure 2), pre-Josephine benefitted from the band of moisture and convection to the west and south while battling the pouch-layer vertical wind shear and dry air impingement from the north and northeast. The Josephine 700-hPa wave is consistent with previous research by Dunkerton et al. (2009) and Wang and Hankes' (2013) typified formation path.

In summary, vertically aligned closed streamlines at 925 hPa and 850 hPa preceded relatively strong convective activity by six to twelve hours. Available low-level moisture may accelerate column moistening within the closed streamlines. The fluctuating vertical shear coincident with dry air inhibited pouch associated convection. As the vertical shear weakened with time and the available moisture returned with a pouch structure still intact that was able to remoisten the column within six to twelve hours producing another burst of convection. The resurgence of convection in the low vertical shear environment allowed for pouch development into TD-11. As TD-11, the idealized wave-pouch was evident with the trough axis crossing the critical latitude at a concentrated area of high OW values within closed streamlines and collocated with sustained deep convection (Figure 16). Josephine strengthened to TS status on 13 August before taking a northwestward track yet again into

vertical shear and dry air. This delicate balance of pouch structure and available moisture with the adverse impact of vertical wind shear and dry air on genesis remains the bane of the TC forecaster. The northward movement into a drier and stronger vertical shear environment ultimately led to the evanescence of Josephine on 16 August.

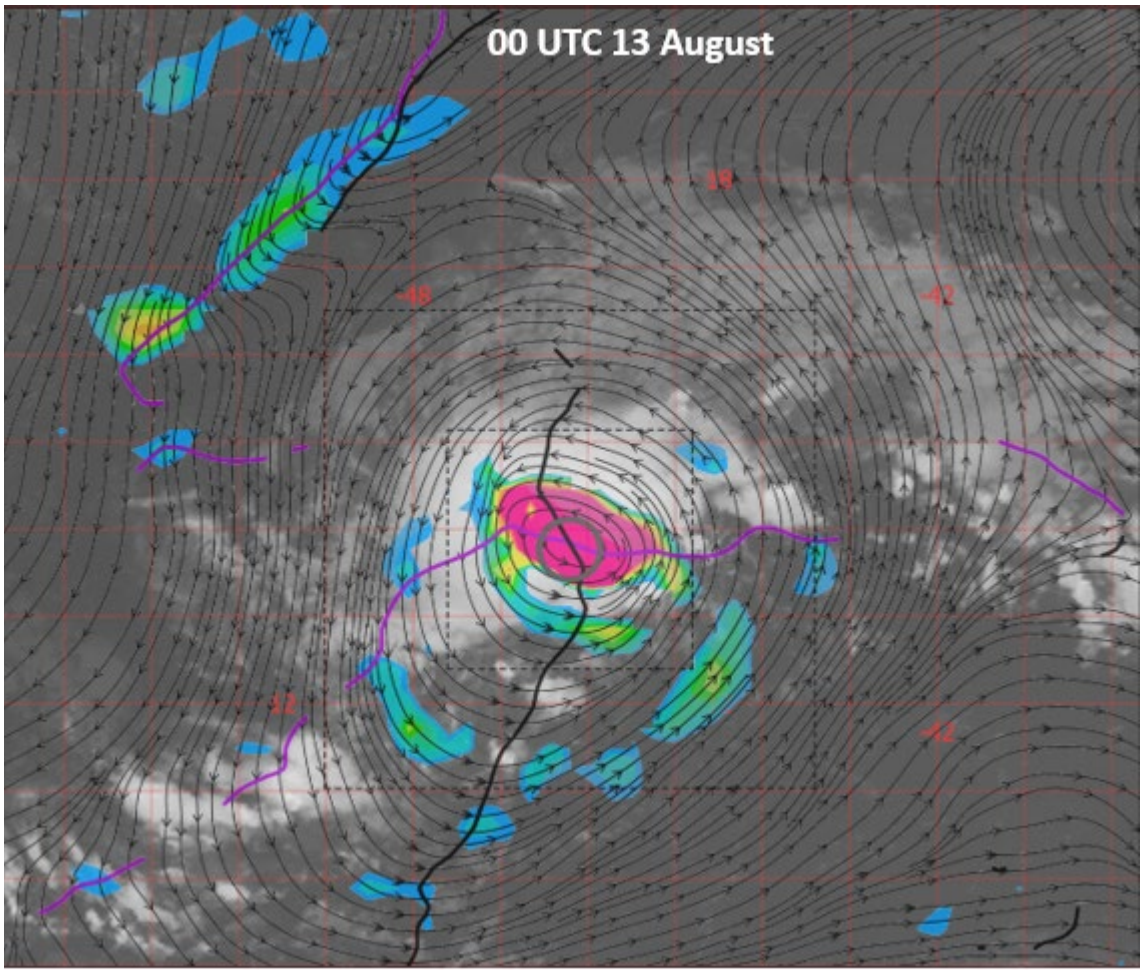

GOES-16 Channel 13 IR imagery overlaid with 700-hPa OW and comoving closed streamlines at 00 UTC 13 August 2020. The trough axis (thick black line) crosses the critical latitude (purple line) inside the closed streamlines. Also, notice the concentrated area of high OW values amongst the deep convection of pre-Josephine as a TD, 12 hours prior to designation as TS Josephine.

Figure 16. Pre-Josephine IR imagery overlaid with OW and comoving streamlines.

B. PRE-ISAIAS

Pre-Isaias propagated along the 12°N typified track at 700 hPa (Figure 17). Unlike the vertically aligned case of pre-Josephine, an independent circulation of high relative vorticity at 850 hPa from the north complicated the formation of Isaias. The 700-hPa and 850-hPa tracks, shown in red and blue, respectively, began in two different locations with distinct compositions. The 700-hPa pouch tracked westward along 12°N within a well-moistened band of air. The 850-hPa pouch at 18°N that tracked southwestward was particularly dry coincident with the SAL. From the indicated tracks, both pouches eventually met and interacted.

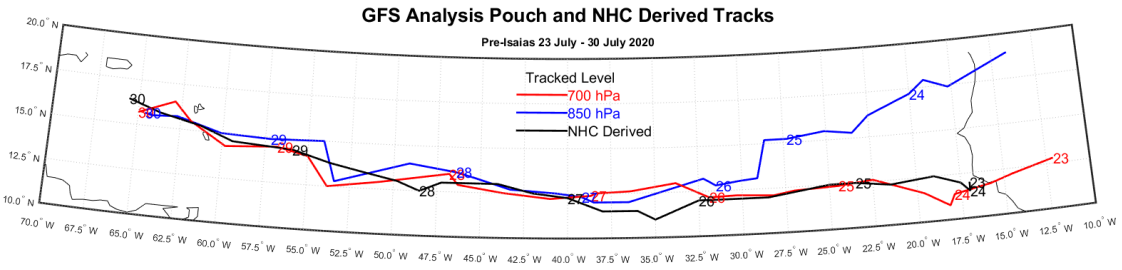

Days marked at 00 UTC, except for the initial 700-hPa at 06 UTC and NHC at 21 UTC.

Figure 17. GFS analysis MP and NHC-derived tracks for pre-Isaias. Adapted from NHC (2020b).

Early on 23 July, pouch analyses revealed a relatively weak 700-hPa trough axis propagating westward over west Africa with adequate relative vorticity and RH. Several isolated OW maxima were depicted by GFS with no dominant feature. The GFS analyses plots in Figure 18 track two dominant features coming off the west African coast on 24 (top) and 25 (bottom) July. The grey circle represents the 700-hPa tracked pouch originally identified and closely corresponds to NHC's initial position and convective activity moving west over the North Atlantic. The color shading nearer 18°N, about six degrees north of the grey circle, represents the 850-hPa pouch. By 25 July (Figure 18, bottom) the two pouches appear to be on a collision course.

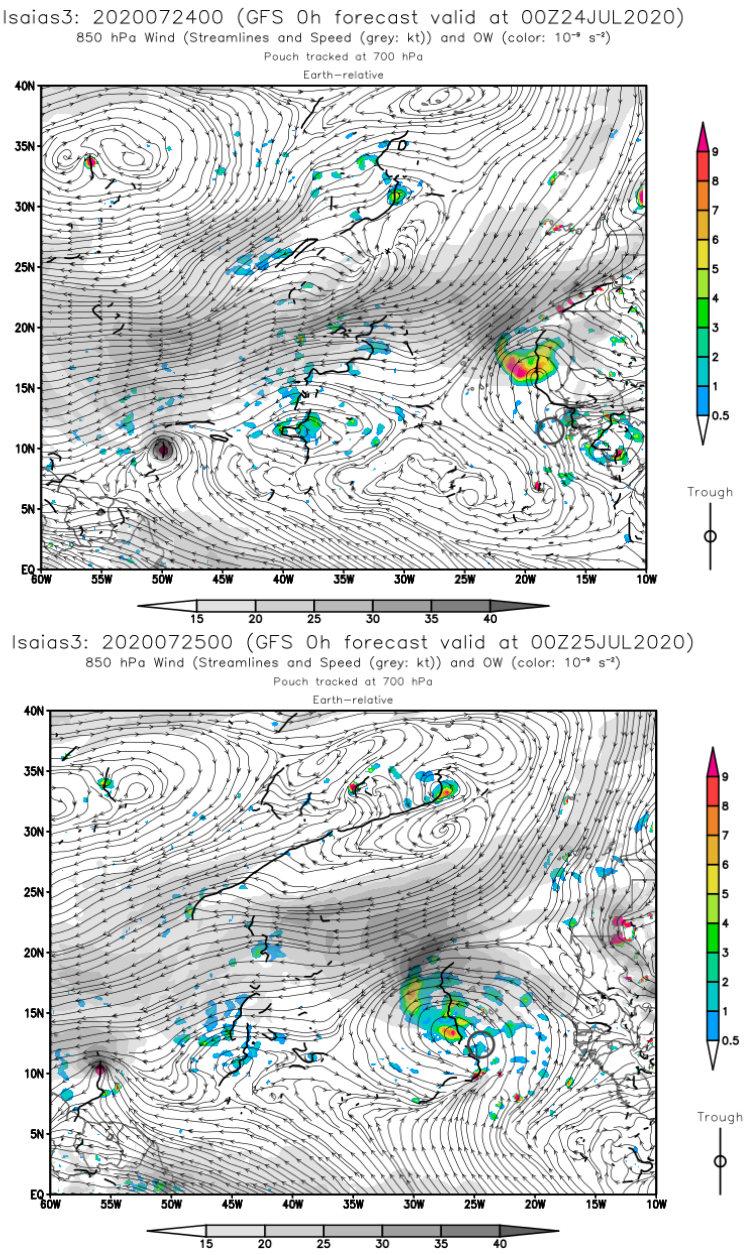

The progression from 00 UTC 24 July (top) to 00 UTC 25 July (bottom) shows an area of high OW at 850 hPa propagating southwestward (color shading) closing in on the westward propagating 700-hPa pouch (grey circle). By 25 July these two pouches begin to interact.

Figure 18. GFS analyses of 850-hPa OW overlaid with Earth-relative streamlines 00 UTC 24 July (top) and 00 UTC 25 July (bottom).

Similar to Figure 18, Figure 19 and Figure 20 depict the positions of the 700-hPa and 850-hPa tracked pouches, respectively, at 00 UTC 24 July 2020. Unlike Figure 18,

Figure 19 and Figure 20 represent the pouches three-dimensionally, from 500 hPa to 925 hPa, with relative vorticity overlaid by comoving streamlines relative to the tracked pouch. A dominant area of 700-hPa high relative vorticity emerged from the coast (Figure 19, second row) at the same time a potential disturbance was noted on NHC's TWO. The 700-hPa tracked pouch retains weakly closed streamlines at 500 hPa and 700 hPa level (Figure 19, top left two panels).

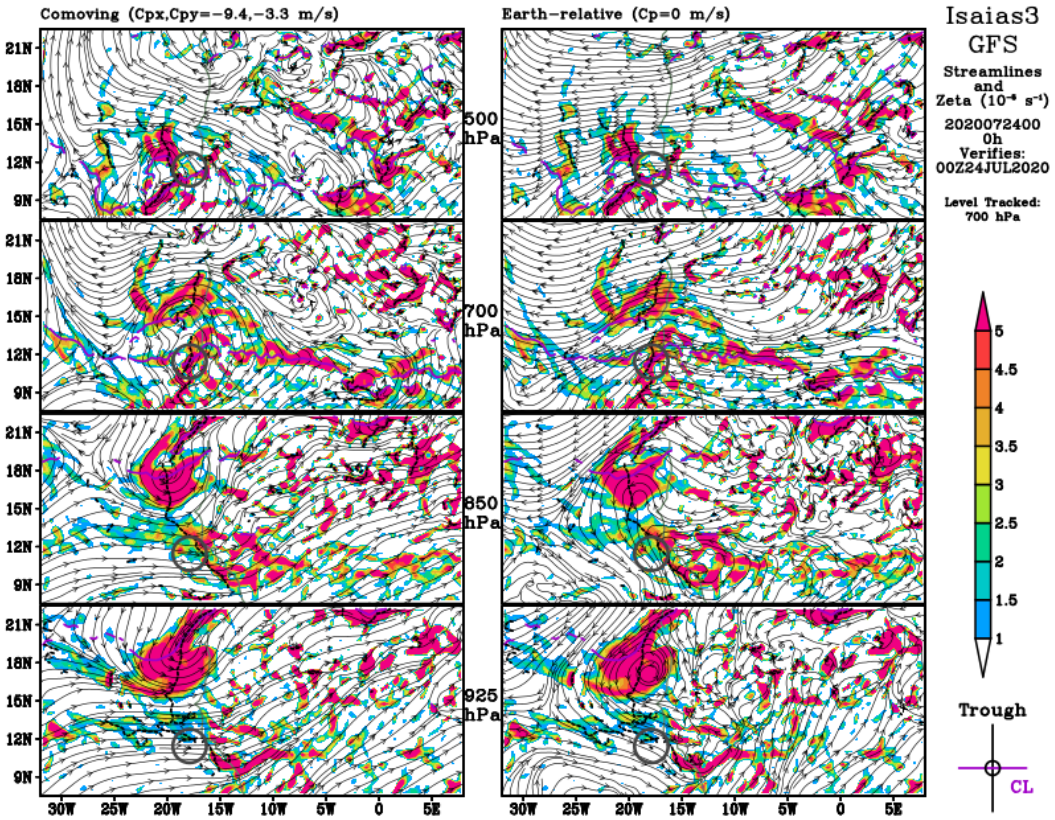

Pre-Isaias relative vorticity plot (color shading) tracking the 700-hPa pouch and streamlines at the four vertical levels of 500 hPa, 700 hPa, 850 hPa, and 925 hPa (top through bottom) at 00 UTC 24 July 2020. The comoving reference frame based on westward (southward) phase speed of 9.4 m/s (3.3 m/s) is on the left; the Earth-relative frame of reference is on the right. The 700-hPa trough with highly localized relative vorticity and trough critical latitude intersection near 12°N in the comoving 700-hPa panel is identified by a grey circle, which is repeated on all panels.

Figure 19. GFS analyses of relative vorticity associated with the 700-hPa pouch.

Simultaneously, a large high relative vorticity area in the 850-hPa level appeared six degrees to the north at 18°N (Figure 19 and Figure 20, third row). This low-level circulation tracked southwestward from 23 to 24 July and had a high value of relative vorticity at both 850 hPa and 925 hPa (Figure 20, bottom two rows). The comoving closed streamlines at 850 hPa and 925 hPa are well-defined (Figure 20, bottom left two panels) in addition to closed streamlines evident in the Earth-relative framework (Figure 20, bottom right two panels) indicating strong cyclonic rotation.

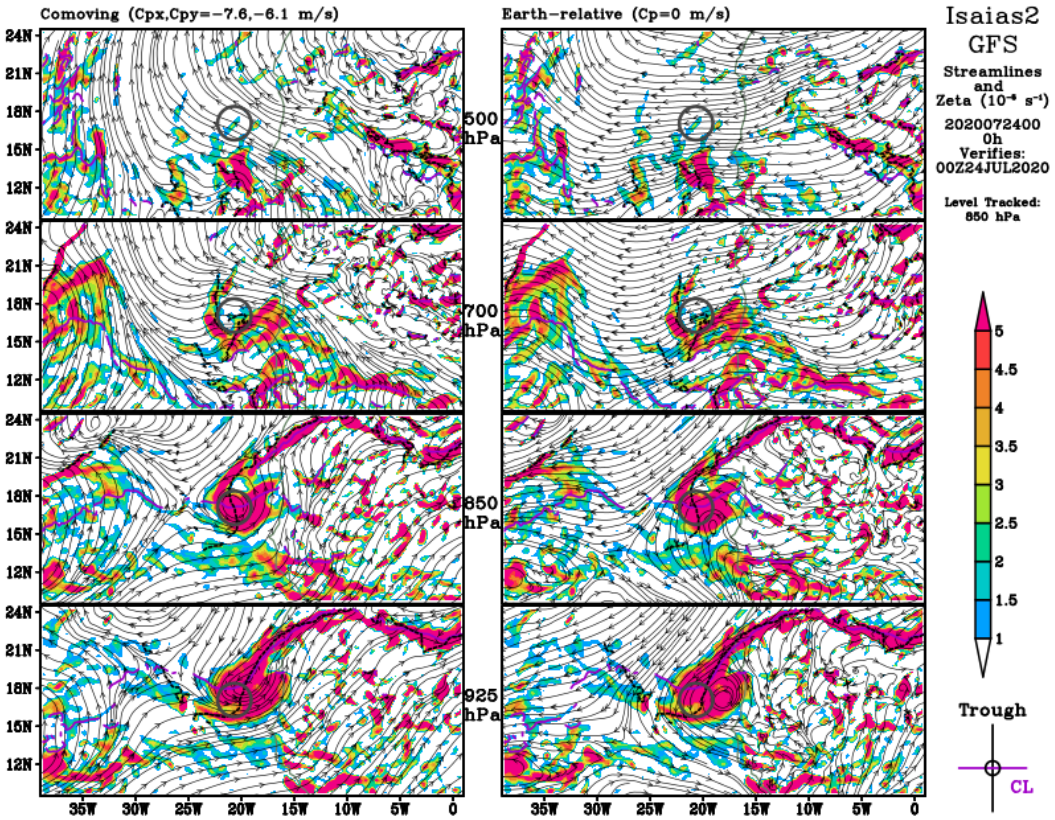

Pre-Isaias wave-pouch identified at the 850-hPa level (corresponds to the third row). The comoving frame of reference based upon a westward propagation velocity of 7.6 m/s southward propagation velocity of 6.1 m/s. The 850-hPa trough with highly localized relative vorticity and trough critical latitude intersection near 18°N in the comoving 850-hPa panel is identified by a grey circle, which is repeated on all panels.

Figure 20. Same as Figure 19, except tracking the 850-hPa pouch.

Corresponding to this low-level pouch, the GFS analyses of RH indicated low available moisture at 925 hPa at 18 UTC 23 July (Figure 21, top left). The remaining plots show a sharp increase in RH near the pouch by 00 UTC 24 July (Figure 21). Considering the southwestward track nearing the ITCZ, the increased RH could be moisture advection into the pouch; however, the increase of RH in the pouch appeared distinct from the moisture to the south. This independent increase in RH within the closed streamlines reinforces the idea that the pouch acts as a protective structure for sustained convective vorticity action. By 06 UTC, RH at 925 hPa substantially increased and appeared to interact with the nearby moisture by 12 UTC (Figure 21, bottom row).

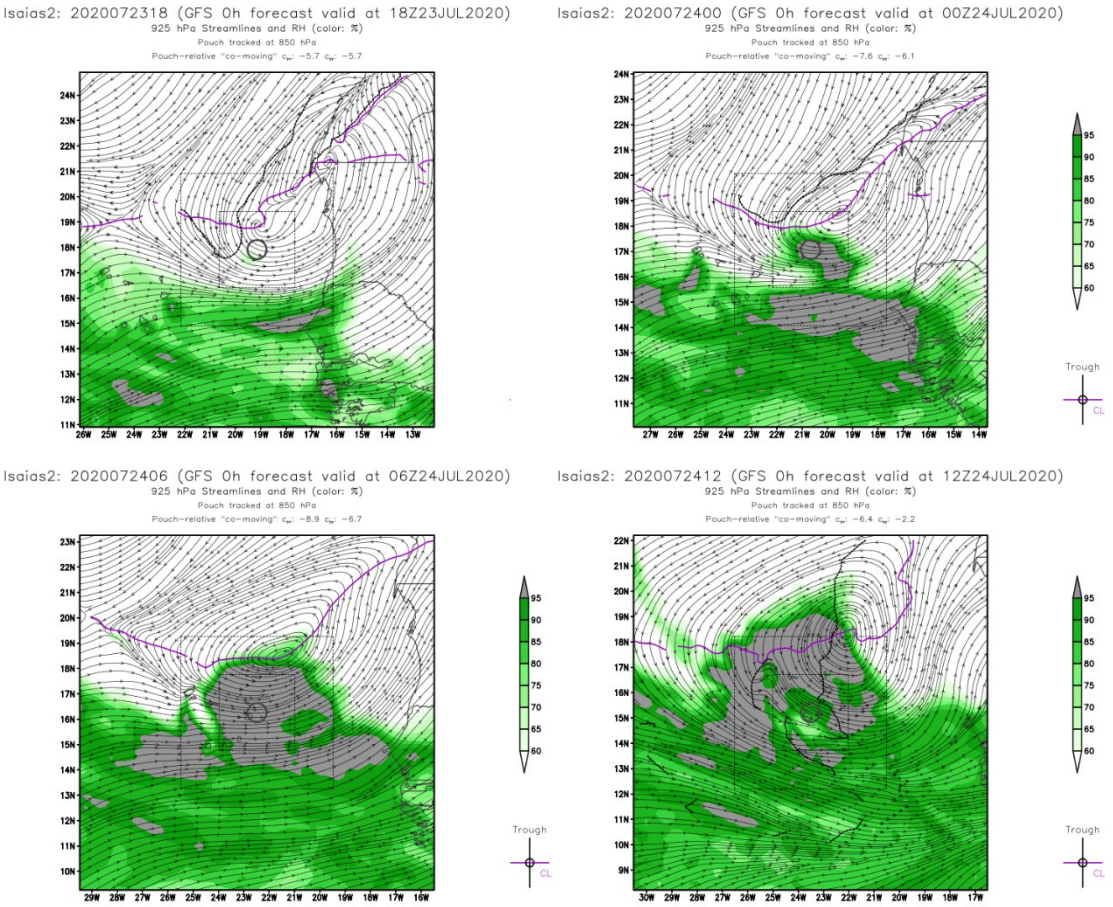

Figure 21. GFS 925-hPa analyses of RH and comoving streamlines for pre-Isaias every six hours from 18 UTC 23 July to 12 UTC 24 July 2020.

Over the next twelve hours, GFS analyses depicted the 925-hPa level with increased RH (not shown), and by 00 UTC 25 July, GFS analyses showed an isolated region of increased RH of 60–65% near the pouch center at 850 hPa (Figure 22, upper left). Over the next 18 hours, the 850-hPa RH rose rapidly with the recirculating moist flow remaining mostly self-isolated (Figure 22). The moistening of this initially dry 850-hPa pouch and its southwestward propagation toward the 700-hPa pouch resulted in further column moistening via vorticity advection preceding pouch associated deep convection.

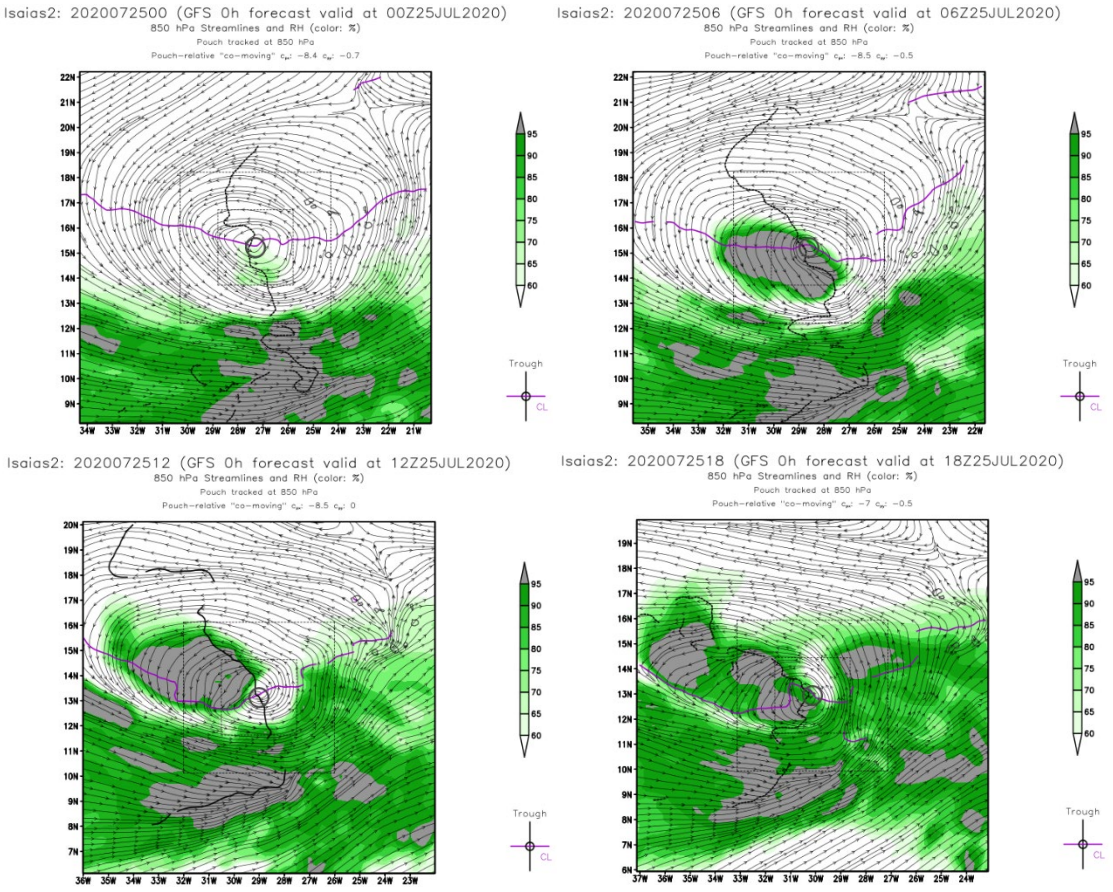

Figure 22. Same as Figure 21, except 850-hPa analyses at 00 UTC through 18 UTC on 25 July 2020.

Considerable deep convection lingered well south of the pouch and NHC positions at 12 UTC 25 July 2020 (Figure 23 top, left column). The GFS comoving analyses (Figure

23 center column) used the 700-hPa tracked pouch. This 700-hPa tracked wave-pouch extended up to 500 hPa and down to 850 hPa with closed streamlines in the comoving reference frame (Figure 23 top, center column). However, the recirculating flow is not yet seen in the Earth-relative reference frame (Figure 23 top, right column). By 18 UTC, some of the convection weakened to the south of the marked positions, but moisture remained evident to the southwest and southeast. Additionally, the pouch, depicted with closed streamlines, reached the 925-hPa (Figure 23 bottom, center column). Closed streamlines at 925-hPa indicated a vertically aligned pouch in the comoving reference frame. Similarly, the Earth-relative plots suggested a vertically aligned pouch except at 500 hPa.

Convection continued to appear unaffiliated with the pouch positions at 00 UTC 26 July (Figure 24 top, left column). GFS analyses depicted closed streamlines in comoving and Earth-relative reference frames indicative of a vertically aligned pouch (Figure 24 top, center and right columns). By 06 UTC, an isolated burst of convection appeared at 12.5°N, 35.5°W just west of the pouch positions and north of the NHC position (Figure 24 bottom, left column). While the pouch remained vertically aligned in the OW Earth-relative reference frame (Figure 24 bottom, right column), the comoving 925-hPa structure temporarily lost its closed streamlines at the given wave phase speed (Figure 24 bottom, center column).

The small convective burst west of the indicated circulation positions grew in area by 12 UTC 26 July 2020 (Figure 25 top, left column). The 700-hPa and 850-hPa pouches remained within a half degree of each other. The 700-hPa tracked pouch returned to vertical alignment through the layer between 500 hPa and 925 hPa in the comoving and Earth-relative reference frames (Figure 25, top, center and right columns). By 18 UTC, pouch and NHC positions became closer in proximity, although convection temporarily weakened near the pouch center, the hook-like shape of cloudiness extending northward to 16°N, 35°W on the east side of the pouch suggested possible circulation (Figure 25, bottom, left column).

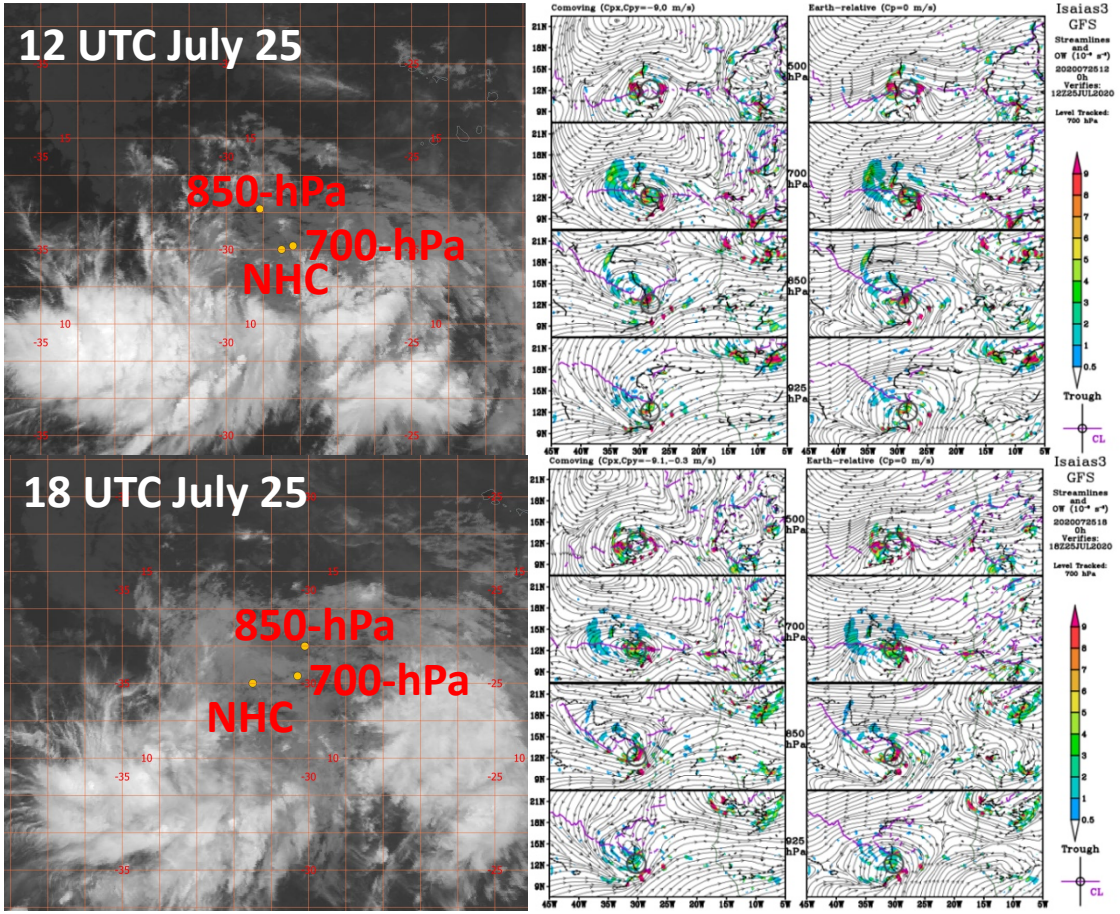

GOES-16 Channel 13 IR (left column) and GFS analyses of OW overlaid with comoving (center column) and Earth-relative (right column) streamlines at four levels (500 hPa, 700 hPa, 850 hPa, and 925 hPa (top to bottom)) on 25 July 2020 at 12 UTC (top half) and 18 UTC (bottom half). Approximated NHC and MP-derived 700 and 850-hPa pouch locations are denoted on GOES-16 imagery with yellow dots. The same 700-hPa pouch locations are denoted with a grey circle on all GFS plots, regardless of underlying level plotted.

Figure 23. Pre-Isaias IR imagery and OW overlaid with comoving and Earth-relative streamline plots at 12 and 18 UTC 25 July 2020.

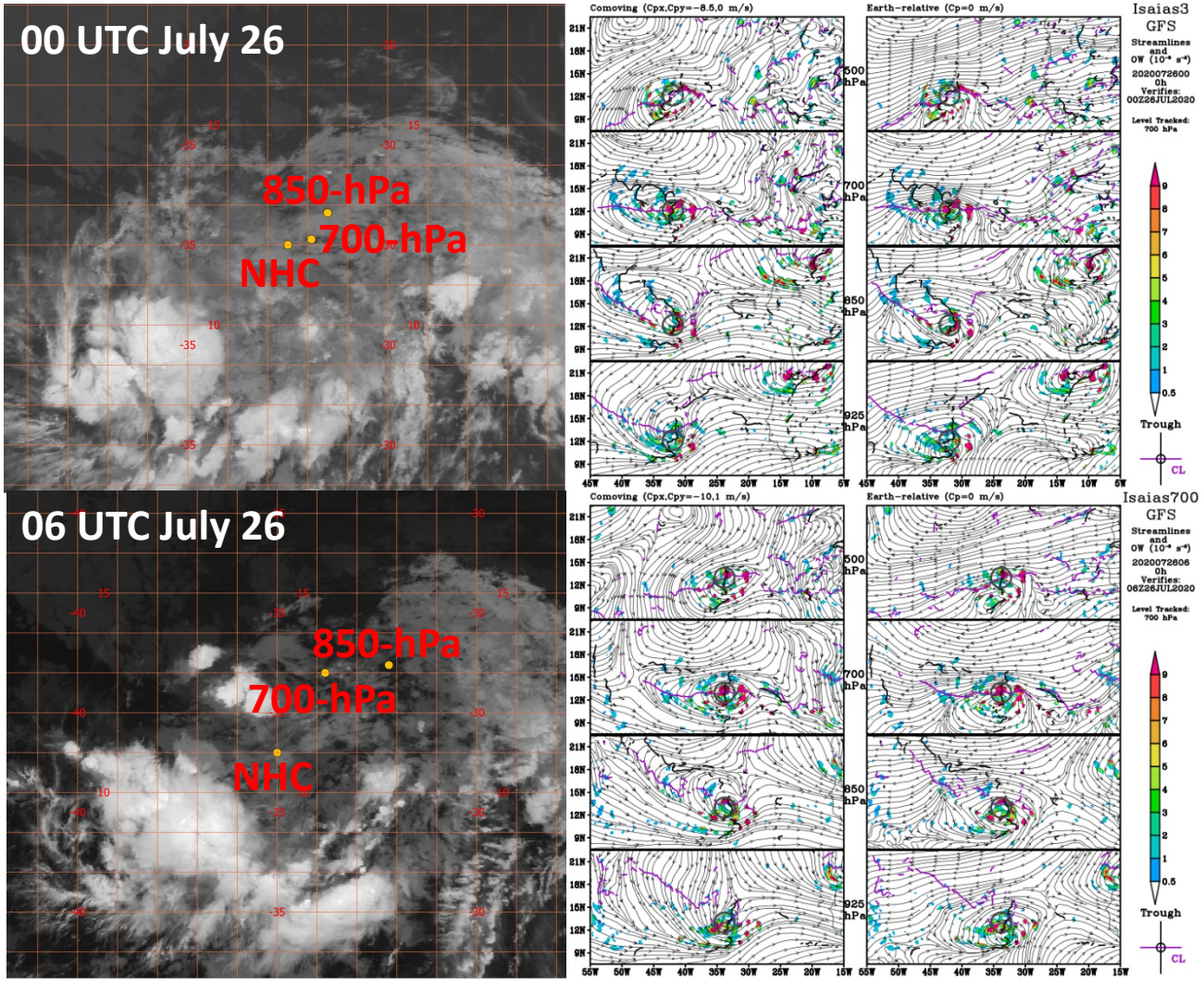

Figure 24. Same as Figure 23, except at 00 and 06 UTC 26 July 2020.

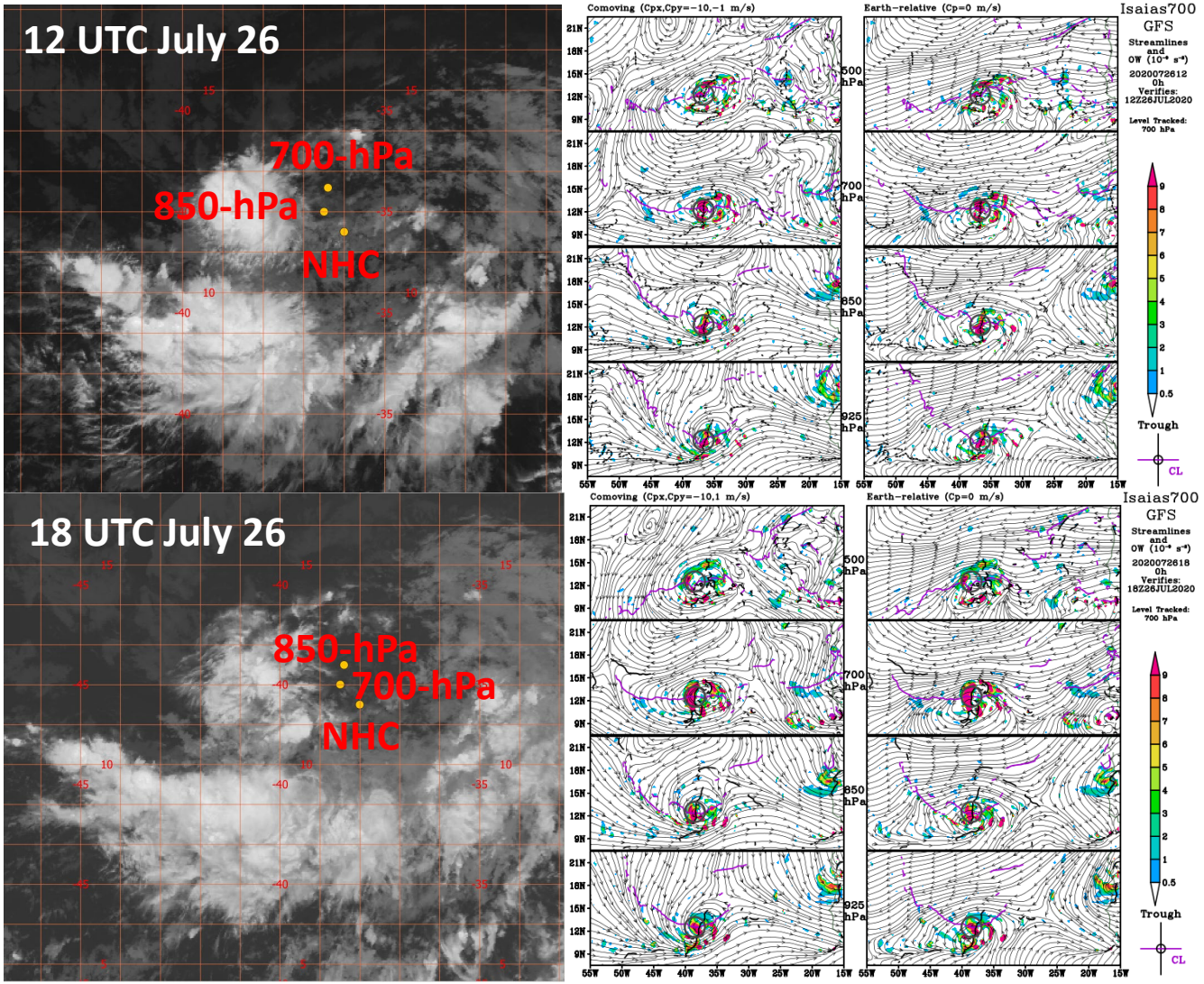

Figure 25. Same as Figure 23, except at 12 and 18 UTC 26 July 2020.

By 18 UTC 25 July, while the two pouch centers remained separate and with limited convection (Figure 23 bottom, left column), the AEW at 700 hPa and the dry, but steadily moistening 850-hPa circulation begin to overlap. Figure 26 depicts the vertical extent of the RH in the vicinity of the pouch, with a minimum of RH at 700 hPa and high values of RH at the other three levels. The moist lower levels, especially at 850 hPa on the western side of the gradually aligning pouch (Figure 23, upper right column), hint at the subsequent burst of convection to the west of the positions twelve hours later at 06 UTC 26 July (Figure 24, lower left column). Deep convective activity contributed to moistening of the entire column that was sustained throughout the remainder of the formation process.

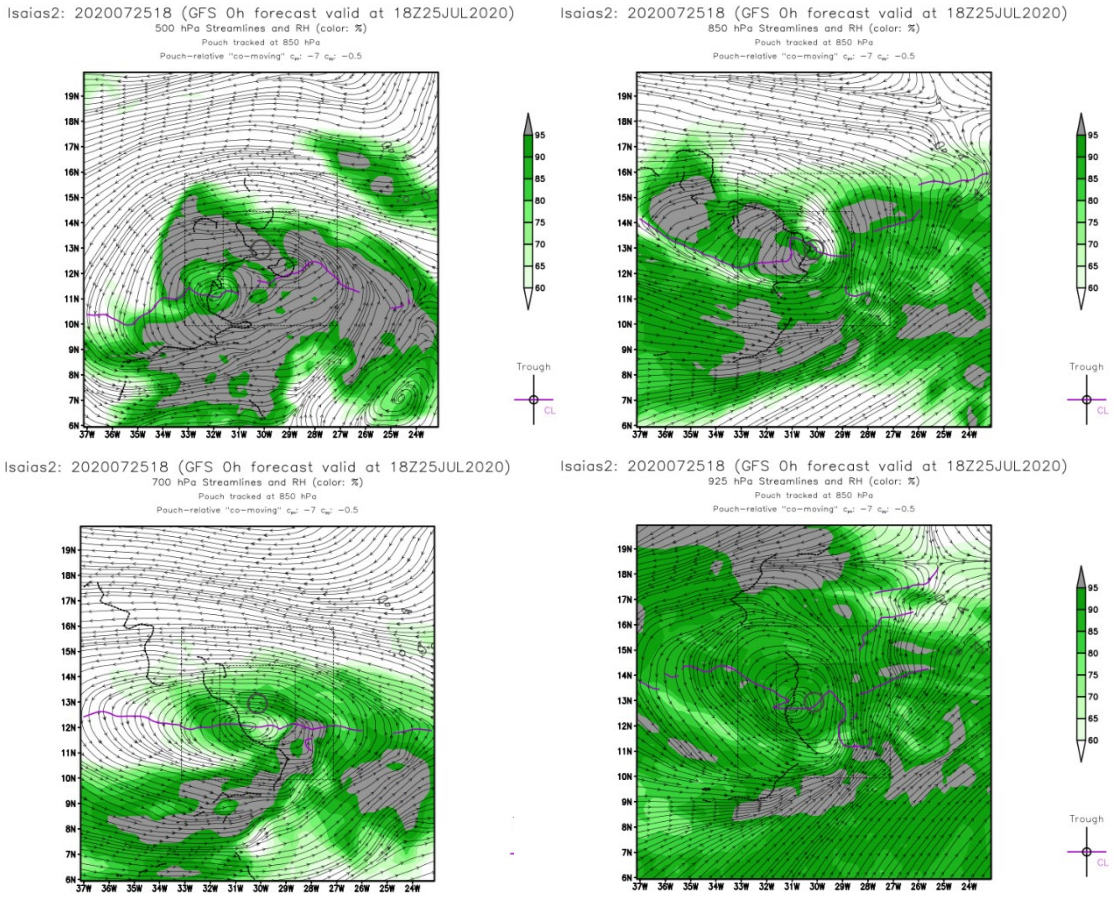

Figure 26. Same as Figure 21, but each level from 500 hPa to 925 hPa at 18 UTC 25 July 2020.

While pinpointing the exact time and location when the two pouches consolidate into one is difficult, identifying this event contextualized the state of the disturbance in a way that can be tracked reliably at either level (700 hPa or 850 hPa). Concerning the independent nature of the dry low-level circulation and the vertical alignment of two disturbances, could the interaction of these two pouches aid genesis? Either disturbance could have developed into a TC, but the vertical alignment of a moist mid-level disturbance with a low-level disturbance appeared to provide the bulk of a single, extended pouch structure over the course of 25 and 26 July.

Moistening within the closed circulation was not evident in IR imagery since low-level moisture must sufficiently rise to condense into clouds at the lifted condensation level (LCL). The persistence of the protective pouch continued to self-moisten the column, which allowed parcels to break above the LCL. Once above the LCL, deep convection is apparent in IR imagery approximately 12 hours later. Even with analysis fields, the intersection of a dry pouch at lower levels tracking from the northeast (initially from 18°N) combining with the 700-hPa level moist pouch originating from the east (12°N) provides a challenging genesis sequence to analyze. Additionally, the isolation of the low-level moistening coupled with the onset of a burst of convection indicates there is an association between a strong vortical structure within a pouch at low-levels and the birth of a potential tropical cyclone. The pouch need not be extremely moist or humid in origin, but in areas of high SST and strong cyclonic vorticity, a TC may emerge. The presence of multiple cyclonic disturbances at different levels colliding and stacking muddies the simple picture. The dynamics of two disturbances stacking may contribute to the genesis process, once atmospheric moisture is sufficient in conjunction with an extended pouch via vertical alignment of the 850-hPa and 700-hPa pouches.

The well-defined pouch continued forming, but with operational uncertainty. Figure 27 presents pre-Isaias as an idealized pouch from the OW and comoving streamline overlay at 00 UTC 28 July; however, the convection remained broad and disorganized in extent around the pouch center and primarily to the west of the pouch center. The ring of convection around the pouch appears to follow the closed streamlines reinforcing the pouch and TC formation. IR imagery without the comoving plot provides an ambiguous

indication of formation. Among the three TCs studied here, Isaias has perhaps the most unique path to formation. This uniqueness is evident in NHC operational forecasts as the disturbance was upgraded from a PTC on 12 UTC 28 July to tropical storm status as TS Isaias on 00 UTC 30 July without the designation of a tropical depression.

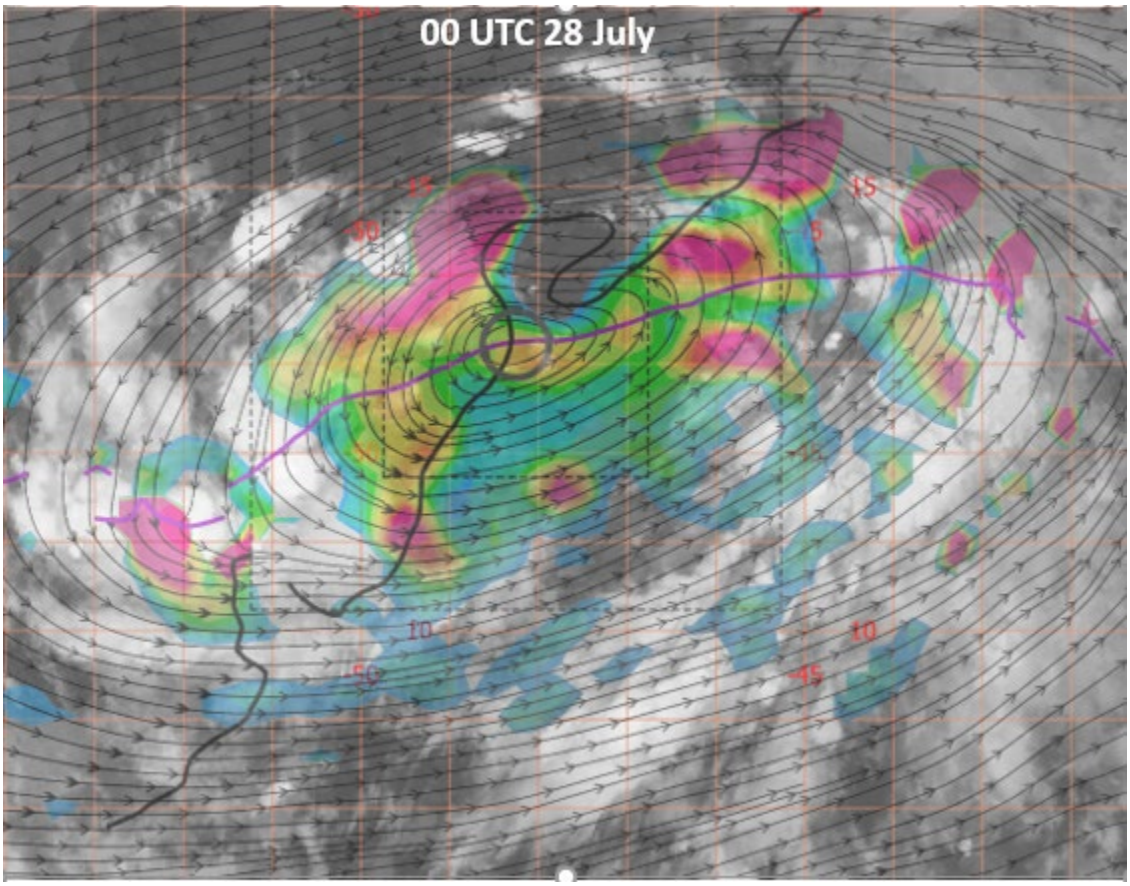

Pre-Isaias prior to designation as a potential tropical cyclone. The GOES-16 Channel 13 IR overlaid with OW inside closed comoving streamlines indicates a well-defined pouch at 00 UTC 28 July 2020. The trough axis (thick black line) crosses the critical latitude (purple line) in the pouch center marking the "sweet spot."

Figure 27. Pre-Isaias IR imagery overlaid with MP OW and comoving streamlines.

C. PRE-LAURA

A month after Isaias, Laura's mid-August formation, near the peak of hurricane season, occurred in a very humid band of air near 11°N. Multiple trough axes existed, resulting in several groups of convective activity. The broad extent of relative vorticity, rather than concentrated within closed streamlines, coincided with the disorganized mass of convective cells that propagated with multiple trough axes across the Atlantic. Moisture in the lower levels was readily available.

Figure 28 provides a cursory glance into the propagation and development of Hurricane Laura. The two pouch tracks in red and blue identify pre-Laura's path at two different levels until its designation as a tropical depression. The disparity of these pouch positions with the NHC track (black line) disparity of position initially and throughout the formation period provides some clue to the challenge that is tropical storm forecasting. There is an approximate ten-degree separation between the two pouches on 18 August, while the NHC track jumps significantly between 17 and 18 August. By 19 August there is consensus on position between the three positioning techniques, which remains for the remainder of the pre-Laura track.

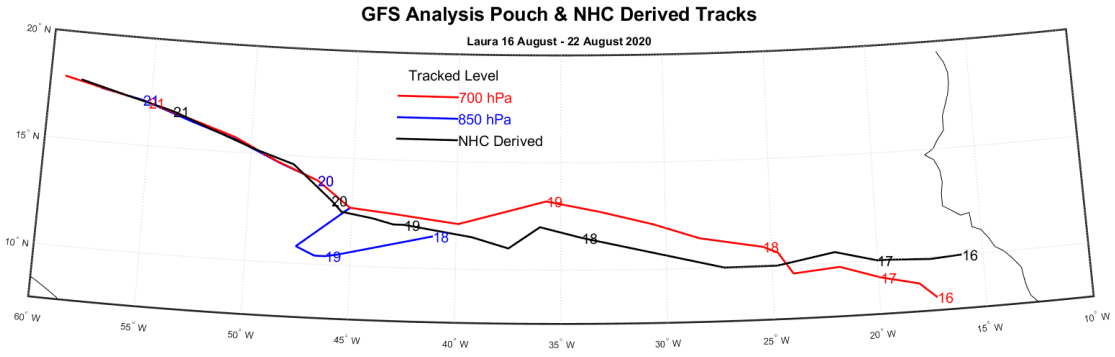

Figure 28. GFS analysis pouch and NHC-derived tracks.
Adapted from NHC (2020b).

The disturbance or series of disturbances that started out as a broad area of clouds and showers emerged off the west coast of Africa on 16 August 2020. Several waves propagated across the Atlantic with minimal organization until 19 August when the wave

transitioned to a tropical depression. Within swaths of relative vorticity, consistent with the operational analysis of a broadly extensive AEW, were small areas of OW (Figure 29). Within the post-analysis, multiple trough axes in the vicinity of the centered trough reflect the broad extent of activity.

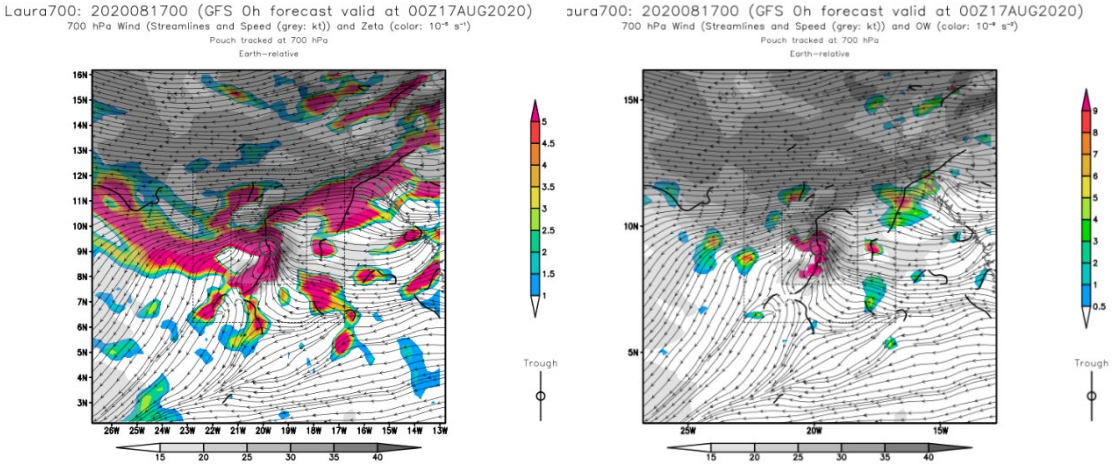

GFS analyses of pre-Laura 700-hPa Earth-relative streamlines overlaid on relative vorticity (left) and OW (right) at 00 UTC 17 August 2020. The 700-hPa pouch center (based on the comoving reference frame) is indicated by a grey circle on both panels. Multiple trough axes exist within a large swath of relative vorticity and corresponds to the disorganized mass identified by forecasters.

Figure 29. GFS analyses of pre-Laura relative vorticity and OW at 00 UTC 17 August.

The development of pre-Laura started with broad and disorganized convection along 11°N. The readily available moisture consistent with the ITCZ and its northern position at the peak of hurricane season produced very favorable atmospheric conditions for cyclogenesis. A disturbance along this band of warm moist air was well protected synoptically from vertical wind shear and dry air intrusion, allowing the formation of multiple pouches. The additional synoptic conditions of a meridional trough near 42°W between two North Atlantic subtropical ridges and a more zonally elongated trough or compilation of troughs along 11°N provided fertile ground for several pouches (Figure 30). Those pouches associated with the meridional trough had little westward phase speed and stayed mostly stationary and shallow relegated to 850 and 925-hPa. The shallow pouches appeared to stay distinct and independent, as depicted by GFS streamline and OW plots.

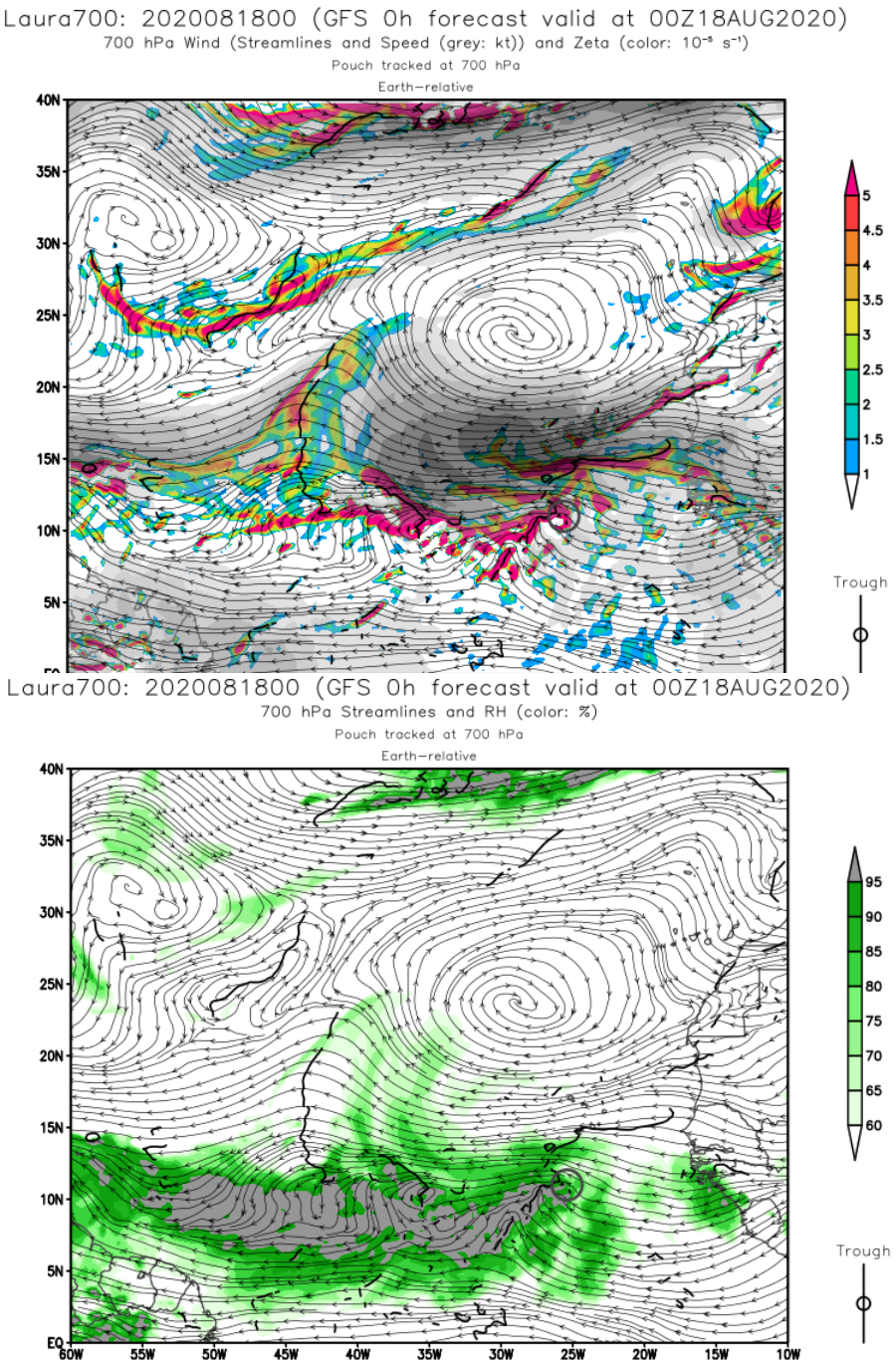

A meridional trough between two subtropical ridges in the North Atlantic. Plots are in the Earth-relative reference frame at 00 UTC 18 August 2020. The grey circle indicates the pouch identified location.

Figure 30. GFS analysis of 700-hPa relative vorticity (top) and relative humidity (bottom).

A broad area of cloudiness extended to the west of the pouch center at 18 UTC 17 August (Figure 31, top left column), which then consolidated into banded convection well west of the pouch center by 00 UTC 18 August (Figure 31, bottom left column). The 4-level GFS analyses of streamlines and OW depicted multiple troughs. Tracked at 700 hPa, the weak pouch highlighted by the grey circle was one of many potential pouches and, given the methods, was the best positional choice. During this time, the pouch at 700 hPa is not extremely strong nor does its presence extend above or below 700 hPa. While there were closed streamlines associated with a meridional trough at about 42°W in the Earth-relative plot, the OW values of the trough were relatively low and broad.

Convection appeared in two distinct areas at 06 and 12 UTC 18 August (Figure 32, left column). The 800-km separation between the 700-hPa pouch and NHC derived positions indicated on the IR imagery hint at the expanse of this disturbance that is in question. Isolated pockets of OW in the GFS analyses extended west of the indicated 700-hPa level tracked pouch within an elongated trough (Figure 32, center and right columns). GFS analyses in the Earth-relative reference frame continue to depict an open wave with high OW values throughout the column (Figure 32, right column). In the Earth-relative plot, nearly closed streamlines are visible around 45°W at 850 and 925 hPa levels, indicating a slowly moving low level pouch well west of the 700-hPa tracked pouch (Figure 33 right column, bottom two panels).

Convection became less distinct with some dissipation at 18 UTC 18 August and 00 UTC 19 August (Figure 34, left column) and remained disorganized. At 18 UTC 18 August, the 700-hPa pouch remained at mid-levels with closed streamlines at only 500 hPa and 700 hPa (Figure 33, top center column). By 00 UTC 19 August the 700-hPa pouch became more apparent in the comoving reference frame with closed streamlines extending down to 850 hPa. Also, a separate stationary 850-hPa pouch far to the west of the 700-hPa pouch persisted (Figure 33, bottom left column). Without significant movement, this 850-hPa pouch was well-defined in the Earth-relative plots along with high OW values near 10°N, 46°W (Figure 33, bottom right column). By 00 UTC 19 August, the 850-hPa tracked pouch appeared to weaken in the Earth-relative plots. Between the two tracked pouches were several areas of moderate to high level OW.

Convection strengthened and organized by 06 UTC 19 August, and this trend continued through 12 UTC 19 August (Figure 34, left column). Pouch and NHC positions remained separated during much of this time, but those positions neared by 12 UTC. As the 700-hPa level pouch tracked westward, some of the high OW areas appeared to become entangled within or on the periphery of the closed comoving streamlines at 700 hPa and 850 hPa (Figure 34, center column). Between 06 and 12 UTC 19 August, the OW area associated with the western 850-hPa pouch remained distinct from the 700-hPa pouch, but without closed streamlines in the Earth-relative plots while the 700-hPa pouch deepened in the comoving plots (Figure 34, center and right columns). Additionally, the strong OW values from the 850-hPa pouch diminished in comparison to the OW values for the 700-hPa pouch from 18 UTC 18 August to 12 UTC 19 August.

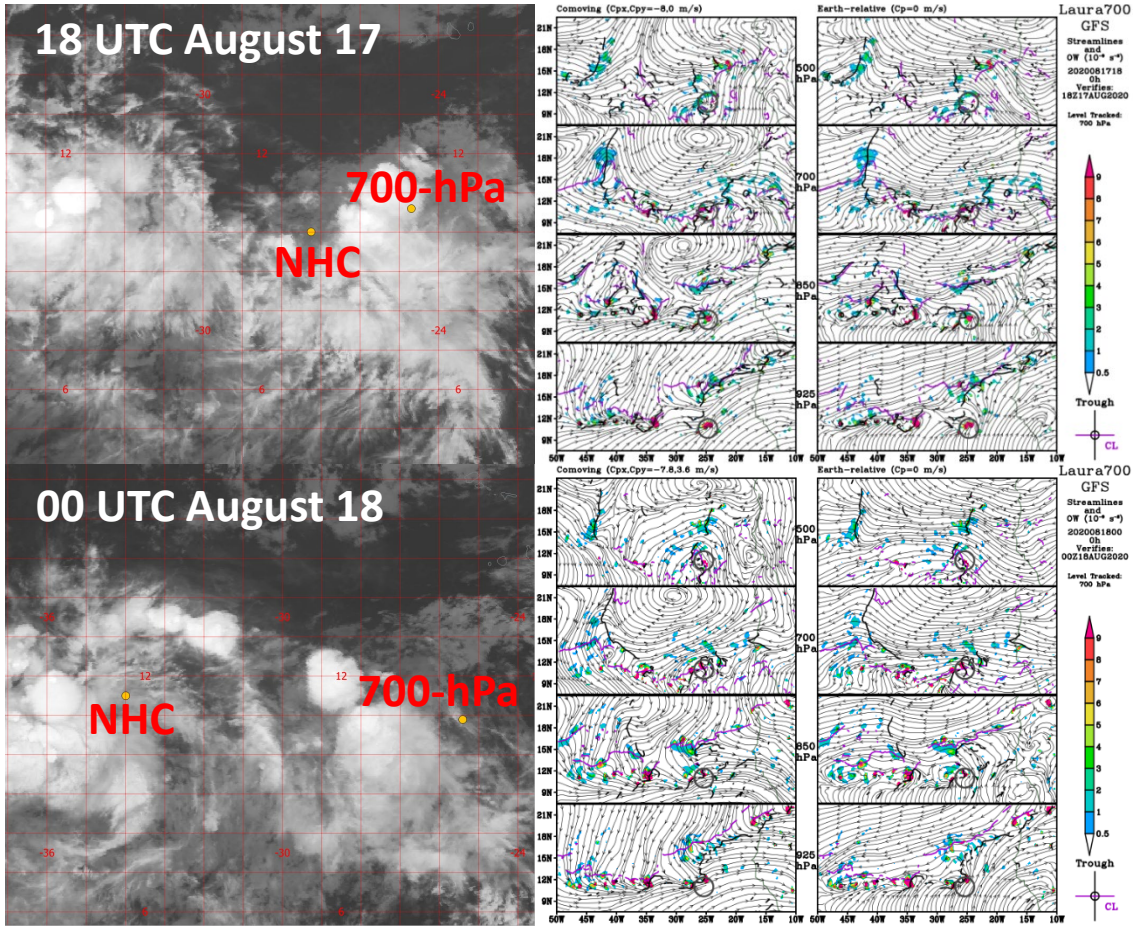

GOES-16 Channel 13 IR (left column) and GFS analyses of OW overlaid with comoving (center column) and Earth-relative (right column) streamlines at four levels (500 hPa, 700 hPa, 850 hPa, and 925-hPa (top to bottom)) at 18 UTC 17 August (top half) and 00 UTC 18 August 2020 (bottom half). Approximated NHC and MP-derived 700-hPa pouch locations denoted on GOES-16 imagery with yellow dots. Same 700-hPa pouch location is denoted with a grey circle on all GFS plots, regardless of underlying level plotted.

Figure 31. Pre-Laura IR imagery alongside OW plots overlaid with comoving and Earth-relative streamlines.

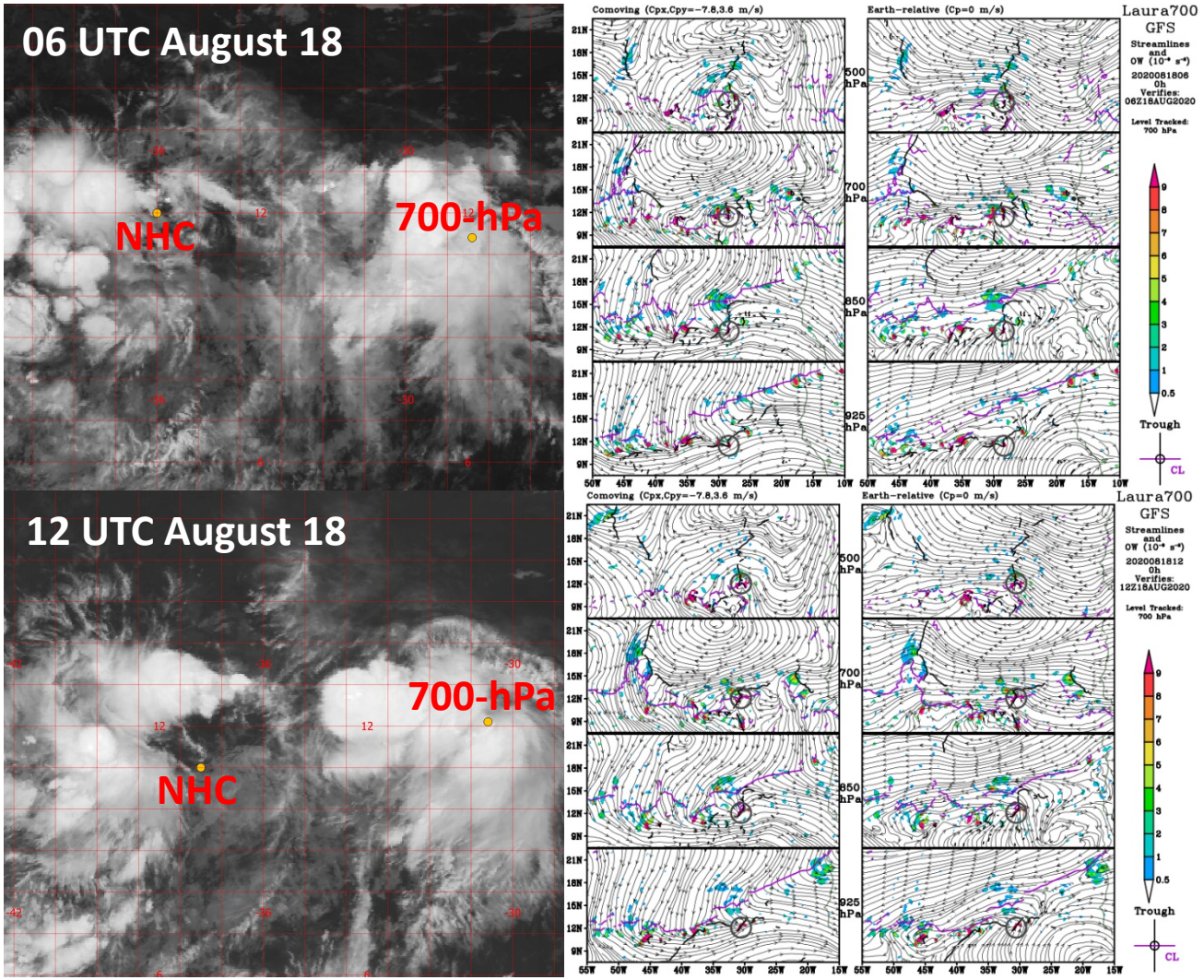

Figure 32. Same as Figure 31, except for 06 and 12 UTC 18 August 2020.

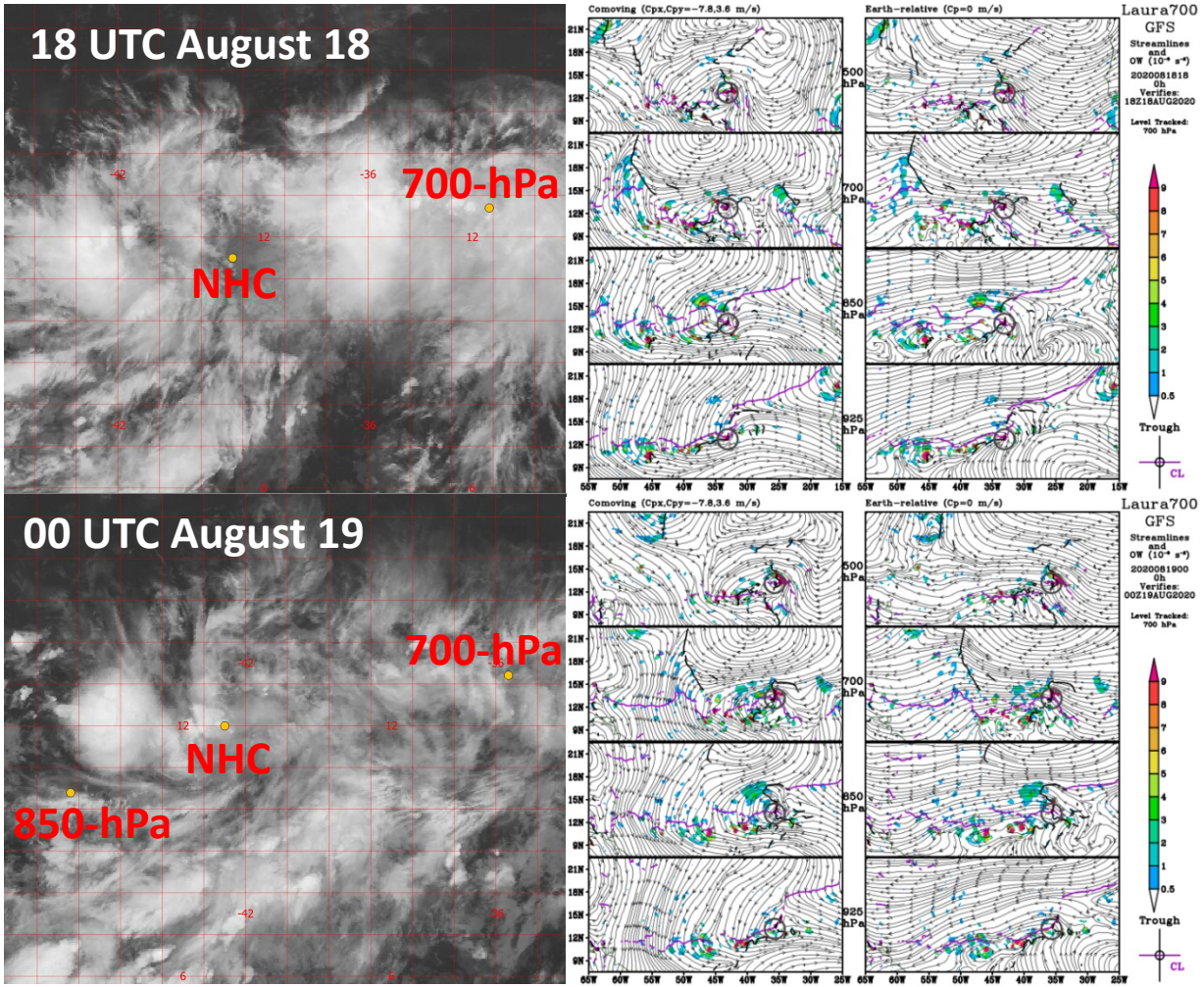

An 850-hPa tracked pouch position becomes evident and is indicated on the satellite IR imagery only.

Figure 33. Same as Figure 31, except for 18 UTC 18 and 00 UTC 19 August 2020.

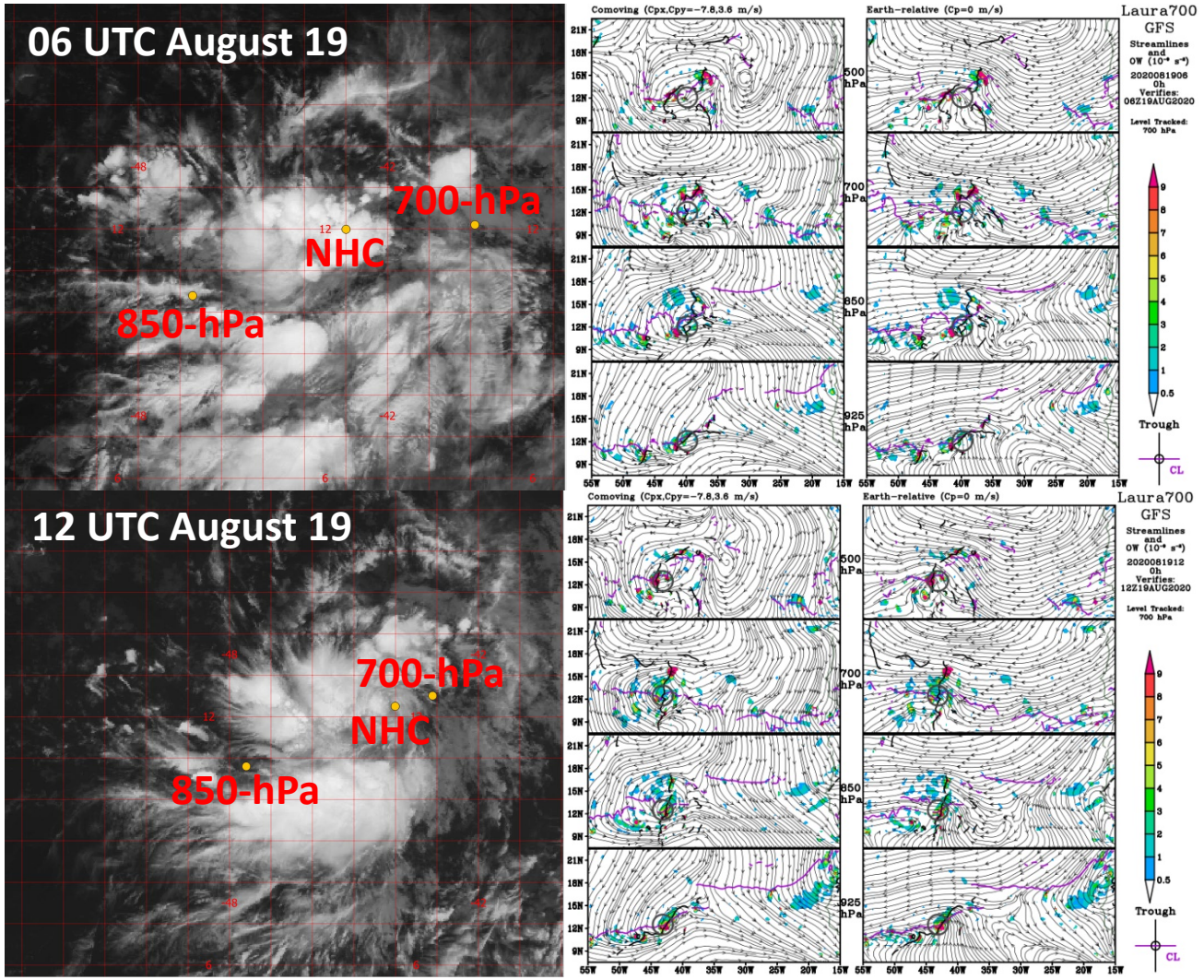

Figure 34. Same as Figure 31, except for 06 and 12 UTC 19 August 2020.

While mid-level vertical wind shear inhibited organization from 17 to 21 August, the vertical wind shear was not strong enough to shear away the pouch (The pouch-layer (left) and deep-layer (right) vertical wind shear provide differing aspects of vertical wind shear. Blue arrows indicate wind velocity at the upper level, 500 hPa (left) and 200 hPa (right); the red arrow represents the wind vector at 850 hPa for both panels; the black arrow indicates the lower-level wind vector subtracted from the upper-level wind vector.

Figure 35). Weakening of the 700-hPa pouch from 19–20 August coincident with reduced RH (not shown), which suggests dry air encroaching upon the pouch. Additionally, at 850 hPa and 925 hPa, the GFS analyses depicted decreased RH in the broad extent of the zonally elongated wave-trough. However, a small pouch extending from 925-hPa to 700-hPa persisted through these adverse shear conditions by 21 August (Figure 36).

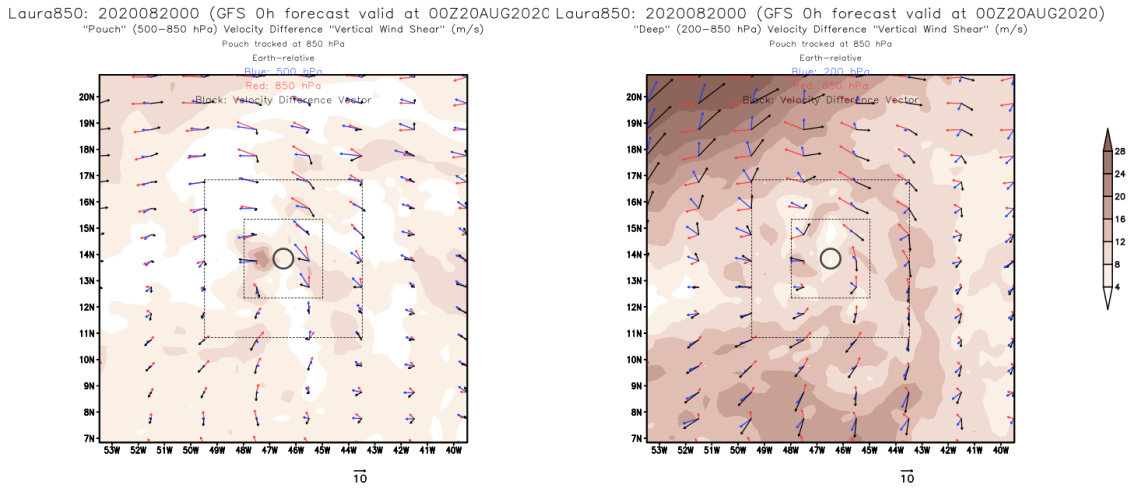

The pouch-layer (left) and deep-layer (right) vertical wind shear provide differing aspects of vertical wind shear. Blue arrows indicate wind velocity at the upper level, 500 hPa (left) and 200 hPa (right); the red arrow represents the wind vector at 850 hPa for both panels; the black arrow indicates the lower-level wind vector subtracted from the upper-level wind vector.

Figure 35. GFS pouch-layer (500-850 hPa) (left) and deep-layer (200-850 hPa) (right) vertical wind shear centered over pre-Laura at 00 UTC 20 August 2020.

The perseverance of the pouch at low levels and eventual cessation of pouch vertical wind shear marked a transition for the system, that, once shifted into favorable conditions, could build via a bottom-up process. By 21 August, the OW in comoving reference frame stacked nicely from 925 hPa to 700 hPa, with the 500 hPa level lagging to the southeast geographically (Figure 36). The Earth-relative plots indicate that the disturbance continued to exhibit an open wave-like structure. The now vertically aligned circulation approached an area

of warm water east of the Caribbean, allowing the tropical depression to strengthen to Tropical Storm Laura with sustained 40-kt winds.

Throughout pre-Laura, several independent areas of high OW values or pouches exist along the longitudinally expansive band of cyclonic relative vorticity and relative humidity. The pouch identified at 700-hPa appeared to attract nearby pouches or isolated high OW areas into its circulation as it deepened and developed along its westward propagation. Several cells of convection in the IR imagery corresponded to these areas of broad cyclonic relative vorticity and isolated areas of high OW values. The 00 UTC 21 August GFS analysis showed multiple OW associated with the wave-pouch at 700, 800, and 925 hPa (Figure 36).

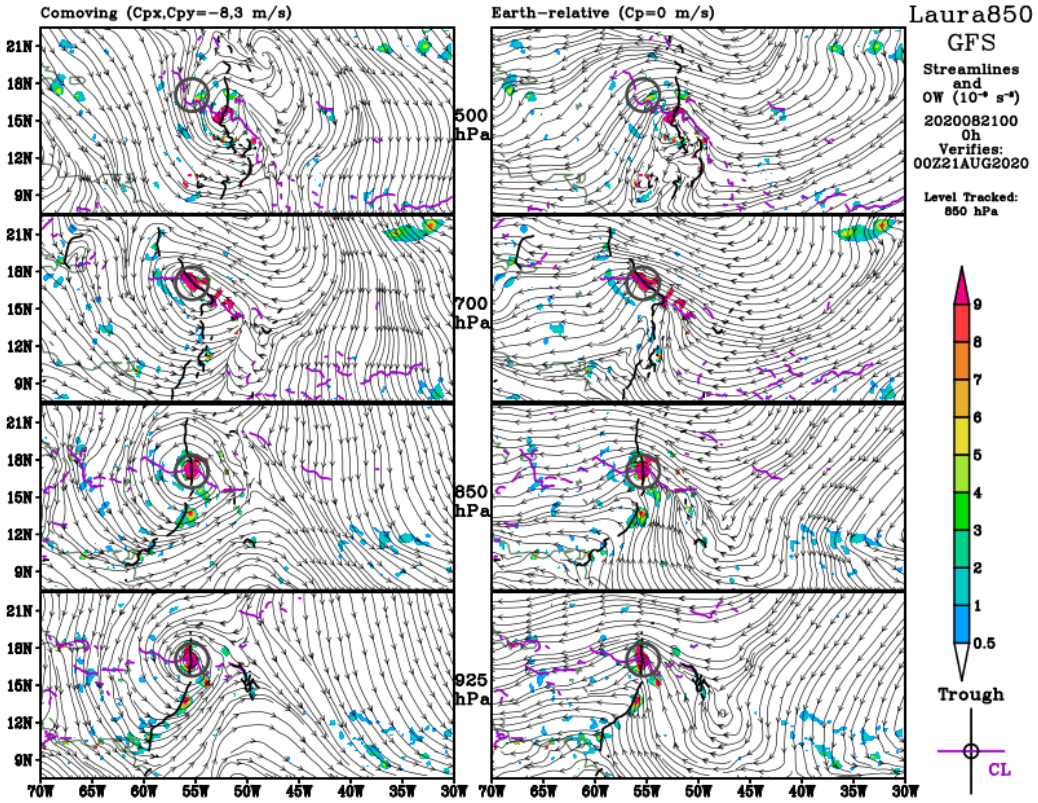

The comoving plots are based on westward propagation velocity of 8m/s and northward propagation velocity of 3m/s phase speeds. The pre-Laura wave-pouch with highly localized OW and trough-critical latitude intersection near 17°N, 55°W in the comoving 850-hPa panel is represented by the grey circle and is repeated on all panels.

Figure 36. GFS analyses of OW (shading) overlaid with comoving and Earth-relative streamlines at 00 UTC 21 August 2020.

The GFS analyses reflect the interaction of multiple pouches from the OW plots (Figure 31 through Figure 34, center and right columns). Compared with relative vorticity plots, OW plots show isolated areas of high OW that better distinguishes the interaction of these centers of spin. However, the role of relative vorticity remains relevant. For instance, on 18 August, the westward propagating 700-hPa pouch at 25°W pursued the slow-moving 850-hPa pouch at 45°W. This interaction led to the consolidation of cyclonic relative vorticity from 00 UTC 18 August to 12 UTC 19 August (Figure 37 and Figure 38).

Despite the temporally coarse six-hour intervals of the GFS analyses, OW plots hint at direct pouch interactions characterized as one or more of the following: (1) elastic interaction (2) partial or complete straining, or (3) partial or complete merging (Prieto et al. 2003). In pre-Laura's case, a main vortex began an elastic interaction with nearby smaller vortices, followed by partial straining of smaller vortices by the main vortex. The straining action occurred as the smaller vortices entered the stream flow of the larger vortex, following the flow southeastward around the larger vortex. As the smaller vortices experienced partial straining and elastic interaction around the east side of the main vortex, the high OW values begin to combine, which suggested partial to complete merger. The continuum of interaction of smaller vortices nearing in orbit around the main pouch reinforces Prieto et al.'s (2003) description and generalization of categories characterized by separation distance, radius size, and vorticity intensity.

Within the context of the MP, the initial elastic interaction characterized a main vortex as an attractor and the smaller vortices orbiting the main vortex. The preservation of the main vortex or pouch and the smaller vortices suggests some inherent protection to the respective pouch structure, like the horizontal shear acting as a shear sheath. The smaller vortices effectively "fall" into the flow of the main pouch as if to orbit its center cyclonically. The horizontal shear of each vortex or pouch protects from strain initially, until the orbit of the smaller vortices continues to near the main pouch center. The horizontal shear associated with smaller vortices breaks down given the strength of the main pouch's horizontal shear, leading to a strain on the smaller vortices as the smaller vortices fall into the flow of the larger vortex and become drawn into the main pouch center. With the protective sheath of the smaller vortices removed, the remaining vortex nears the center initiating a partial or complete merger. This partial or complete merger adds cyclonic vorticity to the inner pouch area and expands the main pouch (Figure 39).

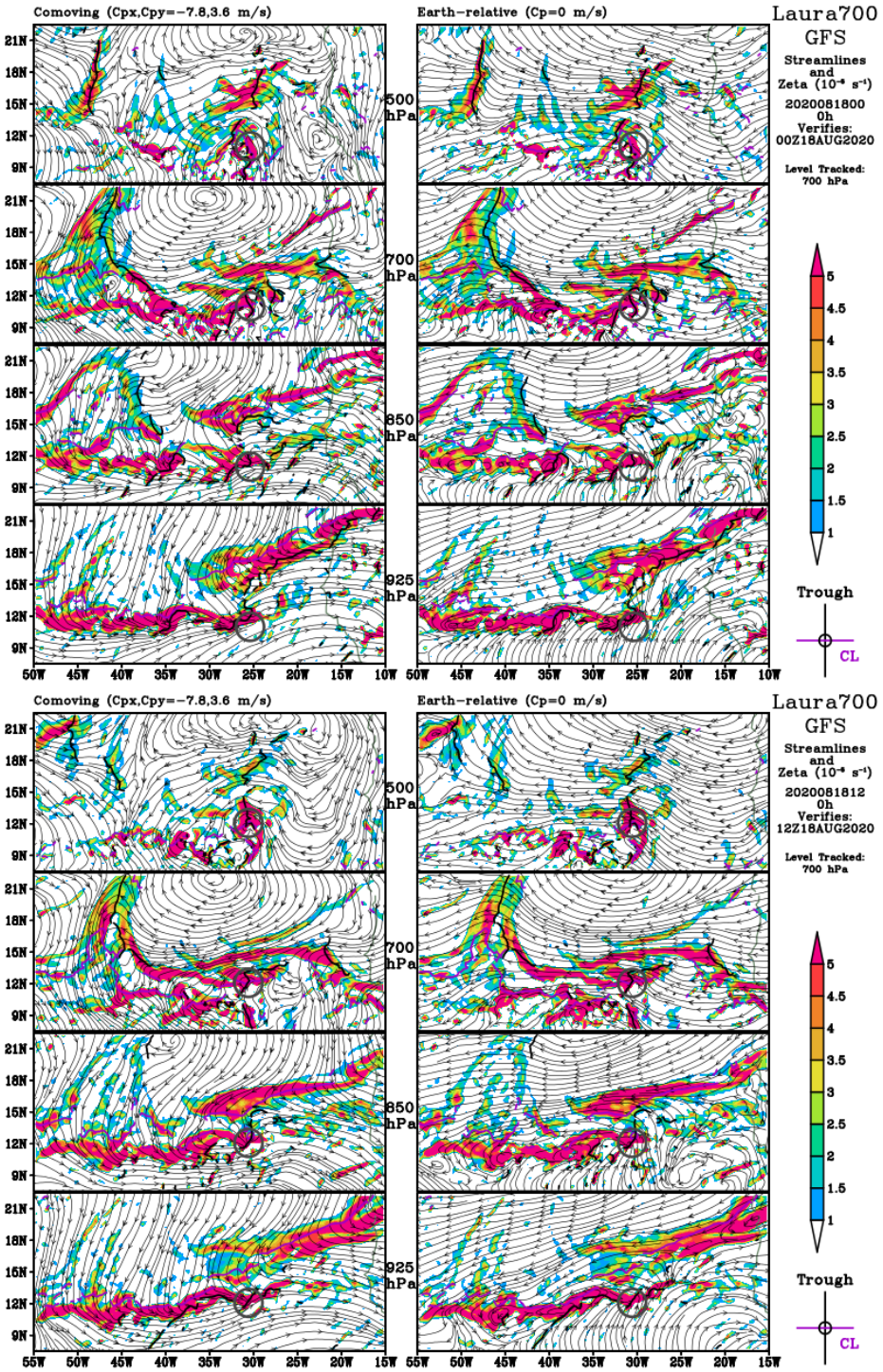

The comoving frame (left column) of reference based on a westward propagation velocity of 7.8m/s and a northward propagation velocity of 3.6m/s. The pre-Laura wave-pouch exhibits broad cyclonic relative vorticity, and its trough-critical latitude intersection near 11°N or 12°N is shown by a grey circle that is repeated in each frame, including the Earth-relative panels (right column).

Figure 37. GFS analysis of relative vorticity (shading) overlaid with streamlines at 00 and 12 UTC 18 August 2020.

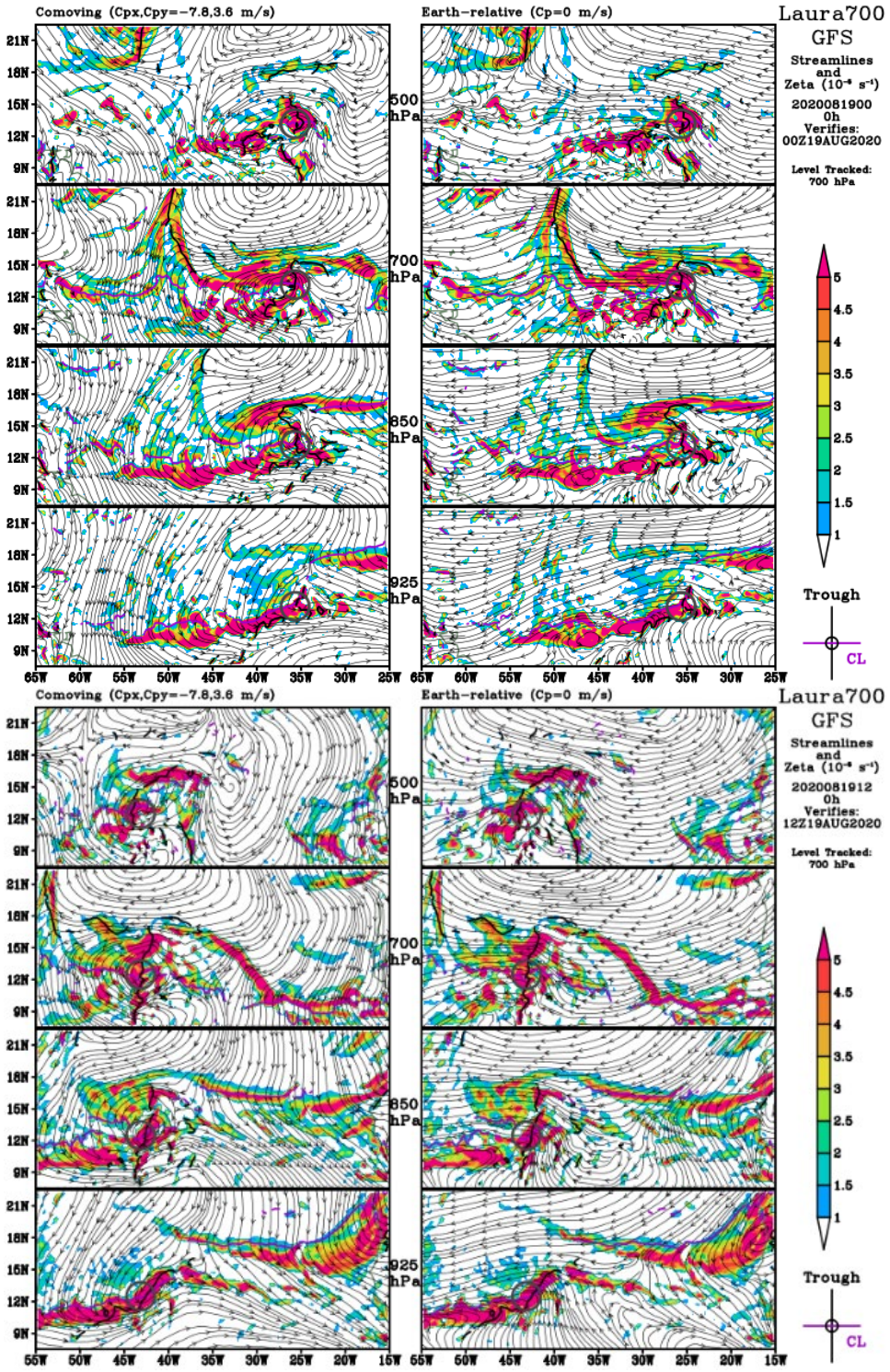

Figure 38. Same as Figure 37, except at 00 and 12 UTC 19 August 2020.

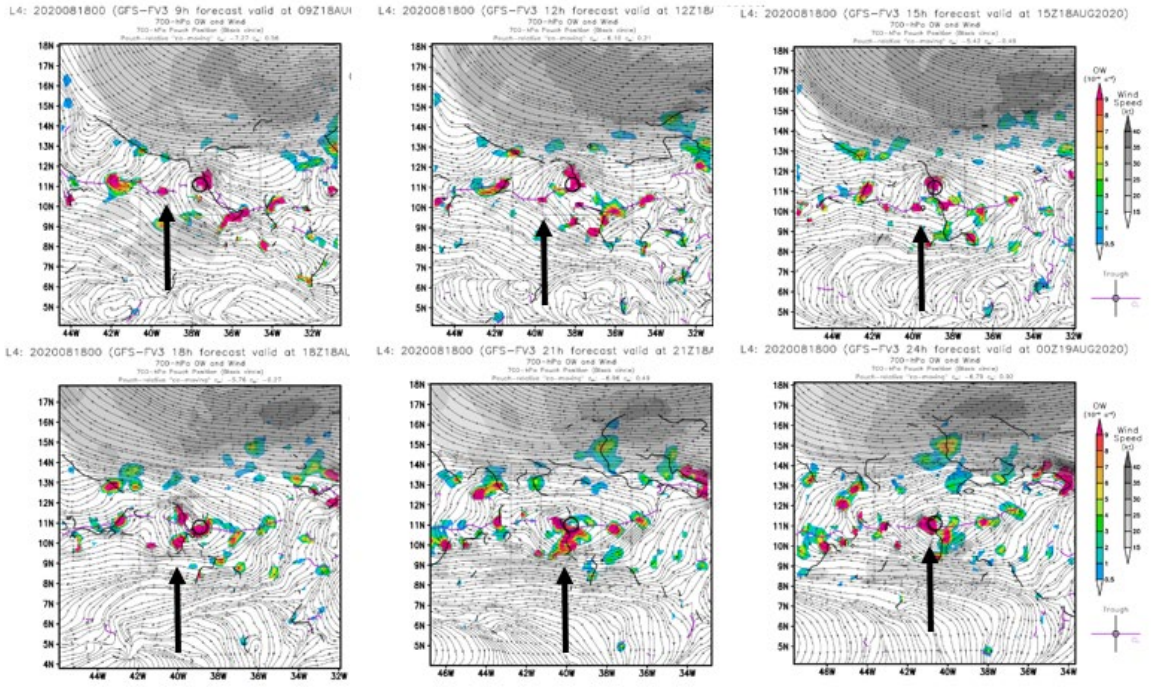

Pre-Laura GFS forecast valid between 9 to 24 hours at three-hour increments. OW and comoving streamline plots illustrate the main pouch (black circle) in the vicinity of smaller vortices. Depending on intensity, the smallest vortices experience partial to complete strain, while larger vortices experience more elastic interaction, then partial strain to partial or complete merger. The arrows follow a smaller vortex as it enters the cyclonic flow and becomes strained (top middle), then partially merges (bottom left), and finally completely merges (bottom middle).

Figure 39. Pre-Laura GFS forecast initialized at 00 UTC 18 August 2020. Source: Rutherford (2020)[1].

Laura's path to development was similar to the context provided by Dunkerton et al. (2009) with a track akin to Wang and Hankes (2013), in which an AEW with a westward propagating pouch at 700 hPa eventually forms into a TS. The pouch level analysis, however, provides insight that distinguishes pre-Laura from the typified 700-hPa level propagation path. Several small areas with high value OW were found within the broad relative vorticity associated with the disturbance. The interaction of these OW areas

[1] https://marsupialpouches.nps.edu/pouches.php?m=gfs&p=COOW700&dtg=2020081800&fh=loop&r=atl&pp=L4&y=2019

became of interest. Rutherford et al. (2018) described the dynamics involved in tropical cyclone formation, but in context of a single somewhat idealized pouch. Additional research evaluated the interaction of multiple vortices within the scope of elastic interaction, vortex strain, or vortex merger (Prieto et al. 2003; Leweke et al. 2016). These experiments were idealized mathematical or numerical solutions that proved valuable in application to pouch interactions.

Despite appearing as an open wave in the Earth-relative plots at 00 UTC 21 August (Figure 36), the series of OW images eventually revealed a pre-Laura pouch that was vertically aligned with comoving closed streamlines at each level from 700 hPa down to 925 hPa, with slight southeastward tilt between 700 hPa and 500 hPa. The GFS 00 UTC 18 August forecast (Figure 39) suggested the progression of pre-Laura at the 700 hPa and 850 hPa levels as akin to starting with zonally oriented OW centers and proceeding to roll them up like a rug. Distinct OW areas appeared to orbit the pouch center even when defined as TD-13 at 00 UTC 20 August (Figure 40). The idealized 700-hPa pouch had a primary convective cell positioned to the northwest of the pouch center, weaker convection circulating south of the pouch, as well as orbiting OW cells within the broader extent of the closed streamlines. This interaction was well illustrated during the 00 UTC 18 August GFS forecast, preserving properties revealed by the conceptual model through the numerical prediction model forecast.

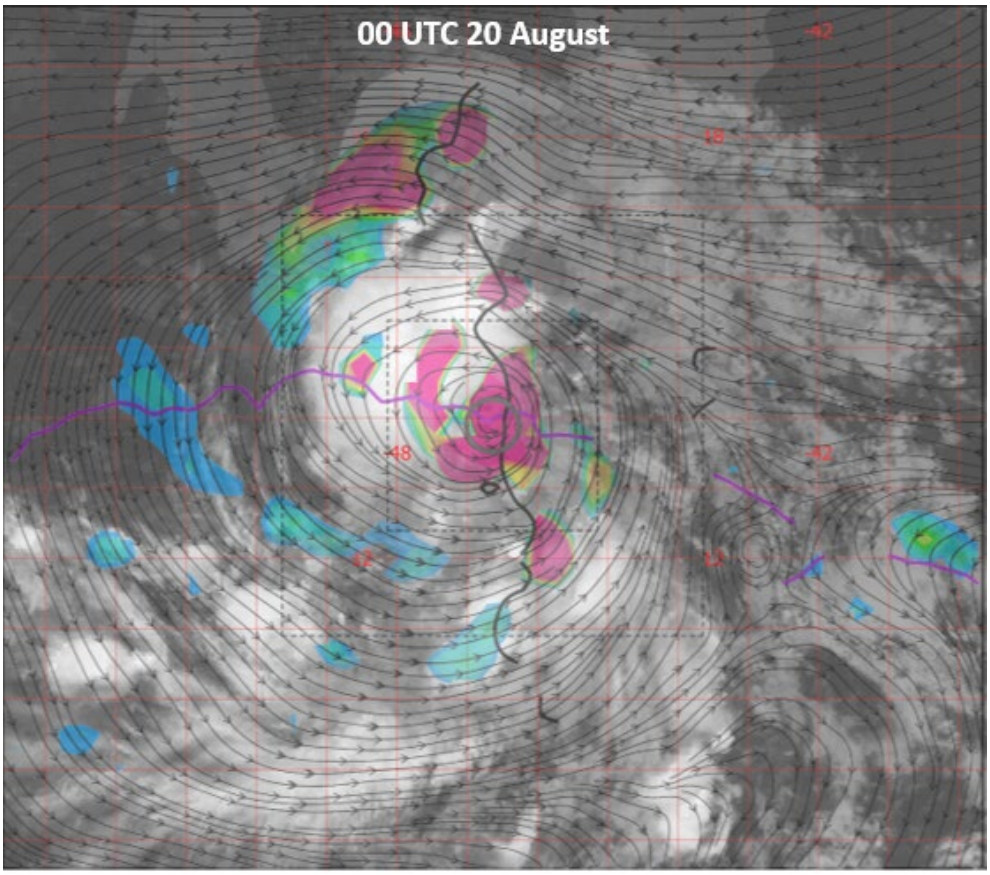

Trough axis (thick black line) crosses the critical latitude (purple line) marking the "sweet spot" at the pouch center. A primary deep convective complex is in the northwest quadrant of the pouch with smaller cells of deep convection wrapping cyclonically around from the southwest to the southeast of the pouch center.

Figure 40. IR imagery for pre-Laura, now TD-13, overlaid with OW and comoving streamlines.

THIS PAGE INTENTIONALLY LEFT BLANK

IV. CONCLUSION AND DISCUSSION

You don't need a weatherman to know which way the wind blows.

—Bob Dylan, 1965

Likewise, it does not take a meteorologist to understand that each tropical cyclone, from wave to depression to storm is unique. The circumstances from which TCs form are highly variable and broad statistical studies tend to gloss over the dynamics and pertinent interactions occurring at different scales that influence TC formation. Evaluating the three storms, Isaias, Josephine, and Laura, sheds some light on the synoptic and mesoscale influences on tropical systems as well as the developing structure at the pouch scale. Based on the present literature and working within the MP conceptual model, the best working definition of a pouch is that of a trough axis and critical latitude intersection corresponding to an area of high cyclonic relative vorticity (with minimal or limited strain and shear deformation) within cyclonic and nearly (or fully) closed streamlines. The following are some observations about pouches consolidated from the results chapter.

Pouch positions do not line up precisely with deep convection, but pouch positions remain in proximity to associated deep convection. This result is not a new take on pouches, but it is helpful in contextualizing the pouch relative to an identified area of potential or persistent convective activity. As a shallow pouch or a wave-trough forms, the convection may be indistinct from a specific pouch and may be associated with the trough passing through an area of relatively high moisture content. Once well-formed, however, a pouch will be moistened by the deep convection and the evaporation of corresponding clouds above the boundary layer. Often, the convective elements in westward propagating pouches in the North Atlantic tend to be west or northwest of the pouch center itself.

Pouches must exist at the lower levels for cyclogenesis to occur; thus, the 700-hPa level pouch is not adequate itself, and the pouch must extend vertically to further develop. This observation reinforces the bottom-up approach to cyclogenesis; not necessarily that pouches originate at low-levels, but that the pouch structure must progressively extend to the lower levels for convergence near the surface to occur. Deep convection already in the

vicinity of a developing pouch may contribute to the downward extension of the pouch, but a sustained pouch and associated deep convection occurs once the pouch structure extends from the surface through the boundary layer. Each cyclone seemed to follow this recipe in one way or another. Isaias had a low-level pouch that experienced column moistening followed by enhanced convection once vertically aligned. Meanwhile, Josephine and Laura were well moistened amidst deep convective areas and required the pouch structure to extend to the lower levels for further development. The troughs and associated pouches that led to the formation of Laura showed that a low-level pouch lacking sufficient relative vorticity was not able to achieve genesis until the 700-hPa level pouch aligned above it.

Direct pouch interactions muddy the certainty of tropical depression formation. Isaias and Laura proved that pouches from different levels as well as the same levels interact. A spectrum of elastic interaction, strain, and merger may develop depending on track and relative pouch positions. Isaias and Laura had two different pouch alignment mechanisms: Isaias formed from two independent troughs, initially separated by six degrees in latitude, come together at one point; and Laura formed from zonal interactions of multiple pouches along approximately the same latitude. The relative vorticity and OW analyses highlighted the concentrated structure of the two pouches that appear to form Isaias, and the broad expanse of the cyclonic relative vorticity plot and the detail in the OW field that encompassed several pouches associated with two main troughs that influenced the formation of pre-Laura.

Pouches may be initially dry or moist. An interesting feature of the Isaias formation was the presence of a dry pouch at 850 hPa characterized by high cyclonic relative vorticity inside nearly closed streamlines in the comoving reference frame. The complexity of Isaias continued when this dry 850-hPa level pouch combined with the moist 700-hPa level pouch. The apparent isolated moistening of the dry pouch at lower-levels occurred when the 850-hPa and 700-hPa level pouches combined. Once both pouches combined, convective bursts in the IR imagery reinforced the RH images, indicating accelerated column moistening. This sequence exhibited vorticity advection vice deep convection as the process that preceded distinct convective bursts appearing on the IR imagery. Once the pouches aligned and extended from the surface to above the boundary layer with increased

RH, the convective bursts appeared approximately 12 hours later. The sequence provided a strong illustration of the pouch structure and associated moisture, indicated by RH, needed in the formation of Isaias.

A. THE MARSUPIAL POUCH PARADIGM APPLIED TO THREE STORMS

In line with the MP conceptual model from Dunkerton et al. (2009), Montgomery et al. (2010b), and the contribution of Wang and Hankes (2013) on the typical AEW track, each storm, Isaias, Josephine, and Laura had 700-hPa cyclonic vorticity disturbances and were trackable from the coast of West Africa, typically around Guinea. Working deeper into Africa, an origin pouch, or a continuous state of high OW, blended into several possible pouch origins without strong confidence in continuing pouch analysis into Africa. Whether disturbances come from the AEJ and its diurnal meandering, or from a westward moving equatorial wave further from the east, is left for future analysis. Suffice to say, that the AEW and associated troughs were not exceptionally large amplitude disturbances, but ones that propagated above a warming ocean, into a region of high relative humidity, and most importantly, minimal to moderate vertical wind shear. These are all properties conducive for sustained deep cumulus convection, resulting in the vertical extension of the pouch. Furthermore, with Isaias and Laura, multiple trough axes, associated with areas of high relative vorticity, interacted in the consolidation of disturbances at different levels and the same level, respectively.

Each storm exhibited nearly closed streamlines in a wave-relative reference frame around cyclonic relative vorticity at low levels (850 hPa and 925 hPa) prior to strengthening into a tropical depression, or potential tropical cyclone in the case of Isaias. Though the mechanisms for developing low level structure differed, achieving lower-level support was a critical component to cyclogenesis and reaffirm previous findings (Dunkerton et al. 2009). Isaias exhibited low-level support most distinctly when the sharp progression of column moistening in a vertically aligned pouch preceded convective bursts. The column moistening at the lower levels then drove the noticeable convective bursts, nearly pinpointing the moment of genesis. For Josephine and Laura, the wave-troughs propagated through well-moistened lower levels amidst areas of deep convection and

contributing to an extension of the pouch to 850 hPa and 925 hPa with nearly closed streamlines.

In each case, a pouch remained trackable at 700 hPa, but that characteristic alone does not tell the whole story. Outlined in each section throughout the results chapter, the discussions illustrated differences with each storm. On a pouch scale, sources of low-level relative vorticity varied. Low-level development of Isaias came from a dry, high relative vorticity structure well to the north that lined up with a relatively weak, 700-hPa wave trough, the superposition of which formed a vertically robust cyclonic vorticity pouch. Meanwhile, Josephine developed from a weak 700-hPa westward propagating wave-trough, and the pouch appeared to extend to 500 hPa before extending to 850 and 925 hPa levels amidst areas of deep convection. Josephine appeared to follow the typical wave path as vertical shear modulated development along a path described by Wang and Hankes (2013). In Laura, two main trough axes generated disturbances within a broad region of well-moistened air. These disturbances would experience elastic interaction followed by partial strain and finally partial to complete merging in the pre-Laura development (Prieto et al. 2013).

B. OPERATIONAL IMPACT AND SUMMARY

On operationalizing this process, a forecaster may add context to their narrative of tropical cyclone formation, in both time and space. The comoving reference frame lifts a veil providing insight into the structure of disturbances prior to conventional Earth-relative model fields and satellite detection and imagery. Though the MP conceptual model uses model inputs from the GFS forecast and analysis, no different from what a forecaster has, the shift to a comoving reference frame allows for advanced insight and increased context for accuracy on the position of a disturbance or several disturbances. Although closed streamlines in the Earth-relative reference frame more clearly indicate cyclonic flow structure and potential activity, the center of Lagrangian circulation and eventual convective activity are not at the Earth-relative circulation center. Moreover, consideration of the phase speed of a parent wave provides a chance to identify cyclonic development in advance of a TC formation by hours, and sometimes, days. The findings outlined in these conclusions provide additional clues that I believe will be helpful to forecasting TC

formation: the onset of sustained convective activity within an approximately vertically aligned pouch, can indicate the highly likely positional and temporal formation of a TC.

An inherent limitation in this analysis is the hindsight bias with regard to post analysis. Real-time forecasters may benefit from the application of MP similar to the effective use of the MP to guide in-situ measurements of areas of potential TC development or interest, e.g., PREDICT (Montgomery et al. 2012). The analysis within this discussion attempted to compare MP products with real-time NHC products to gain operational insight, but relevancy outside the timeline of the storm remains a limitation. Additionally, while generalizations cannot be made from the short and incomplete narrative of three storms, there are some key takeaways relevant to operational forecasters:

1. The observation of the pouch structure that extends from 700 hPa to 850 hPa and 925 hPa indicates the likely further development into a tropical cyclone.

    a. Deep convection, a mechanism that induces convergence of cyclonic vorticity in the lower troposphere, including near the surface contributes to the downward extension of the pouch. This process was evident in pre-Josephine and pre-Laura within a moist atmosphere.

    b. Without deep convection present, vorticity advection as a result of the combination or interaction of two or more pouches (or vortices) can provide the pouch structure needed for to sustain deep convection within the pouch and related self-moistening. This process was most evident in Isaias.

2. Uncertainty in the forecast of TC formation within the MP may provide insight to the modulating effects of pouch-layer vertical wind shear and direct pouch (vortex) interactions.

    a. Vertical wind shear is inimical to convection associated with developing TCs and this shear may also impinge on the pouch and open up dry air pathways into the pouch. Vertical wind shear is a

forecast variable for all disturbances and was the dominant theme in the pre-Josephine case.

b. Direct pouch (or-vortex) interactions may contribute to the benefit or detriment of a tropical disturbance. Pre-Isaias and pre-Laura experienced multiple pouches (or vortices) that influenced the formation and surrounding uncertainty of formation. Limited temporal and spatial resolution prevented a detailed analysis. Higher temporal resolution is needed to improve our understanding of these interactions on TC formation. However, some degree of interaction (i.e., elastic interaction, strain, or merger) was evident in the analyses and model figures.

Happy hurricane hunting!

C. THOUGHTS FOR FUTURE OPERATIONS AND RESEARCH

Additional research may attempt to link the pouch structure to convective activity and TC formation for future storms. The anecdotal analysis of three storms lacks the sample size to determine statistically significant findings. Rather, the process and evaluation of these three storms and future storms may contribute to a larger context of research attempting to pinpoint positional certainty and mechanisms pertaining to disturbances or pouches as they progress or fail to progress.

As much as the post-analysis of these three storms through the lens of the MP provides insight and nuance to operational forecasts, there warrants a discussion about operationalizing the process where possible. As previously discussed in the methods chapter, the MP conceptual model is straightforward and intuitive, but applying the concept comes with a lot of work. Some of that work is self-imposed on the Montgomery Research Group without an individual dedicated to the enhancement of the process beyond producing the minimum products. An immediate boon to operational context to the MP would be to include graphics on a six-hour increment with the model fields that are available. However, this enhancement would add considerable work given the current process to determine pouches four times a day. A careful determination on how to

automate, through machine learning or some other variant of artificial intelligence may aid in this process for routine or easy pouch determinations. Given the contextual difficulty in determining pouches throughout the process, having a premade reference for basin wide on a six-hour basis would narrow the scope when considering OW, relative vorticity, RH, along with the equivalent potential temperature and tracer.

Rutherford et al.'s (2018) approach to automation considered a total span of 72 hours, 36 previous to an analysis and 36 forecasted. This methodology to refine pouch determination does extremely well for developed storms and even pouches near or a part of waves, see 00 UTC 18, 19, and 20 August[2] MP GFS based forecast. False positive pouches do nonetheless occur, and there lacks a coherent labelling between analysis efforts, which along with the challenge of sequentially positioning pouches gives an operator the impression that pouches appear, disappear, and jump around throughout the period. Some of this may reflect the nonlinearity of the underlying model outputs in addition to the real-world variation over 24 hours wherein, as an example, deep convection develops and dissipates around a parent wave along its path of propagation. Jumping from high OW areas across six hours intervals or 24 hours works within a continuity time frame best when the system is fully developed. To counter the false positives, there is a probability of verification that provides users with a probability of a given pouch reaching tropical storm status in a period of five days. This probability product provides a useful operational tool in addition to the other products.

Lastly, with regard to operationalizing the pouch products, many calculations are done in MATLAB or GrADS. The probability of verification relies on machine learning in MATLAB given a database to draw from. Retooling or finding an automated way to add seasons to update and reinforce this tool would contribute to the robustness of the verification tool. However, stepping outside the MATLAB and GrADS reliance, as

[2] 18 August: https://marsupialpouches.nps.edu/global.php?m=gfs&p=EROW700&dtg=2020081800&fh=loop&r=atl&

19 August: https://marsupialpouches.nps.edu/global.php?m=gfs&p=EROW700&dtg=2020081900&fh=loop&r=atl&

20 August: https://marsupialpouches.nps.edu/global.php?m=gfs&p=EROW700&dtg=2020082000&fh=loop&r=atl&

difficult as it is, could add significant value to compute time, capability, and output delivery options. Finding a simple way through GIS to allow for the manipulation of the phase speed to generate custom comoving plots could increase operational and research analysis within the conceptual framework.

APPENDIX: OPERATIONAL FORECASTS FROM NHC

A. JOSEPHINE

The forecast discussion for Figure 41 identifies precipitation and convection associated with a westward propagating tropical wave. Forecasted to develop slowly and enter unfavorable conditions with low chance of development (NHC 2020a).

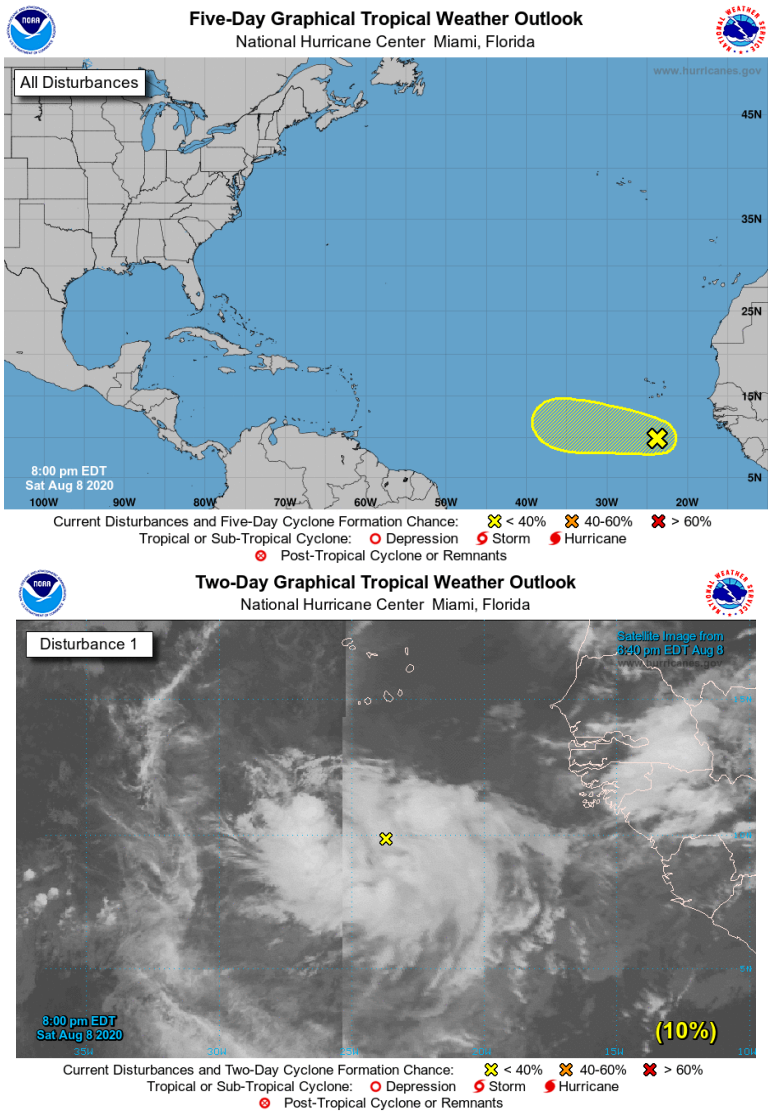

Figure 41. Initial identification of convection with a tropical wave at 2313 UTC 8 August 2020. Source: NHC (2020b).

Forecast discussion indicates continued development led to a center of circulation along with an areas of low pressure. Convection and precipitation continue to organize as the disturbance moved northwestward in the tropical Atlantic (Figure 42). Unfavorable conditions later in the week may inhibit storm development (NHC 2020a).

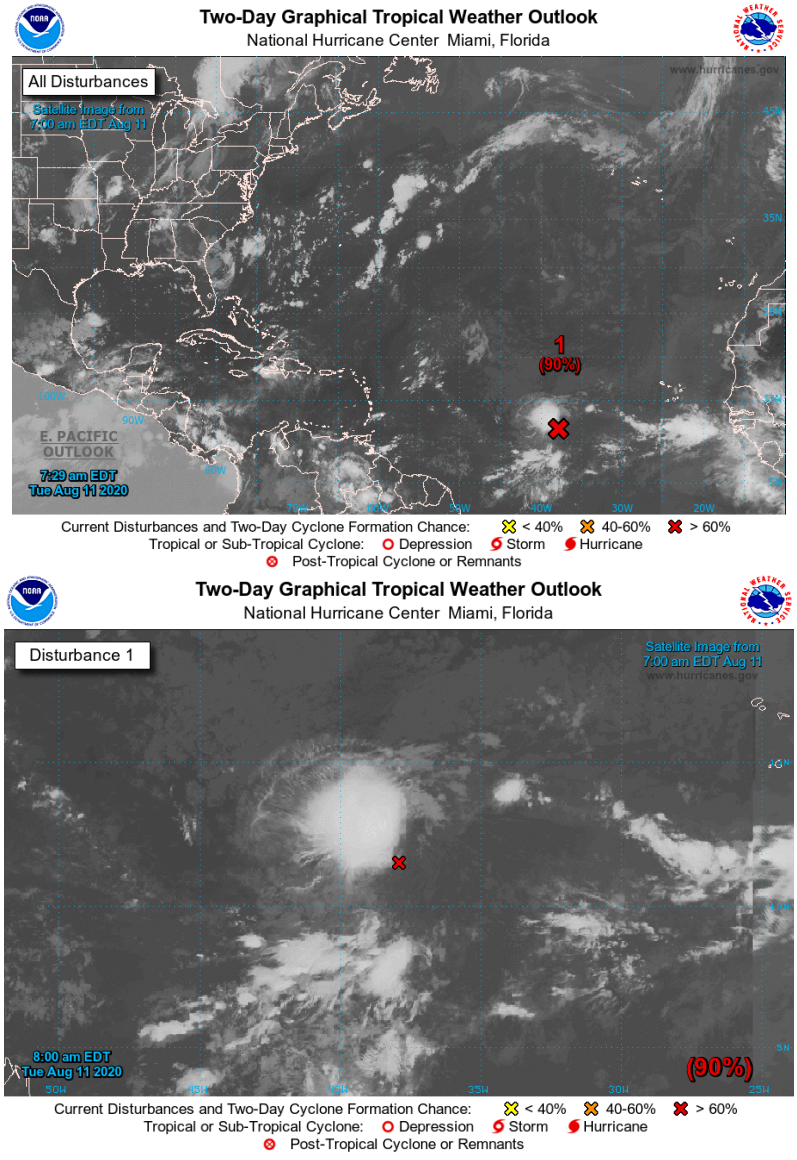

Figure 42. Developing system seen more organized at 1130 UTC 11 August 2020. Source: NHC (2020b).

The initial advisory for TD-11 occurs at 2100 UTC 11 August. The advisory identifies TD-11 with a center at approximately 11.7°N, 40.0°W while moving west at a heading of 280° at 14kts with sustained winds of 30kts (NHC 2020a).

The forecast discussion draws on ASCAT-C data noting that the circulation tightened with deep convection forming. From the discussion, a mid-tropospheric high will buoy the track south, but may weaken allowing the storm to track northward. Further, satellite imagery and SAL evaluation show the depression protected from the dry air. Decreasing easterly shear will also encourage TC development in the short term before increased westerly or southwesterly shear develops considerably weakening the system (NHC 2020a).

By 13 August, Josephine was named and on a northwestward track (Figure 43). The path veered further north and into the dry air and increased vertical shear in the environment that is approximately coincident with the SAL. Within four days, Josephine was sheared apart and dissipated in the North Atlantic.

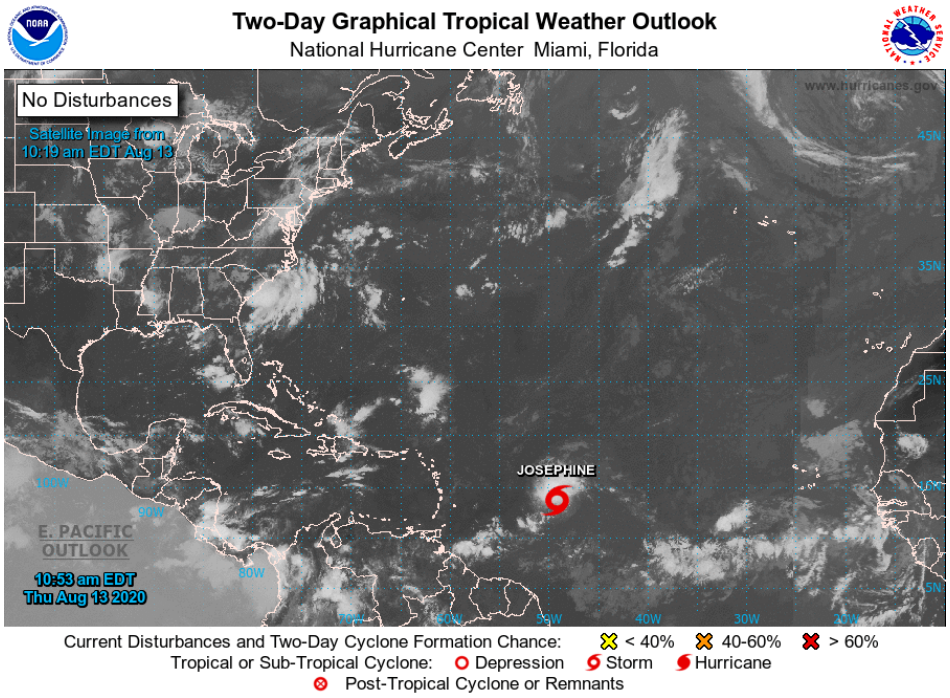

Figure 43. Tropical Storm Josephine at 11453 UTC 13 August 2020. Source: NHC (2020b).

B. ISAIAS

The discussion presents a tropical wave off the African Coast with westward propagation, some development is possible (NHC 2020a). The sentiments of the forecast discussion are illustrated in Figure 44, where a disturbance on the coast of Africa will develop in an area outside of the Leeward Islands prior to entering the Caribbean.

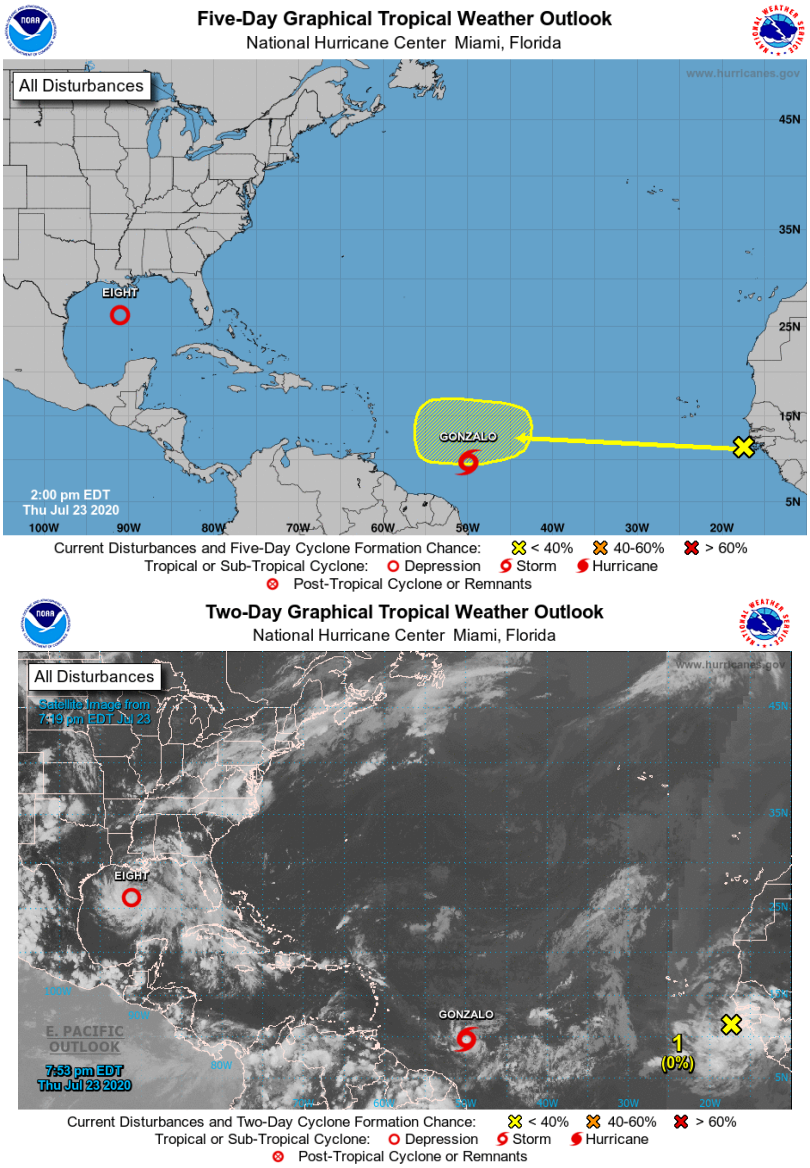

Figure 44. NHC's first identification and prediction of a disturbance on the west coast of Africa at 2353 UTC 23 July 2020. Source: NHC (2020b).

The discussion depicts the tropical wave as a broad area of clouds and unorganized precipitation and convection consistent with Figure 45 (bottom). The forecasted is for continued westward movement at 13 kts with development into a TD in the central tropical Atlantic (NHC 2020a).

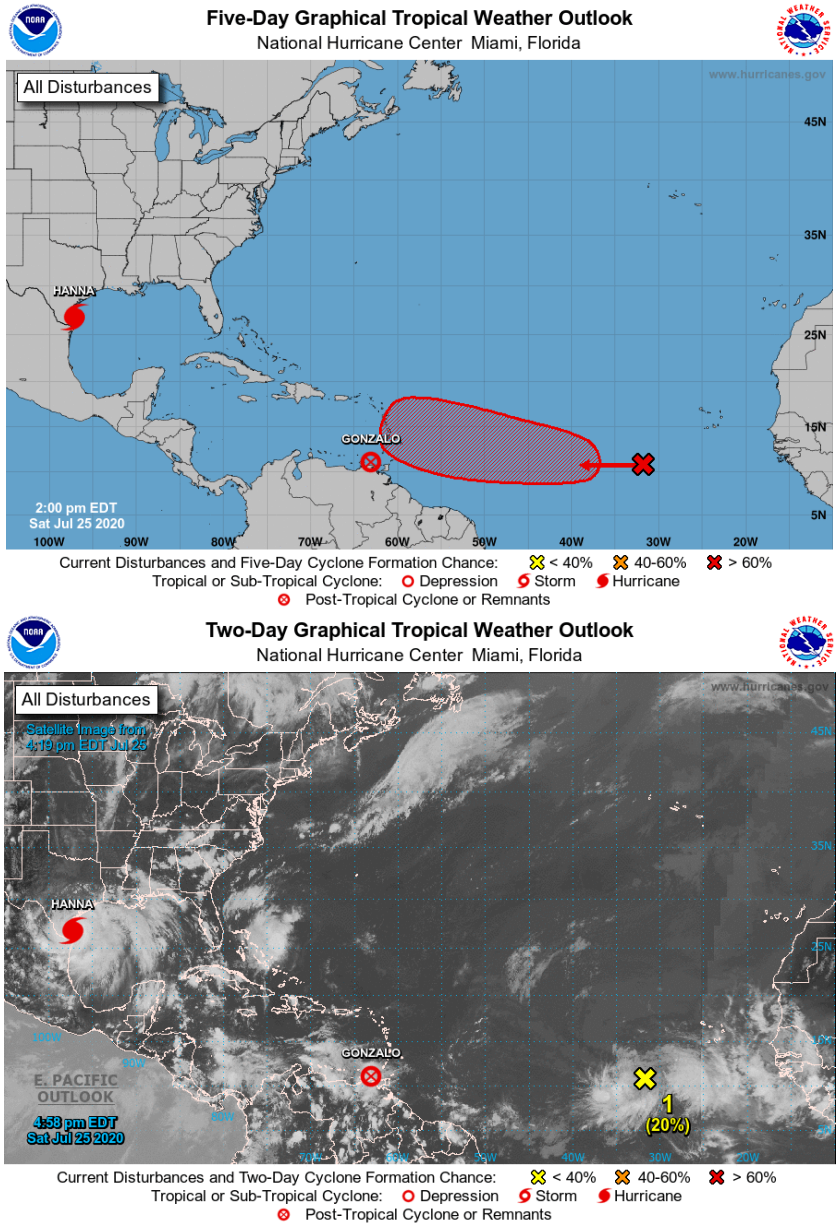

Figure 45. Continued development at 2058 UTC 25 July 2020. Source: NHC (2020b).

The first advisory issued for Potential Tropical Cyclone Nine occurs at 1500 UTC 28 July (Figure 46). The center is approximated near 13.8°N, 53.7°W at a 280° heading traveling at 20 kts with sustained winds reaching 35kts (NHC 2020a). Forecaster discussion identified an elongated circulation without a well-defined center from satellite imagery. Dry air located north of the system is forecasted to hinder development immediately before yielding to into favorable condition for TC development. The forecast expects the system could be a tropical storm near the Leeward Islands (NHC 2020a).

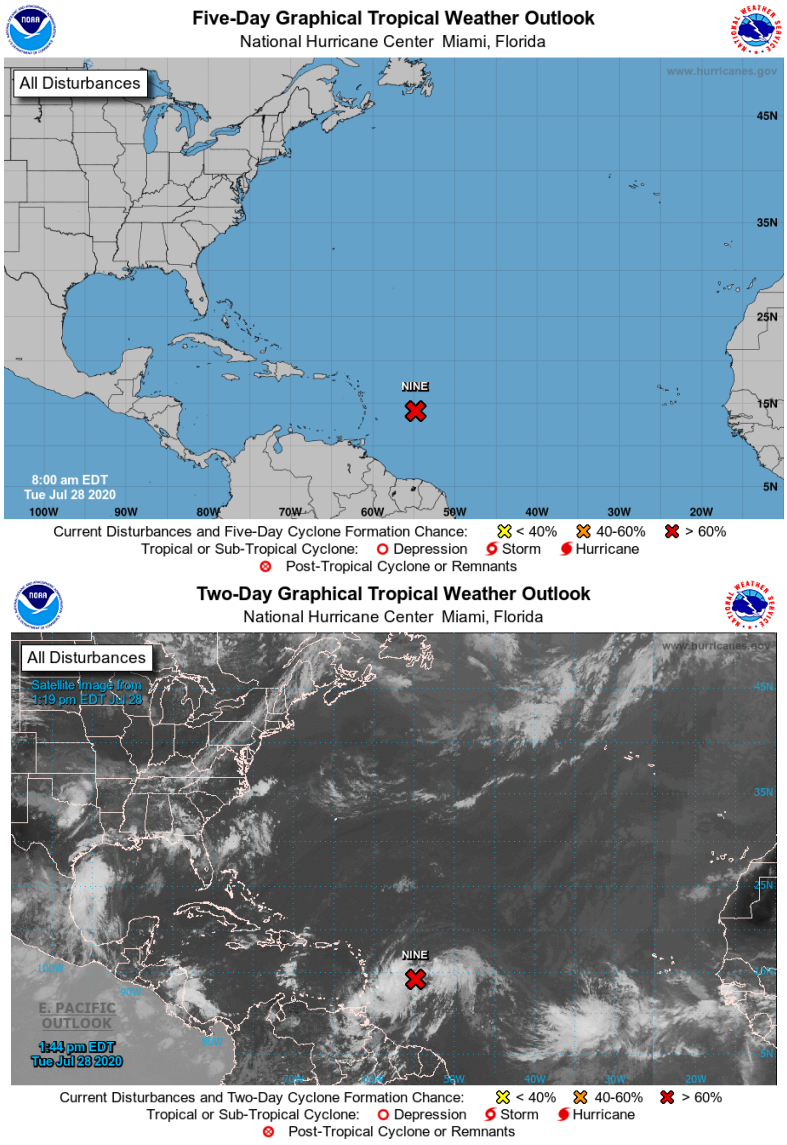

Figure 46. Potential tropical cyclone NINE at 1744 UTC 28 July 2020. Source: NHC (2020b)

The forecast discussion centers on an elongated area of low pressure producing tropical storm force winds indicated from NOAA buoy 41040. A center of the system or of circulation is not apparent from satellite imagery. While not yet an organized storm, favorable conditions will not inhibit further circulation and organization of the system as it tracks toward the Leeward Island at about 15 kts. NHC never identifies Isaias as a tropical depression and instead calls the disturbance a potential tropical cyclone. This distinction seems arbitrary at first, but a closer look at the difference between a TD, TS, and what is now a PTC reveals the lack of organization of the system with no well-defined center (Latto et al. 2021; Brennan 2021). Simultaneously, the operational constraint of issuing advisories on a poorly organized tropical disturbance even with strong model consensus in cyclone formation over the next few days contributed to maintaining the distinction from a TD. The Potential Tropical Cyclone NINE (PTC9) label persisted for about 36 hours before direct upgrading to Tropical Storm Isaias (NHC 2020a). In PTC9 advisory 6 discussed sustained winds of 45 mph, which is above the TS threshold. The next advisory named the tropical storm, indicating an organized center in the discussion (NHC 2020a).

Tropical Storm Isaias passes the Leeward Islands shifting to a north northwestward track. Isaias tracks over the Dominican Republic and strengthens into a hurricane before passing over the Bahamas east of Florida, when Isiaias weakened into a tropical storm. Tropical Storm Isaias takes a track northward up the Atlantic coast and makes landfall as a category one hurricane near the border of North Carolina and South Carolina and continues following near the east coast before dissipating into flow over eastern Canada.

The narrative is that of a tropical disturbance associated with an AEW that propagates westward as loosely assembled convection slowly organizes into a tropical storm. The delay in organization tends to rely on some dry air intrusion from the SAL tracking north of the system, or at least a barrier for moisture in the propagating wave. The discussions identified elongated areas of pressure, clouds, and convection reinforcing an interaction that does not lead to wave dissipation, only inhibition, due to the SAL.

C. LAURA

Pre-Laura is identified as a tropical wave off the west coast of Africa propagating westward at 15–20mph with low development probability over the next five days (Figure 47) (NHC 2020a).

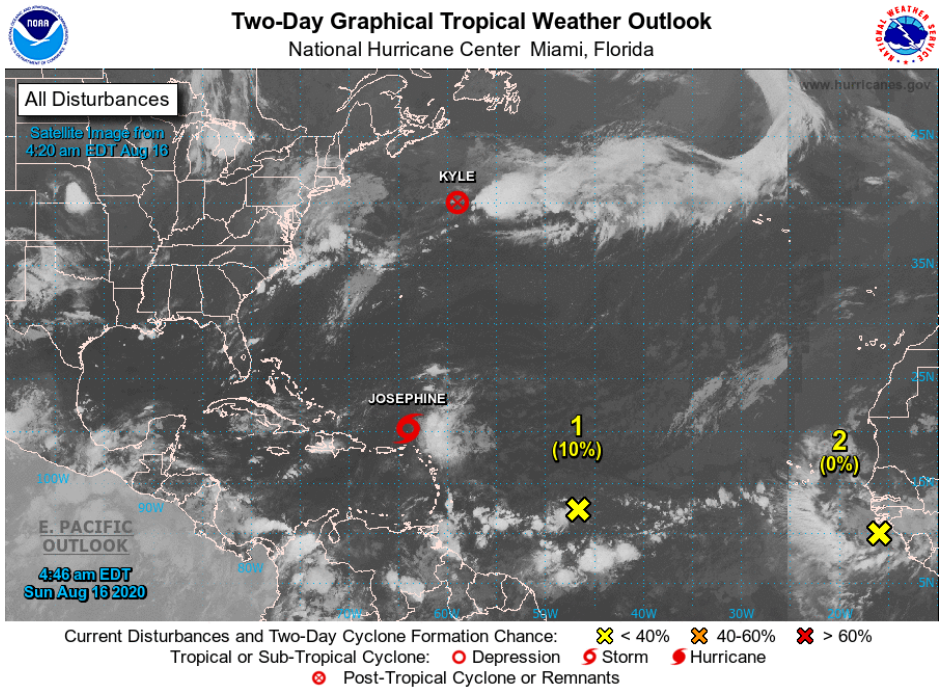

Figure 47. Initial indication of westward propagating AEW at 0847 UTC 16 August 2020. Source NHC (2020b).

The forecast discussion noted that the large area of low pressure organized with more defined banding around the center (NHC 2020a). The system continues to propagate westward at 15–20 mph and should encounter favorable environmental conditions for development (Figure 48).

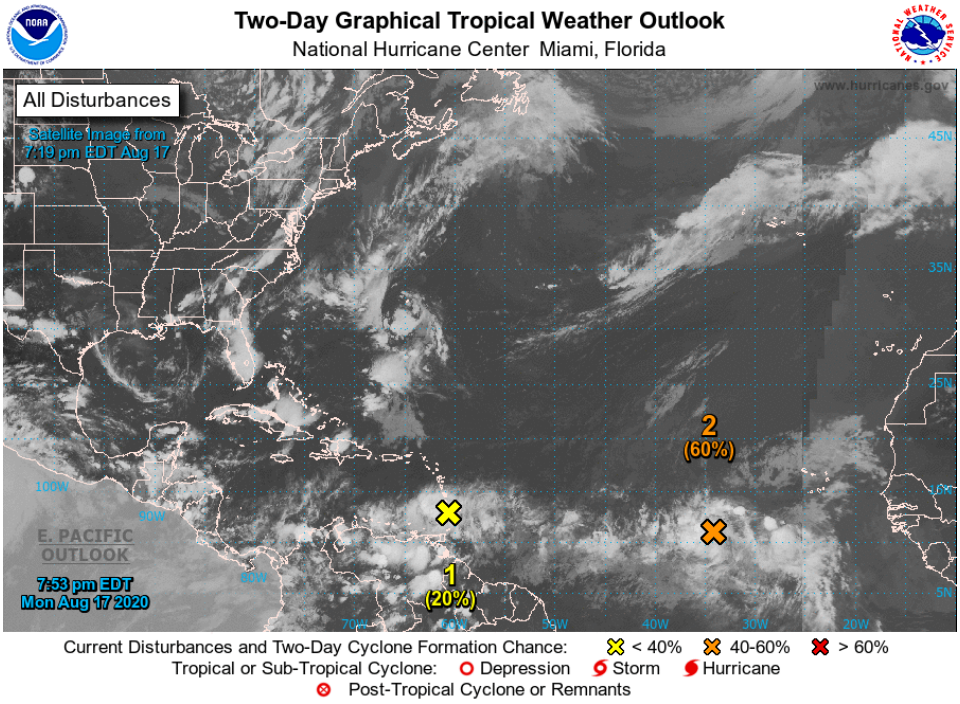

Figure 48. Tropical wave progressing westward with increasing probability of development at 2354 UTC 17 August 2020. Source: NHC (2020b).

Transitioning into a tropical depression, pre-Laura remained poorly organized even after naming, as center of circulation was difficult to determine by aircraft and satellite (Figure 49). Forecasters identified that circulation between levels remained separated with mid-level shear and dry air entrainment inhibiting moist convection. Despite high uncertainty around the position, the gradual increase of persistent wind up to 40 kts led to naming the system Tropical Storm Laura.

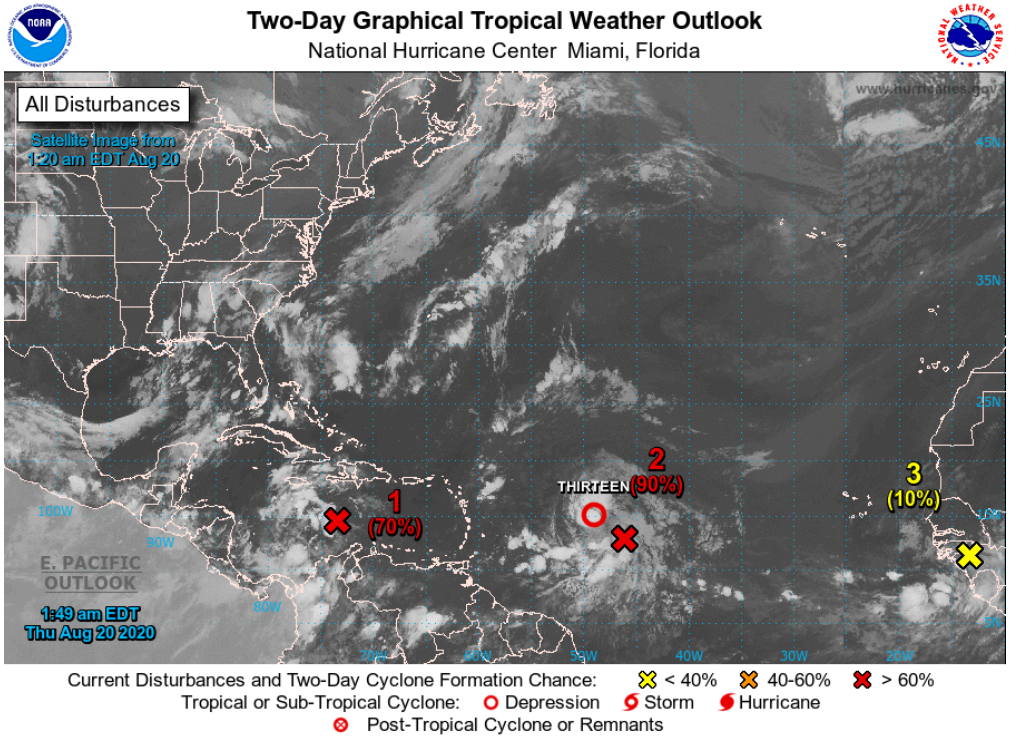

Figure 49. Tropical Depression THIRTEEN at 0550 UTC 20 August 2020. Source: NHC (2020b)

Newly named TS Laura continued on a northwestward track toward the Caribbean Sea (Figure 50). Laura sustained TS status through much of its traverse across the Caribbean Sea and intensified after passing just south of Cuba. The warm waters of the Gulf of Mexico allowed Laura to intensify to a category four hurricane before making landfall on the border between Texas and Louisiana.

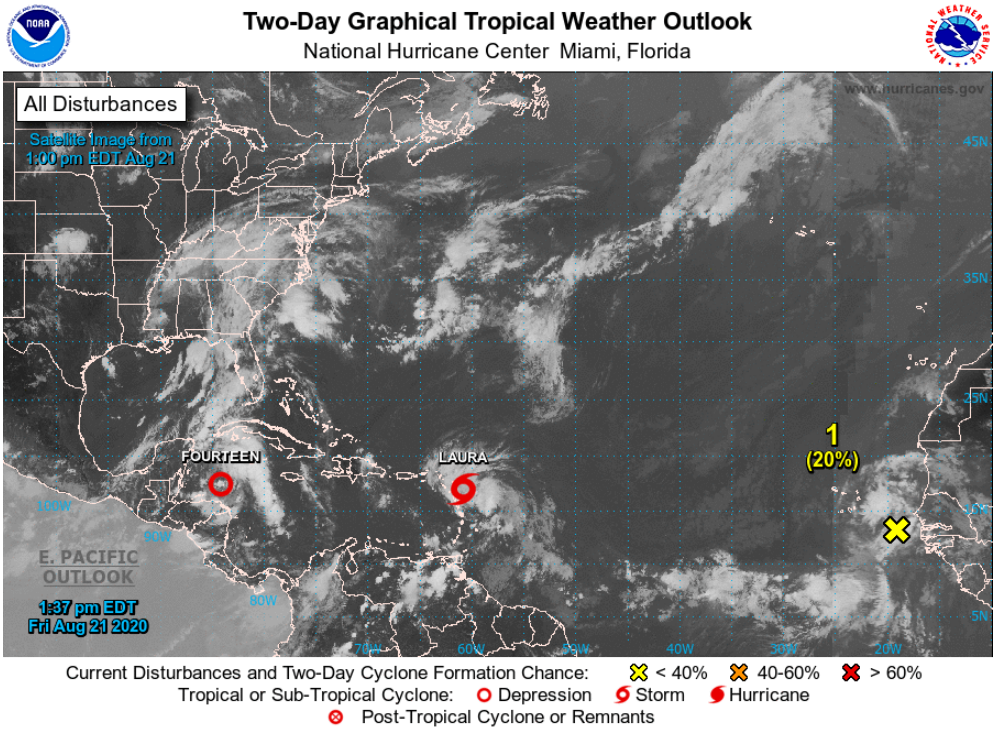

Figure 50. Tropical Storm Laura at 1737 UTC 21 August 2020. Source: NHC (2020b)

THIS PAGE INTENTIONALLY LEFT BLANK

LIST OF REFERENCES

Bell, G., M. Rosencrans, H. Wang, E. Blake, C. Landsea, R. Pasch, and S. Goldenberg, 2020: NOAA 2020 Atlantic hurricane season outlook. Accessed 21 April 2021, https://www.cpc.ncep.noaa.gov/products/outlooks/hurricane2020/May/hurricane.shtml.

Brennan, M., 24 May 2021: Potential tropical cyclone nine. Electronic communication.

Chan, J. C. and R. T. Williams, 1987: Analytical and numerical studies of the beta-effect in tropical cyclone motion. Part I: Zero mean flow. *Journal of the Atmospheric Sciences,* **44**, 9, 1257-1265.

Dritschell, D. G. and D. W. Waugh, 1992: Quantification of the inelastic interaction of unequal vortices in two-dimensional vortex dynamics. *Physics of Fluids: Fluid Dynamics,* **4**, 1737, https://doi.org/10.1063/1.858394.

Dunkerton, T. J., M. T. Montgomery, and Z. Wang, 2009: Tropical cyclogenesis in a tropical wave critical layer: easterly waves. *Atmospheric Chemistry and Physics,* **9**, 5587–5646.

Freismuth, T. M., B. Rutherford, M. Boothe, and M. T. Montgomery, 2016: Why did the storm ex Gaston (2010) fail to redevelop during the PREDICT experiment? *Atmospheric Chemistry and Physics,* **16**, 8511–8519, DOI: 10.5194/acp-16-8511-2016

GDAL/OGR contributors (2021). GDAL/OGR Geospatial Data Abstraction software Library. Open Source Geospatial Foundation. URL https://gdal.org

Gray, William M., 1975: Tropical Cyclone Genesis. CSU-ATSP-234, 121 pp, https://mountainscholar.org/bitstream/handle/10217/247/0234_Bluebook.pdf?sequence=1&isAllowed=y

Knapp, K. R., H. J. Diamond, J. P. Kossin, M. C. Kruk, C. J. Schreck, 2018: International Best Track Archive for Climate Stewardship (IBTrACS) Project, Version 4. *ibtracs.last3years.list.v04r00.csv*. NOAA National Centers for Environmental Information. Accessed 12 February 2021, doi.org/10.25921/82ty-9e16.

Leweke, T., S. Le Dizes, and C. H. K. Williamson, Charles, 2016: Dynamics and Instabilities of Vortex Pairs. *Annual Review of Fluid Mechanics,* **48**, 507–541. 10.1146/annurev-fluid-122414-034558.

Latto, A., A. Hagen, and R. Berg, (2021) National Hurricane Center Tropical Cyclone Report: Hurricane Isaias. Accessed 30 April 2021, https://www.nhc.noaa.gov/data/tcr/AL092020_Isaias.pdf.

Montgomery, Michael T., and Coauthors, 2012: The Pre-Depression Investigation of Cloud-Systems in the Tropics (PREDICT) Experiment: Scientific Basis, New Analysis Tools, and Some First Results. *American Meteorology Society,* **93** (2): 153–172, https://doi.org/10.1175/BAMS-D-11-00046.1.

Montgomery, M. T., L. L. Lussier III, R. W. Moore, and Z. Wang, 2010a: The genesis of Typhoon Nuri as observed during the Tropical Cyclone Structure 2008 (TCS-08) field experiment – Part 1: The role of the easterly wave critical layer. *Atmospheric Chemistry and Physics,* **10**, 9879-9900. www.atmos-chem-phys.net/10/9879/2010/.

Montgomery, M. T., Z. Wang, T. J. Dunkerton, T. J. 2010b: Coarse, intermediate and high resolution numerical simulations of the transition of a tropical wave critical layer to a tropical storm. *Atmospheric Chemistry and Physics*, **10**, 10803-10827, DOI:10.5194/acp-10-10803-2010.

National Hurricane Center and Central Pacific Hurricane Center (NHC), 2020a; 2020 Tropical Cyclone Advisory Archive. Accessed 06 February 2021, https://www.nhc.noaa.gov/archive/2020/.

NHC, 2020b; 5-Day GTWO (June 2014 – Present) archive. Accessed 06 Feburary 2021, https://www.nhc.noaa.gov/archive/xgtwo/gtwo_archive_list.php?basin=atl.

NHC; Glossary of NHC Terms. Accessed 21 February 2021, https://www.nhc.noaa.gov/aboutgloss.shtml#t.

Prieto, R., B. D. McNoldy, S. R. Fulton, and W. H. Schubert, 2003: A Classification of Binary Tropical Cyclone-Like Vortex Interactions. *Monthly Weather Review,* **131**, 2656–2666, DOI:10.1175/MWR2610Supl1.

Reinhard, B. J. 2021: National Hurricane Center Tropical Cyclone Report: Tropical Storm Josephine. NOAA National Hurricane Center. Accessed 6 February 2021, https://www.nhc.noaa.gov/data/tcr/AL112020_Josephine.pdf.

Rutherford, B., M. A. Boothe, T. J. Dunkerton, and M. T. Montgomery, 2018: Dynamical properties of developing tropical cyclones using Lagrangian flow topology. *Royal Meteorological Society*, **144**, 218–230. DOI:I0.1002/qj.3196.

Rutherford, B. 2020: Automated Lagrangian pouch tracking. Naval Postgraduate School and Northwest Researh Associated. Accessed 6 February 2021, https://marsupialpouches.nps.edu/.

Schmit, T. J., P. Griffith, M. M. Gunshor, J. M. Daniels, S. J. Goodman, and W. J. Lebair, 2017: A closer look at the ABI on the GOES-R series. *Bulletin of the American Meteorological Society.* **98**, 4, 681-698. DOI/10.1175/BAMS-D15-00230.1.

Smith, R. K., 1991: An analytic theory of tropical cyclone motion in a barotropic shear flow. Q. J. R. Meteor. Soc., **117**, 685-714.

Sutyrin, G. G. and G. R. Flierl, 1994: Intense vortex motion on the beta plane: development of the beta gyres. *American Meteorological Society,* **51**, 5, 773-790.

Wang, Z. and I. Hankes, 2013: Characteristics of Tropical Easterly Wave Pouches during Tropical Cyclone Formation. *Monthly Weather Review*, **142**, 626–633, DOI: 10.1175/MWR-D-13-00267.1

Wang, Z., M. T. Montgomery, and T. J. Dunkerton, 2010: Genesis of pre–Hurricane Felix (2007). Part I: The role of the easterly wave critical layer. *J. Atmos. Sci*., **67**, 1711–1729, doi:10.1175/2009JAS3420.1.

University of Wisconsin—CIMSS (2020) CIMSS Tropical Cyclones Data Archive. http://tropic.ssec.wisc.edu/archive/

THIS PAGE INTENTIONALLY LEFT BLANK

INITIAL DISTRIBUTION LIST

1. Defense Technical Information Center
   Ft. Belvoir, Virginia

2. Dudley Knox Library
   Naval Postgraduate School
   Monterey, California